CHALMERS
UNIVERSITY OF TECHNOLOGY

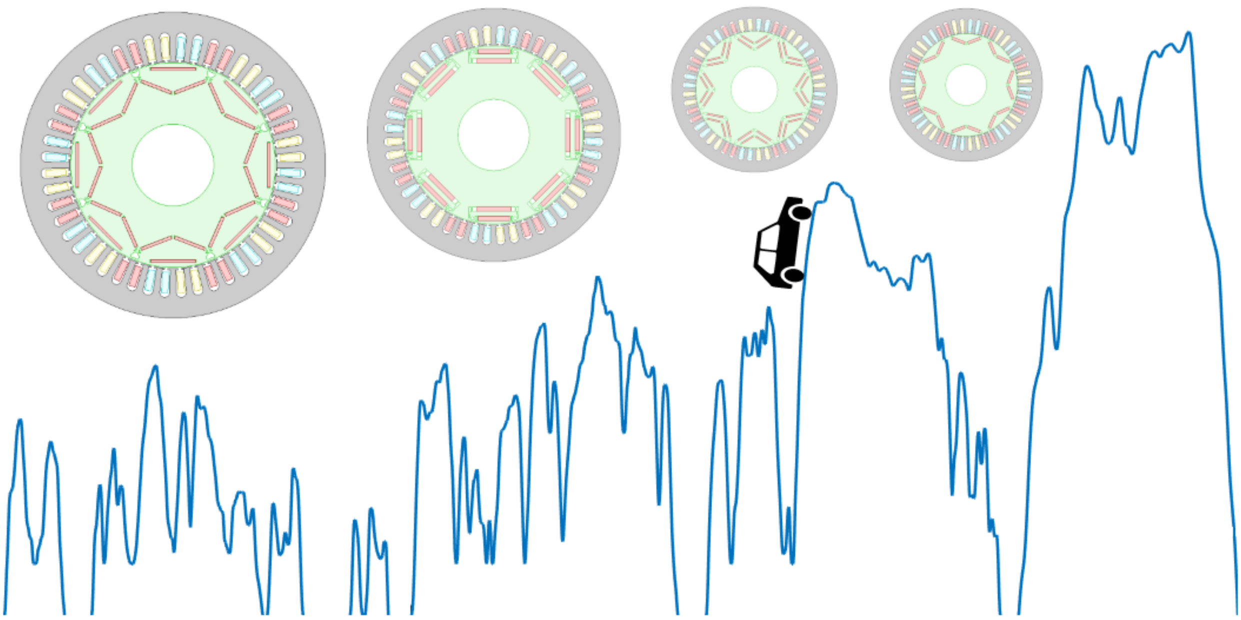

Electric machine design based on drive cycle analysis

Master's thesis in Electric Power Engineering

Bharadwaj Raghuraman, Tom Gyllensten

Department of Electrical Engineering
CHALMERS UNIVERSITY OF TECHNOLOGY
Gothenburg, Sweden 2019

Master's thesis 2019

Electric machine design based on drive cycle analysis

Bharadwaj Raghuraman, Tom Gyllensten

CHALMERS
UNIVERSITY OF TECHNOLOGY

Department of Electrical Engineering
Division of Electric Power Engineering
Chalmers University of Technology
Gothenburg, Sweden 2019

Electric machine design based on drive cycle analysis
Bharadwaj Raghuraman and Tom Gyllensten

Supervisor: Torbjörn Thiringer, Chalmers University of Technology and Elisabet Jansson, Volvo Cars
Examiner: Torbjörn Thiringer, Dept. of Electrical Engineering

Master's Thesis 2019
Department of Electrical Engineering
Division of Electric Power Engineering
Chalmers University of Technology
SE-412 96 Gothenburg
Telephone +46 31 772 1000

Printed by Chalmers Reproservice
Gothenburg, Sweden 2019

Electric machine design based on drive cycle analysis
Bharadwaj Raghuraman and Tom Gyllensten
Department of Electrical Engineering
Chalmers University of Technology

Abstract

In this thesis, the design of electric machines with respect to real-world driving cycles has been carried out. The thesis can be divided into two parts where the first aims to characterize electric machine operation from real-world driving data. The data consists of an extensive amount of measurements taken from over 500 cars which amount to 110 000 individual trips and 39000 hours of driving. The data mainly consists of speed over time and combining this with two vehicle models, Volvo S60 and Volvo XC90, electric machine operating regions are found. All the trips extracted from the database, are characterized as either Urban, Rural or Highway. The most common operating regions, as well as regions that have the highest energy consumption for each drive type is found. Also, additional investigations of how people drive, and what differentiates the driving types from each other are studied in terms of acceleration and energy consumption. In the second part, eight electric machines are modeled with the goal of meeting the requirements found from the database analysis. The most important factor in this thesis is to have high efficiency where most energy is consumed. For the machines, four different rotor topologies are modeled. The eight machines then go through improvements with the goal of increasing efficiency. Also, additional analysis in the form of demagnetization and mechanical properties is carried out. It was found that most consumers drive in low torque (20- 30 Nm) and relatively high speed (6000 - 9000 RPM) regions in the torque-speed map of the machine. Also, two different silicon steel materials with vastly different prices for the stator and rotor laminations were considered. It was found that the initial high cost of the expensive silicon steel machine can be compensated by higher efficiency during the lifetime operation of the machine. Overall, it was found that different driving types and different car models can benefit from choosing a machine more suitable for that specific application.

Keywords: Real world driving cycles, Electric machine, Modeling of electric machine,Electric machine analysis, Demagnetization.

Acknowledgements

We would like to take this opportunity to thank all those who helped us in the execution of this work. Foremost, we would like to thank our supervisor and examiner Prof. Torbjörn Thiringer for his support, encouragement and persistent commitment towards his students . Furthermore, we would also like to express our sincere gratitude towards our supervisor at Volvo Cars , Elisabet Jansson for many fruitful discussions and endless support. Additionally, we would also like to thank all members of the Electromagnetic design team at Volvo cars for their consistent support.

Bharadwaj Raghuraman and Tom Gyllensten
Göteborg, Sweden
July, 2019

Contents

1
Introduction

1.1 Background

The automotive industry is going towards rapid electrification and this has given rise to a renewed interest in electric machine design with high performance, high efficiency and suited for the customer needs. With increased electrification, electric cars are being used in all kinds of driving scenarios, from city driving, highway driving and also high-performance driving. Due to this wide range of driving scenarios, a common approach to electric machine design is not optimal. Hence, a more targeted approach to electric machine design based on the type of customer and his/her needs is required.

1.2 Previous work

Numerous approaches have been adopted in electric machine design for automotive propulsion applications by analyzing drive-cycle data. [1] presented a specialized design evaluation tool for the design of electric machines. The influence of different parameters on the powertrain was also studied. But the drive cycles considered for the design were legislative drive-cycles such as UDDS, HWFET and US06 mainly for the US the market. [2] presented different optimizations for the design of permanent magnet synchronous machines (PMSM) targeting drive cycles such as NEDC, Artemis and a combination of NEDC and Artemis legislative drive cycles. [3] presented optimization specific to interior permanent magnet machine designs based on drive-cycle data. Here, V shaped magnet design was considered for optimization and the NEDC and Arthemis drive cycles were considered. [4] presented an extensive optimization approach for Permanent Magnet Assisted Synchronous Reluctance machine (PMASR) using legislative drive cycles such as UDDS and US06. [5] presented an approach to electric machine design where in average efficiency over a driving cycle was used as an important parameter to analyze and design machine, based on drive cycle analysis. As noted from above, most of the work carried out in the electric machine design is based on legislative drive cycles which might not give a true representation of the driving done by a normal customer. Also, some of the legislative drive cycles are quite old and might not truly present the performance requirements for the electric machine. In this thesis, we would like to fill this void by analyzing a large database of real-world driving and base the electric machine design on the database.

1.3 Aim

The aim of this master thesis is to first analyze numerous real-world driving cycles and characterize the most common operating regions of various categories of cars and map these operating regions to the electric machine operating regions. Second, to derive the requirements of the electric machine from the above drive-cycle analysis and to design an electric machine optimized towards the operating points where most energy is spent while driving. To find this machine, multiple rotor designs will be compared against each other.

1.4 Scope

A publicly available database of drive-cycles is used to derive the requirements of the electric machine design. Electric machine design will be carried out in a simulation environment and no hardware prototype will be built due to time constraints. A detailed analysis of the cost of manufacturing the machine is not included but a judicious choice of materials to keep the overall cost of the machine to a minimum will be carried out. Also, the project lasts over a 20 week time period. During that time the goal is to investigate at least two types of motors on different driving cycle types.

1.5 Method

The main tasks of the master thesis are as follows:

1) Conduct a literature study on Permanent Magnet Synchronous Machine (PMSM) design and on MySQL database management system to read drive-cycle data.
2) Develop scripts to read drive-cycle data from the database.
3) Characterize extracted drive cycles in terms of speed.
4) Analyze drive-cycles with different driving patterns and derive important conclusions on the most common operating regions.
5) Map the derived operating regions to the operating regions of an electric machine and extract requirements for electric machine design.
6) Design a PMSM machine based on the derived requirements.
7) Performance selected geometric variations on the electric machine and evaluate the impact on the result.
8) Derive the electric machine performance indices and efficiency maps.
9) Compare the machines in terms of efficiency with results from drive cycle analysis.
10) Additional analysis in terms of demagnetization and mechanical analysis.

2
Theory

2.1 Drive cycle

A drive cycle is defined as a series of data-points which represents the speed of a vehicle over time. Driving cycles are either created theoretically or recorded using real-world driving. Standardized drive cycles are often used to test a vehicle's fuel consumption and CO_2 emissions. With the advent of electric vehicles, drive cycles are now often used to size the electrical powertrain components, especially the battery. Even though standardized drive-cycles are often used for powertrain size, these cycles miss the interaction of a vehicle with its environment which is an essential part of sizing. These interactions can be clearly captured in real-world driving scenarios and hence in this thesis, numerous real-world drive cycles are used to classify driving behaviors or drive patterns and also to design electric machines for a pure-electric car architecture.

2.2 Database

The real-world driving cycles used in this thesis are collected as part of the Swedish car movement data project [6] conducted between June 2010 and September 2012. The database contains data of 714 privately owned cars that are registered in Västra Götaland county or Kungsbacka municipality of Sweden. Out of the total 714 cars, 528 cars have data exceeding 30 days and over 450 cars more than 50 days.

2.3 Basics of Vehicle dynamics

The behavior of a car on the road with a specified motor is heavily dependent on the parameters of the car. Vehicle dynamics modeling is essential to the design of the car's powertrain and aims to represent the real car as close as possible. With the help of a good model, accurate simulations with specific drive train specifications can be carried out. The goal in this thesis is to calculate the amount of torque and speed needed at the motor shaft in order to meet the different drive cycles. The second purpose is to investigate the operating points for every drive cycle. Hence a comprehensive car model which takes into account various loads on the vehicle is required. Each car in the database is represented as a device and the database does not provide information about the specific car type that a device corresponds to. Therefore all the cars from the database are considered to have equal weight and a general model for the car is constructed. However since the sizing of the power train is dependent on vehicle parameters such as weight and air resistance, two different cars are modeled. Two car's models representing Volvo's heaviest and lightest cars namely XC90 and S60 are used for analysis [7][8]. Some important factors that affect vehicle dynamics are detailed below.

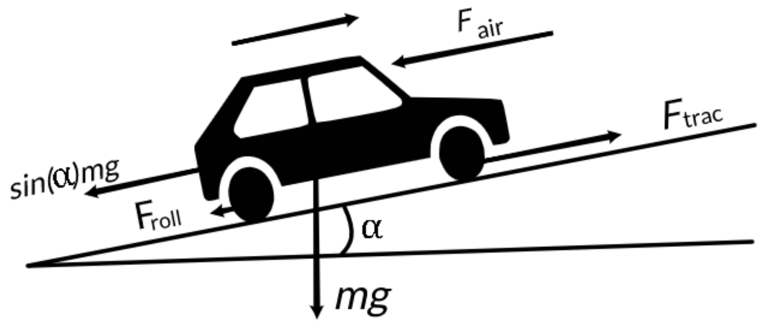

Figure 2.1: Forces on a vehicle

2.3.1 Air resistance

Aerodynamic drag is a force that increases quadratic with speed according to

$$F_{air} = \frac{1}{2}\rho A C_d v^2 \tag{2.1}$$

where ρ is the air density and v is the velocity of the vehicle. The force arises due to the mass flow of air around the car when the car is traveling. The resistance from the air is the main force to overcome when running a car on a flat surface. It is therefore desirable to have as small resistance in the air as possible. The two factors that contribute to this is the frontal cross-sectional area of the car (A) and the drag coefficient (C_d). The latter is a coefficient that tells how "streamlined" or "sleek" a car is. This coefficient is measured in a wind tunnel. During the development process of the car, C_d is optimized due to the interest in reducing fuel consumption. This can be observed from the data of XC90 vehicle whose C_d value changed from 0.4 to 0.32 from 2002 to the present version [8]. Normally C_d value is between 0.25 - 0.35.

2.3.2 Rolling resistance

A car's rolling resistance occurs due to the contact between the soft tires of a car and the surface given by

$$F_{roll} = C_r mg \cos\alpha \tag{2.2}$$

where m is the mass of the vehicle and g is acceleration due to gravity. The magnitude of the resistance offered is a complex factor dependent on up to seven different factors [9]. These factors end up in a coefficient (C_r) that together with the car's weight and road gradient gives an approximate force that needs to be overcome to get the car rolling. In this thesis, all car's assumed to have the same rolling resistance coefficient.

2.3.3 Grading force

Grading force is the force required when moving up or downhill. This force together with the acceleration force is often the biggest contributor to the total traction force needed to propel the vehicle forward. This force can either be positive or negative and can therefore either help or resist the forward motion of the car given by

$$F_{grade} = mg \sin \alpha \tag{2.3}$$

In this thesis, the grading force is excluded from the total traction force to simplify the database analysis. Instead, calculations are done to make sure that the specified machines can handle gradients as required by legislation.

2.3.4 Acceleration force

Acceleration force is the largest contributor to the total traction force and is a major factor in the sizing of electric machines and is given by

$$F_{Acc} = m\frac{dv}{dt} \tag{2.4}$$

where m is the mass of the vehicle and $\frac{dv}{dt}$ the change in speed. Due to customer requirements of high performance cars, this term tends to be the highest contributor to the total force requirement.

2.3.5 Traction Force

The total tractive force is given as the sum of all the forces required to meet the specific driving conditions in terms of acceleration, grading, air resistance, and rolling resistance and is given by

$$F_{trac} = F_{acc} + F_{roll} + F_{grade} + F_{air} \tag{2.5}$$

The torque required from the machine is in direct relation to the total tractive force.

2.4 Permanent Magnet Synchronous Machine

Numerous electric machine topologies have been studied and in use as a propulsion system in electric vehicles [10]. The two most common electric machine topologies are Induction machines and Permanent Magnet Synchronous Machine (PMSM) [11]. Compared to an induction machine, a PMSM has high power density, high efficiency and is lightweight which are crucial factors for electric vehicle application [11]. This thesis focuses on the design and analysis of PMSM machines for electric vehicles.
Permanent magnet synchronous machines generally consist of a wound stator similar to an induction machine and a permanent magnet rotor. Typical PMSM used in electric vehicles are of three-phase type supplied by an inverter setup.

2.4.1 PMSM electric equivalent circuit

Representation of a PMSM using a dynamic equivalent circuit is generally carried out in the dq reference frame. The d-axis refers to the main flux path of the magnets and the q-axis leads the d-axis by 90-degree electrical angle. The $d-q$ axis of a 4 pole interior permanent magnet rotor is shown in figure 2.2.

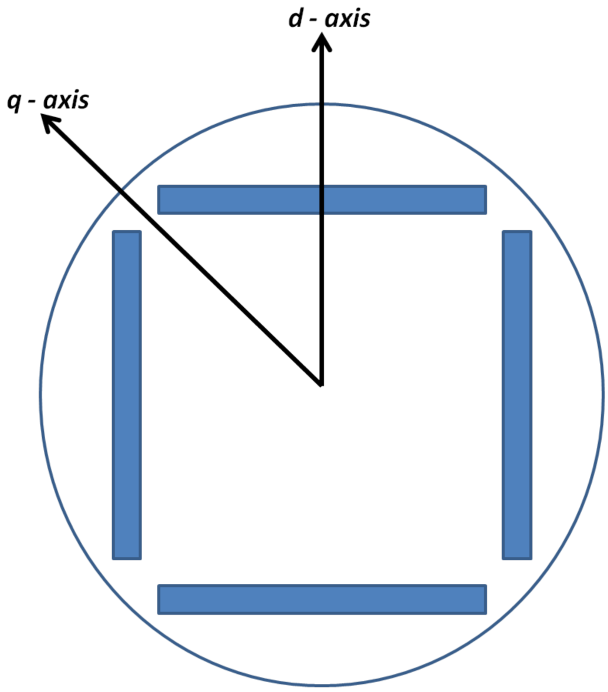

Figure 2.2: dq - axis of a PMSM machine

The voltage equations describing the PMSM machine in the d-q reference frame are given by

$$U_{sd} = R_s i_{sd} + L_{sd}\frac{di_{sd}}{dt} - \omega_r L_{sq} i_{sq} \tag{2.6}$$

$$U_{sq} = R_s i_{sq} + L_{sq}\frac{di_{sq}}{dt} + \omega_r L_{sd} i_{sd} + \omega_r \Psi_m \tag{2.7}$$

where R_s is the stator winding resistance,L_sd is the stator inductance along the d axis, L_sq is the stator inductance along the q axis, ω_r is the electric speed in rad/s, Ψ_m is the magnet flux linkage, i_{sd} is the current along d axis and i_{sq} is the current along q axis. The corresponding equivalent circuits are shown in fig. 2.3.

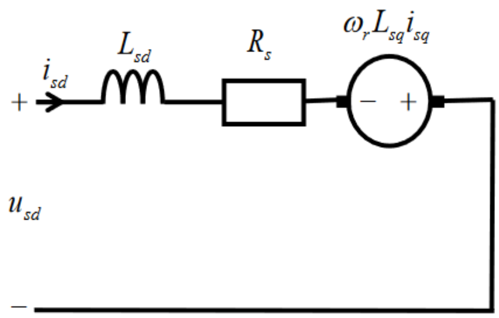

(a) d - axis equivalent circuit

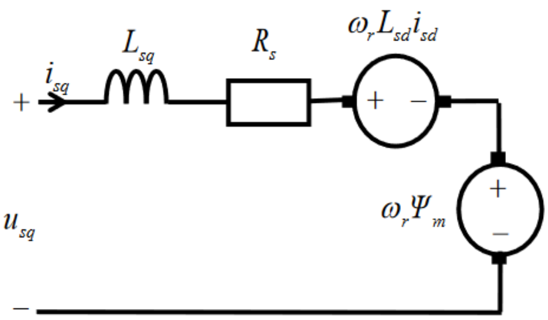

(b) q - axis equivalent circuit

Figure 2.3: Equivalent circuits

The electromagnetic torque (T_e) generated by the machine is given by

$$T_e = \frac{3n_p}{2}\left\{\Psi_m i_{sq} + (L_{sd} - L_{sq}) i_{sd} i_{sq}\right\} \tag{2.8}$$

From the torque equation, we can see that there are two components of torque. One is due to the magnets and one is due to the difference between the reluctance paths along with the d and q axis of the machine. We can write T_e in terms of current magnitude (I_{mag}) and the current angle (β) and it is given by

$$T_e = \frac{3n_p}{2}\left\{\Psi_m I_{mag} \sin\beta + (L_{sd} - L_{sq}) I_{mag}^2 \sin\beta\cos\beta\right\} \tag{2.9}$$

A typical variation of torque and its components with respect to the current angle is shown in figure 2.4

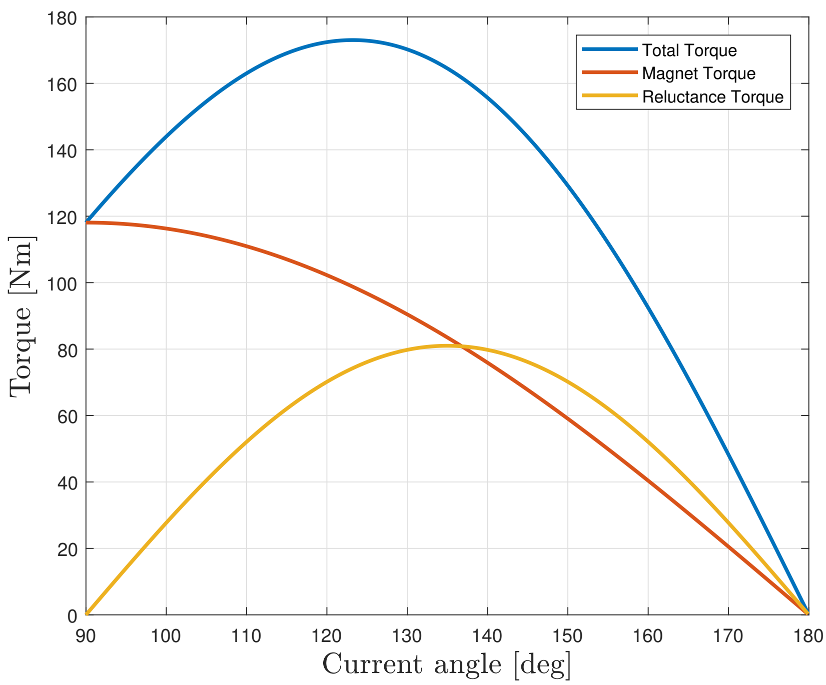

Figure 2.4: Torque and its components in a PMSM machine

2.5 PMSM control strategies

Control of PMSM is an integral part in an electrical drivetrain system for achieving maximum machine performance. Many different control strategies have been evolved [12] to maximize/minimize different parameters such as efficiency or reduce the current used. Two such control strategies that are discussed and used are. Maximum Torque per Ampere control where we try to minimize copper losses to achieve the required torque [13]. Minimum loss control tries to minimize the total electromagnetic losses (copper loss + iron losses) in the machine to achieve the required torque set-point [14].

2.5.1 Maximum Torque per Ampere (MTPA)

The MTPA algorithm is one of the most widely used and well known control strategies for control of PMSM machines [12]. MTPA control tries to achieve the requested torque while ensuring that the copper loss is minimized. As copper losses compromise a large part of the total losses in the machine, the MTPA algorithm helps in achieving high efficiency, which is very important for automotive propulsion applications.

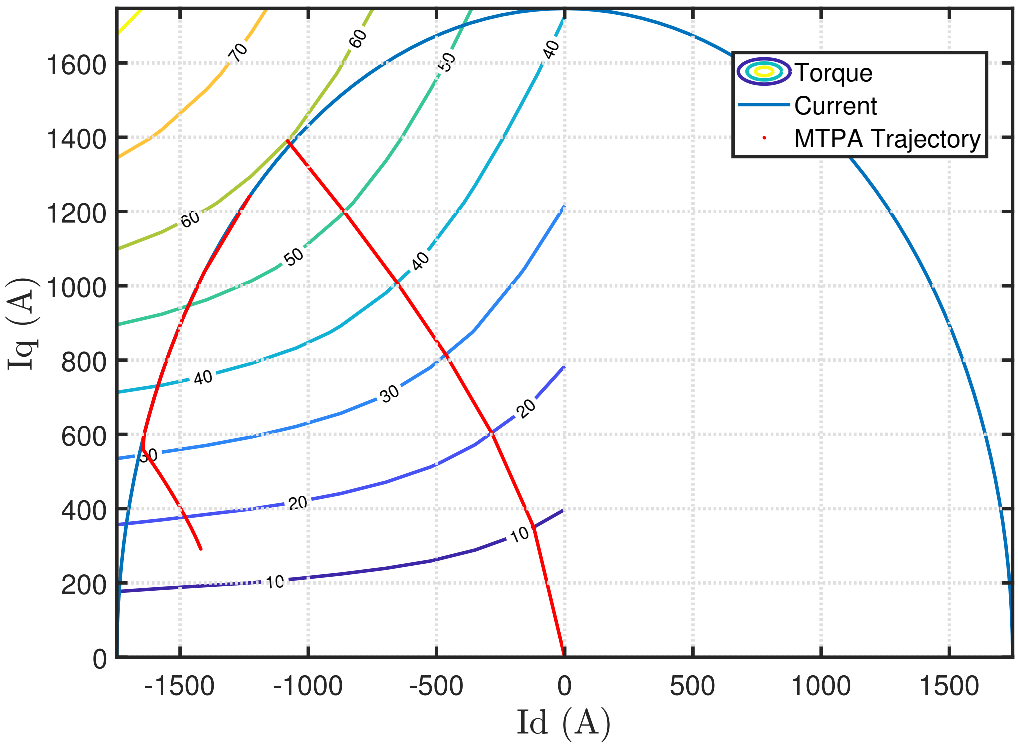

Figure 2.5: MTPA Trajectory

MTPA control can be subdivided into three main regions of operation:

1. Current trajectory before the voltage limit is reached (MTPA region) .

2. Current trajectory after the voltage limit is reached and field weakening is applied (Field weakening region).

3. Current trajectory in the high speed region when the voltage ellipse falls within the current circle. The current is minimized by following the maximum torque per voltage (MTPV region) line.

From (2.9), we can observe that the torque produced by a PMSM machine is mainly controlled by the current magnitude (I_{mag}) and the current angle (β). Copper losses in a machine are proportional to the square of the current (I_{mag}^2) flowing in the windings. The current angle for the reference torque generation with the least current magnitude is achieved by

$$\frac{dT_e}{d\beta} = \frac{3n_p}{2}\left\{\Psi_m I_{mag}\sin\beta + (L_{sd} - L_{sq})I_{mag}^2 \sin\beta\cos\beta\right\} = 0 \tag{2.10}$$

From this, the variation of the current angle in the MTPA region is given by

$$\cos\beta = \frac{\Psi_m}{4(L_{sd} - L_{sq})I_{mag}} - \sqrt{\frac{1}{2} + \left(\frac{\Psi_m}{4(L_{sd} - L_{sq})I_{mag}}\right)^2} \tag{2.11}$$

These equations are valid only if constant L_{sd}, L_{sq} and Ψ_m are assumed. A detailed description of the MTPA control can be found in [13].

2.5.2 Minimum Loss control

At high speeds, the core losses of the machine is a significant proportion of the total losses and hence just reducing the copper losses by MTPA control might not be an optimal solution. Minimum Loss control [15] tries to address this problem by trying to achieve the requested torque demand and also ensure the least total loss in the machine. Copper losses(P_{cu}) in a machine is given by

$$P_{cu} = \frac{3}{2}R_s I_{mag}^2 \tag{2.12}$$

where R_s is the stator winding resistance. Core losses are generally separated into hysteresis (P_{hyst})and eddy current losses(P_{eddy}) [16]. In addition to the traditional core and copper losses, another component, stray losses(P_{stray}), which are due to the higher winding space and slot harmonics are also considered. The empirical expressions for hysteresis loss is given by [16],

$$P_{hyst} = k_h B^{\gamma}\omega \tag{2.13}$$

where k_h is the hysteresis loss coefficient, B is the magnetic flux density and $\gamma \approx 1.8 - 2.2$ and ω is the electrical speed.The eddy current loss is given by [16],

$$P_{eddy} = k_e B^2\omega^2 \tag{2.14}$$

where k_e is the eddy current loss coefficient. The stray loss calculation is difficult and is generally expressed as [16],

$$P_{stray} = k_{st} B^{1.5} \omega^{1.5} \tag{2.15}$$

where k_{st} is the stray loss coefficient. Minimum loss control tries to achieve the torque request (T_{req}) subject to the constraints,

$$min(P_{cu} + P_{hyst} + P_{eddy} + P_{stray}) \tag{2.16}$$

$$T_e - T_{req} = 0 \tag{2.17}$$

$$(\omega L_{sd} i_{sd} + \omega \Psi_m) + (\omega L_{sq} i_{sq})^2 \leq U_{max}^2 \tag{2.18}$$

$$i_{sd}^2 + i_{sq}^2 \leq I_{max}^2 \tag{2.19}$$

where T_e is the generated electromagnetic torque, U_{max} and I_{max} are the maximum available voltage and current limits to the machine. A detailed description of the minimum loss control can be found in [15].

2.6 Analytical design of PMSM machines

Electric machine design is an iterative procedure in order to achieve the desired result. As electric machine design involves numerous parameters, an exact analytical solution is often impossible. Hence here we will discuss the initial design of the machine based on analytical equations which are then used to perform finite element analysis and get a better result. Some of the important parameters which have to be estimated in finite element analysis are:

1. Main dimensions
2. Air gap length
3. Winding configuration
4. Slot and teeth dimensions
5. Core depth and outer dimensions, and
6. Initial magnet dimensions

Prerequisites required for the initial estimation of the parameters are as follows:

1. Maximum and Rated Output Power
2. Maximum and Rated Torque
3. Maximum and Base speed
4. Available DC voltage
5. Pole number of the machine

For all the designs, a 400 V DC bus is assumed and a 8 pole machine (P) is considered.

2.6.1 Rotor dimensions

The main dimensions of the machine mainly refer to the air gap diameter(D_{airgap}) and the active length (L_{stack}) of the machine as shown in Fig. 2.6.

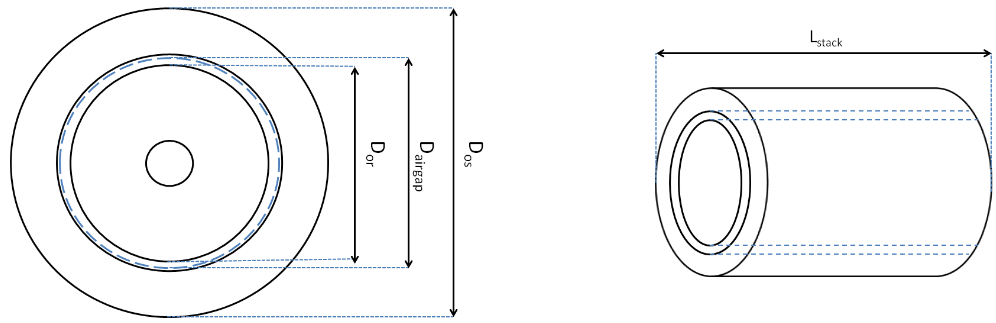

(a) Machine dimensions

(b) Stack length

Figure 2.6: Machine dimensions

Two main factors contributing are the magnetic and electric loading on the machine. Magnetic loading(B_δ) is the maximum value of the magnetic flux density in the air gap, and electric loading (A) refers to the maximum linear current density of the machine [17] given by

$$A = \frac{I_u}{\tau_s} \tag{2.20}$$

where I_u is the maximum value of slot current and τ_s is the slot pitch given by

$$\tau_s = \frac{\pi D}{Q_s} \tag{2.21}$$

where D is generally used for the rotor outer diameter or stator inner diameter neglecting the air gap length, and Q_s is the number of slots. The torque (T) generated by a machine is directly proportional to the product of the electric and magnetic loading known as shear stress and the volume of the rotor [17], i.e

$$T = \sigma_F 2\pi r_r^2 l_e = 2\sigma_F V_r \tag{2.22}$$

where r_r is the radius of the rotor, l_e is the active or stack length of the machine, V_r is the rotor volume and σ_F is the sheer stress given by

$$\sigma_F = \frac{AB_\delta \cos\zeta}{2} \tag{2.23}$$

where ζ is the spatial phase shift between the fundamental components of A and B_δ. By knowing the torque requirement of the machine and using the above approach the volume of the rotor can be estimated. Various approaches have been investigated on the distribution of rotor volume into the length and diameter of the rotor. [18] defines a term called aspect ratio (K_{ratio}) defined as the ratio between the active length and the pole pitch of the machine

$$K_{ratio} = \frac{L_{stack}}{\tau_p} \tag{2.24}$$

where the pole pitch τ_p is given by

$$\tau_p = \frac{\pi D}{P} \tag{2.25}$$

and P is the number of poles. As stated in [18], as the value of K_{ratio} is increased, the weight, cost and the inertia of the motor decreases but increases the linear current density A. The author recommends a typical value of 1-2 for the aspect ratio. Here an aspect ratio of 2 is chosen for all the designs to reduce cost and weight and still manage the increase in current density.

2.6.2 Air gap length

Air gap length (δ) of a machine is a significant parameter in the design process. Air gap length has major effects on the losses and efficiency of the machine. A small air gap length has the benefit of lower magnetizing current in case of induction machines or lower magnet content in case of a PMSM, but a small value of air gap also increases the eddy current losses due to the permeance harmonics created by the slots in the stator. Empirical formulas are generally used to calculate the air gap length as there is no theoretical optimal solution. The empirical formula stated in [17] is used for calculation in this thesis and is given by

$$\delta = \frac{0.18 + 0.006{P_{max}}^{0.4}}{1000}[m] \tag{2.26}$$

where P_{max} is the maximum output power of the machine in Watts.

2.6.3 Winding Configuration

The two main types of winding configuration are the integral slot winding and the fractional slot windings. In integral slot windings, the number of slots per pole per phase is an integer and in a fractional slot winding, the number of slots per pole per phase is a fraction. Integral slot windings are known to provide a higher sinusoidal distribution of the MMF compared to fractional slot windings while on the downside use more copper for the windings[17]. As a higher sinusoidal MMF distribution helps in reducing the core loss in the machine which then translates to better efficiency at higher speeds, in this thesis, integral slot windings are considered. Considering number of slots per pole per phase (q) as 2, we get a symmetrical winding configuration[17], the total number of slots in a three-phase machine (Q_s) is given by

$$Q_s = 3Pq \tag{2.27}$$

One of the important parameters for the configuration of the windings is the winding factor (K_w) which is the product of the winding distribution factor (K_d), pitch factor (K_p) and the skewing factor (K_s).

Distribution factor - K_d

If all the coils of one phase per pole are allotted into one slot, it is considered as a concentrated winding where the total back EMF is the arithmetic sum of the back EMFs of all coils under one phase per pole. But to get a more sinusoidal flux distribution, the coils of per pole per phase can be distributed to more than one slot and hence is called a distributed winding. And hence the total back EMF is the vector sum of induced EMF per coil[17]. Due to this, the total back EMF by the distribution of the winding is reduced as compared to the concentrated winding, and the reduction of back EMF is given by a factor called Winding distribution factor (K_d). The fundamental component of the distribution factor (K_{d1}) is given by

$$K_{d1} = \frac{\sin\left(\frac{\pi}{2m}\right)}{q\sin\left(\frac{\pi}{2mq}\right)} \tag{2.28}$$

where m is the number of phases. For three-phase machines K_{d1} can be reduced to

$$K_{d1} = \frac{1}{2q\sin\left(\frac{\pi/6}{q}\right)} \tag{2.29}$$

Pitch factor - K_p

Pole pitch (y_Q) of a machine is defined by the number of slots per pole given by

$$y_Q = \frac{Q_s}{P} \tag{2.30}$$

In a full pitch winding the coil ends are separated exactly by one pole pitch slots or 180^o electrical angle. However, in short pitching is the pitch between the coil ends less than a full pitch or the angle is less than 180^o[17]. Short pitching of coils is one of the many ways of reducing the amount of copper used in the winding and also when done correctly can enhance the sinusoidal current linkage. On the downside short -pitching reduces the flux linkage and hence more turns of coils is required to get the same back EMF as a full pitched coil[17]. This can be quantified in terms of pitch factor (K_p) whose fundamental component is given by

$$K_{p1} = \sin\left(\frac{y}{y_Q}\frac{\pi}{2}\right) \tag{2.31}$$

where y represents the pitch expressed in the number of slots and the ratio (y/y_Q) the relative shortening.

So, the winding factor K_w expressed in terms of the fundamental components of the distribution and pitch factor is

$$K_{w1} = K_{d1}K_{p1} \tag{2.32}$$

Given the required base speed (w_b) of the machine and the operating DC bus voltage (U_{dc}), the number of turns per phase(N_s) can be calculated as

$$N_s = \frac{\sqrt{2}U_{ph,rms}}{w_b K_{w1} L_{stack} \tau_p B_{av}} \tag{2.33}$$

where $U_{ph,rms}$ is $U_{dc}/\sqrt{6}$ and B_{av} is $\frac{2}{\pi}B_{\delta}$.

To reduce the thickness of the wire used, the current path is generally split up into a number of parallel paths (a), such that the ratio of number of poles (P) and number of parallel paths (a) is an integer [18]. The number of conductors in a slot is given by

$$z_Q = \frac{6aN_s}{Q_s} \tag{2.34}$$

If z_Q is a fraction, it is rounded off to the next integer and the new value for the number of turns is calculated by

$$N_{s,new} = \frac{z_Q Q_s}{6a} \tag{2.35}$$

2.6.4 Slot and teeth dimensions

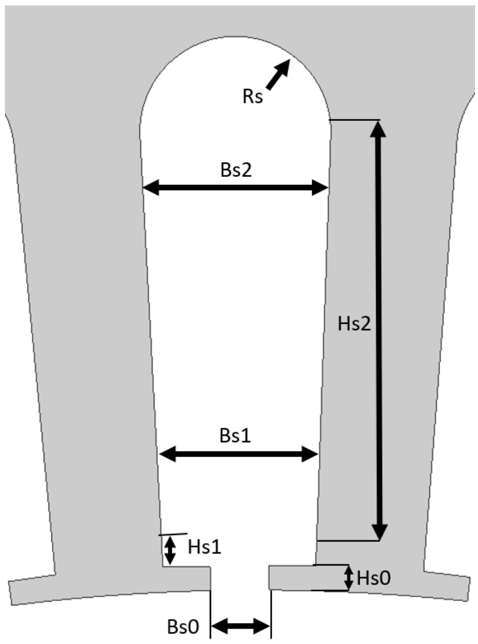

Figure 2.7: Parameters for slot design

The slot and the teeth dimensions of a machine is highly related to the maximum amount of current and the current density allowed due to thermal constraints. For a given maximum power of the machine, the RMS value of the phase current at peak power is given by

$$I_{s,ph} = \frac{P_{max}}{3\phi\rho U_{ph,rms}} \tag{2.36}$$

where ϕ and ρ are the assumed power-factor and efficiency respectively. Assuming an RMS current density of J_{rms}, the total conductor area(A_{cond}) is calculated as

$$A_{cond} = \frac{I_{s,ph}}{aJ_{rms}} \tag{2.37}$$

As we cannot utilize the entire slot area to fill with copper, a parameter called fill factor(K_{cu}) is introduced, which is the ratio of slot area to the copper area. Fill factor is generally between 0.4-0.5 [17]. From this, the slot area(A_{slot}) can be calculated as

$$A_{slot} = \frac{A_{cond}}{K_{cu}} \tag{2.38}$$

Generally, the conductors are split into a number of strands that carry the current parallelly and this also makes it easier to wind the machine. The actual current density of the machine after the above design procedure is given by

$$J_{rms,act} = \frac{I_{s,ph}}{aN_{strands}A_{strand}} \tag{2.39}$$

where a is the number of parallel paths, $N_{strands}$ is the number of strands and A_{strand} is the copper area in each strand.

An initial value of the tooth width(T_{width}) can be calculated by[17],

$$T_{width} = \frac{\tau_s B_\delta}{K_{fe} B_t} \tag{2.40}$$

where τ_s is the slot pitch ($\pi D_{is}/Q_s$), K_{fe} is the iron factor($\approx$ 0.97-0.98)[17], and B_t is the maximum allowable flux density in the teeth ($\approx$ 1.8 T - 2T) [17].

Slot dimensions can be obtained from the area of the slot and also by treating the slot as a trapezoid. Hence, area of the slot can be expressed as,

$$A_{slot} = \frac{B_{s1} + B_{s2}}{2} H_{s2} \tag{2.41}$$

where B_{s1},B_{s2} and h_{slot} are as shown in the figure. Also for ease of manufacturing, a slot opening of 2.5 mm is considered. Assuming B_{s1} as $1.25(\tau_s - T_{width})$ and the ratio of $B_{s2}/B_{s1} \approx 1.2 - 1.4$, the initial height of slot(H_{s2}) can be calculated[17].

2.6.5 Core depth and outer dimensions

The stator core depth is the thickness of back iron in the stator required to facilitate the flux distribution. It can be calculated as[17],

$$T_{stator} = \frac{D_{is} B_\delta}{P K_{lamination} B_{core}} \tag{2.42}$$

where D_{is} is the inner stator diameter, P is the number of poles, $K_{lamination}$ is the lamination factor ($\approx$ 0.97 - 0.98) and B_{core} is the maximum allowable flux density is the stator/rotor core ($\approx$ 1.5 - 1.6 T). A similar approach can be used to find the thickness of the rotor core.

Finally, the outer diameter of the stator is found to be,

$$D_{os} = D_{is} + 2(H_{s2} + T_{stator} + H_{s0}) \tag{2.43}$$

where h_{s0} is as shown in the figure.

2.6.6 Initial Magnet dimensions

Magnet sizing of interior permanent machines is very difficult by just using the analytical approach due to the varied configurations of magnet placement and also the non-linearity of the magnet circuit. Hence, an initial estimate of the magnet is found using an analytical approach and then the final values are obtained using finite-element analysis. Analytical sizing for two different magnet configurations are dealt with here, namely, the flat similar to Fig. 2.2 and the single layer V shape magnet design. Flat magnet design is one of the most simple interior permanent magnet machine designs, where the magnets are just embedded inside the rotor structure rather than on the surface of the rotor. With the magnets embedded inside, we can take advantage of the reluctance torque due to the variation in the reluctance along the direct and quadrature axis of the rotor. One of the essential parameters required for the initial magnet sizing is the effective air-gap length of the machine due to the presence of the slots. Effective air-gap length can be calculated by using the carter coefficient for scaling the air-gap length [18]. Carter coefficient (K_{carter}) is given by

$$K_{carter} = \frac{\tau_s}{\tau_s - b_0 + \frac{4g}{\pi}\ln\left[1 + \frac{\pi}{4}\frac{b_0}{\delta}\right]} \tag{2.44}$$

where τ_s is the slot pitch, b_0 is the slot opening and δ is the air-gap length. The effective air-gap length (δ_{eff}) is given by

$$\delta_{eff} = K_{carter}\delta \tag{2.45}$$

The initial magnet thickness can be assumed to be $\approx$(3 - 4.5)δ_{eff} [18] and the width of the bridge (W_{bridge}) can be assumed to be 2 - 2.5 mm based on the mechanical rigidity constraints. An important parameter for the calculation of the width of the magnet is the pole-arc to pole-pitch ratio (γ).[19] states a value of 0.68 for the pole-arc to pole-pitch ratio for reduced cogging torque and hence the value of 0.68 is used here. The width of the magnet is then given by [20],

$$W_{magnet} = 2\left(\frac{D_{or}}{2} - W_{bridge}\right)\sin\left(\frac{\gamma\pi}{P}\right) \tag{2.46}$$

A similar approach can be adopted for the V- shape magnet design. In addition to the magnet thickness and magnet width, the magnet angle is an important factor in the design process. There are no analytical optimum solutions for magnet angle and hence a parametric sweep of the angle is required to compare the requirements to the obtained solution. A detailed mechanical design based on magnet thickness, width and angle can be found in [21].

2.7 Finite Element Method

Finite element analysis (FEA) is a numerical method of computation where in complex geometries and non-linear material properties are involved. In FEA, the geometry is broken down into a large number of smaller finite elements. The smaller finite elements are connected to each other by nodes and the field equations are applied to each of the elements and boundary conditions are used to solve for the entire geometry. The non-linear magnetic fields within the electric machines and their relation to the sources are described using Maxwell's equations. The differential form of Maxwell's equations are,

$$\vec{\nabla} \cdot \vec{B} = 0 \tag{2.47}$$

$$\vec{\nabla} \times \vec{H} = J \tag{2.48}$$

$$\vec{\nabla} \times \vec{E} = -\frac{\partial \vec{B}}{\partial t} \tag{2.49}$$

(2.47) indicates that the there is no source present. (2.48) describes the interaction of the magnetic field intensity(H) with the electric current density (J).(2.49) presents the induction of an electric field (E) due to a time varying magnetic flux density (B).

Two hypothetical quantities called magnetic vector potential ($\vec{A}$) and electric scalar potential(Φ) are used to simply the electromagnetic problem [22] at hand and they are related by

$$\vec{B} = \vec{\nabla} \times \vec{A} \tag{2.50}$$

$$\vec{E} + \frac{\partial \vec{A}}{\partial t} = -\vec{\nabla}\Phi \tag{2.51}$$

Equations (2.50), (2.51) coupled with equations (2.47), (2.48) and (2.49) is used to calculate the electromagnetic quantities in a FEA simulation tool.

The torque generated by a machine is also calculated in a FEA tool with the help of Maxwell's stress tensor[22]. According to this, the magnetic field strength between two bodies create a stress (σ_F) on the object surfaces given by

$$\sigma_F = \frac{1}{2}\mu_o H^2 \tag{2.52}$$

This can be further decomposed into radial and tangential components, where in the tangential component($\sigma_{F,tan}$) is of greatest interest for torque production and given by

$$\sigma_{F,tan} = \mu_o H_n H_{tan} \tag{2.53}$$

The total torque (T) produced can be calculated by integrating the stress tensor over a cylinder Γ that confines the total rotor. The torque expression is given by

$$T = \frac{L_{stack}}{\mu_o} \int_{\Gamma} \vec{r} \times (\vec{B} \cdot \vec{n})\vec{B} dS - \frac{B^2 \vec{n}}{2}) d\Gamma \tag{2.54}$$

Variants of the tangential stress tensor expression are also used for calculation of torque in different software tools.

3

Drive cycle Analysis

3.1 Data Extraction

The database [6] used for this thesis consists of over 230 million rows of data. This is stored in an online database management system and can be accessed by a programming language called MySQL. Handling of the massive database has been made easy with the use of Structured Query Language (SQL), through which it is possible to sort information into various categories and also to extract the categorized data to a local computer. The database provides numerous parameters, but the main goal has been to extract speed over time and sort these after individual cars and trips.

3.2 The validity of the data

Over 110 000 individual trips spread across 500 individual cars have been analyzed and used in this thesis. We believe that this amount of data gives a good representation of driving patterns and validate the conclusions made in this thesis. But since the data is collected mostly around Gothenburg city, the data might be biased towards city driving.

3.3 Characterization of driving trips

One of the main goals of this thesis is to investigate the possibility of finding different patterns in the database of drive cycles. Several authors have done various investigations on the basis of categorization [9] [1] and have broadly come up with three main categories namely Urban, Rural and Highway driving. These drive styles result in the operation of the electric machine at different torque-speed operating points. The procedure followed to categorize the trips into the aforementioned categories is explained below.

3.3.1 Trip Characterization

Each device has a number of trips. The variation of trip duration is very wide, from a couple of minutes to a couple of hours. Every trip, as mentioned before, is characterized as either Urban, Rural or Highway. The conditions for the characterization can be found in table 3.1.

Table 3.1: Trip Characterization

Trip characterization terms			
	<60km/h	60-90km/h	>90km/h
Urban	>60% of time	<30% of time	<5% of time
Rural	30% of time	>60% of time	<15%of time
Highway	-	-	>60% of time

3.4 Vehicle model

A car manufacturer often has a wide span of different car models in their product portfolio. These models range from small sedans to large Sport Utility Vehicles(SUV), and this leads to varied properties such as weight, drag coefficient, cross-sectional area and wheel diameter. Today when buying a new car it is often possible to choose between different combustion engines. The picks that are available are selected by the manufacturer that they consider suitable for the car. It is also possible to choose a combustion engine based on the performance level required and the usage behavior of the customer. A similar case can also be argued for electric vehicles where in the customer can choose a certain powertrain based on his need of performance and efficiency. With this in consideration, two different car models are picked to be analyzed in this thesis. To get as wide span as possible, Volvo's heaviest and largest car XC90 and Volvo's currently smallest and lightest car, S60 are picked. The data for these cars can be found in Table 3.2 [7] [8]. The weight of the cars mentioned is the maximum permissible weight as given by the manufacturer.

Table 3.2: Vehicle parameters

Vehicle parameters		
Parameter	XC90	S60
Total weight (kg)	3010 kg	2282 kg
Drag coefficient (C_d)	0.32	0.28
Rolling resistance (C_r)	0.2	0.2
Cross sectional area (m^2)	2.82 m^2	2.28 m^2
Wheel diameter (m)	0.5m	0.5m

3.4.1 Simulink model

A vehicle model is a simplified representation of the forces acting on the vehicle during its motion. In this thesis, the vehicle model is used to extract the electric machine requirements so that it can largely satisfy the speed and torque demands offered by all the trips of the database. The vehicle is modeled with help of the QSS toolbox library[add source] in MATLAB/Simulink environment. QSS library provides the building blocks of a powertrain such as the drive cycles, vehicle model which takes into account the forces described in section 2.3, transmission model, energy converter(electric machine or ICE) and finally a source of energy(petrol, diesel or battery). For the conversion of driving cycle to electric machine torque and speed, vehicle and transmission models are used and instead of using the built-in drive cycles, the car model is fed with the database specified drive cycles. as shown in figure 3.1.

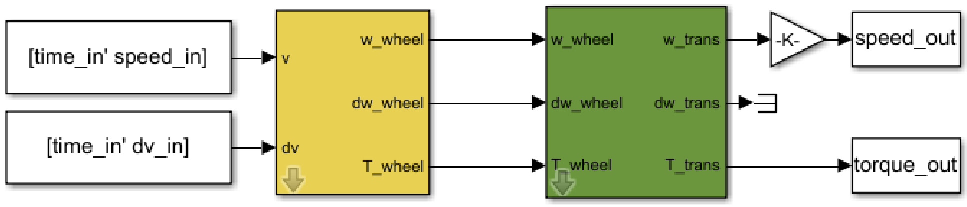

Figure 3.1: Vehicle dynamics model

The car model is also fed with the data of XC90 or S60 vehicle parameters to get the corresponding operating regions. The result of the simulation is then collected as operating points(torque vs speed) that the designed machines have to meet.

3.4.2 The selection of gear ratio and its impact

The selection of the car's gear ratio has a high impact on the operating torque and speed limits of the machine. Comparing with ICE torque-speed characteristics, where a multi-stage gearbox is necessary to be able to satisfy the demands of the driving. Electric machines however have a different torque-speed profile where they can produce maximum torque from very low speeds. This in combination with the possibility of reaching high speeds often results in a simplified gearbox design often having one fixed gear ratio.

This gear ratio is an important parameter as this determines the maximum torque and speed limits the electric machine has to operate at.

Mechanical output power of a electric machine (P_m) is defined as

$$P_m = \tau\omega \tag{3.1}$$

where τ is the torque measured at machine shaft and ω is the speed of the machine.

Wheel power P_{wheel} is defined as

$$P_{wheel} = \omega_{wheel} T_{wheel} \tag{3.2}$$

where ω_{wheel} is wheel shaft speed and T_{wheel} is wheel shaft torque defined by $F_{tractive} \times Radius_{wheel}$. If we assume no losses, $P_{wheel} = P_m$ then

$$\omega_{wheel} = \frac{\omega_{machine}}{N_{gear}} \tag{3.3}$$

$$T_{wheel} = \tau N_{gear} \tag{3.4}$$

For the same power output P_{wheel}, as seen from (3.3) and (3.4) a high gear ratio will result in a high-speed machine with a lower peak torque and a higher base speed and similarly a low gear ratio will result in a slower spinning machine and lower base speed, but the ability to develop higher torque. To have a starting value for the design, the gear ratio is picked to be 10 as it is close to the famous electric car manufacturer Tesla(9.73) [23]. A gearbox efficiency of 98 % is assumed in all cases.

3.5 Determination of machine operating points from drive cycle data

Each trip in the database is a representation of the vehicle motion in terms of speed vs time. This data is combined with the vehicle model described above to obtain the operating torque and speed values of the electric machine for each time step. The car model converts the speed vs time data into the total tractive force needed to meet the drive cycle at that time instance. With help of the car model's gear ratio and wheel diameter, it also defines the machine speed and torque that is required to meet the car velocity and acceleration. An example of this can be seen in figure 3.2.

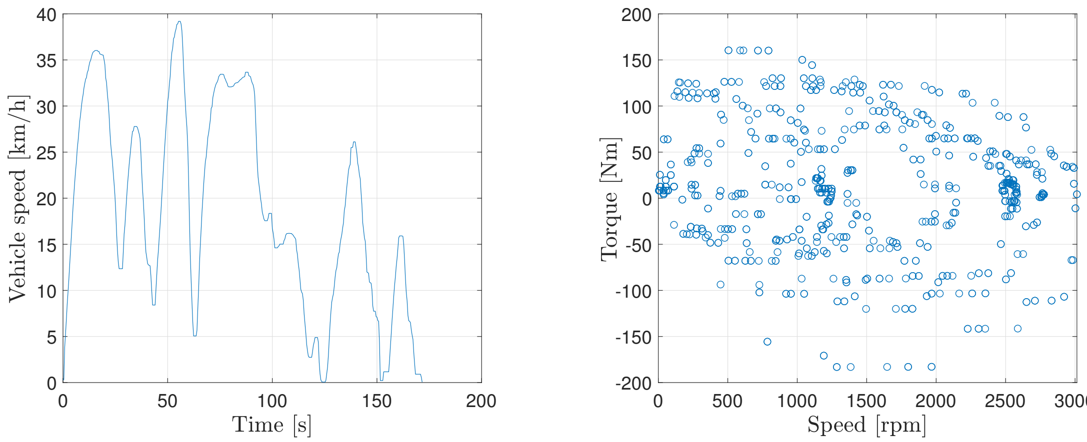

(a) **(b)**

Figure 3.2: Figure a) showing an Urban drive cycle. Figure b) showing corresponding electric machine operating points.

3.5.1 The differences between the Urban, Rural and Highway

As stated before, each trip in the database is categorized as either Urban, Rural or Highway in terms of table 3.1. Three investigations carried on the categorized data are,

1. Most common operating regions of each category

2. Relative positive acceleration (RPA) of each category
3. Energy consumption per driven km.

The most common operating regions of each category are found by dividing the torque-speed map into bins of equal sizes and then counting the number of occurrences of each operating point in those bins. The result of this can be found in figure 3.3 and 3.4. The figures are showing data for the XC90 vehicle. The color bar shows percentage of the largest bin value. It is seen from the plots that for the Urban category the most common operating points are close to 0. It is also seen that the most common operating points for Highway corresponds to 117 km/h, which makes sense as the Highway speed limit in Sweden is between 110-120 km/h. Sub figure 3.4b illustrates the operating points of all the trips irrespective of the category. It can be seen that operating points close to 0 are still the most common operating points.

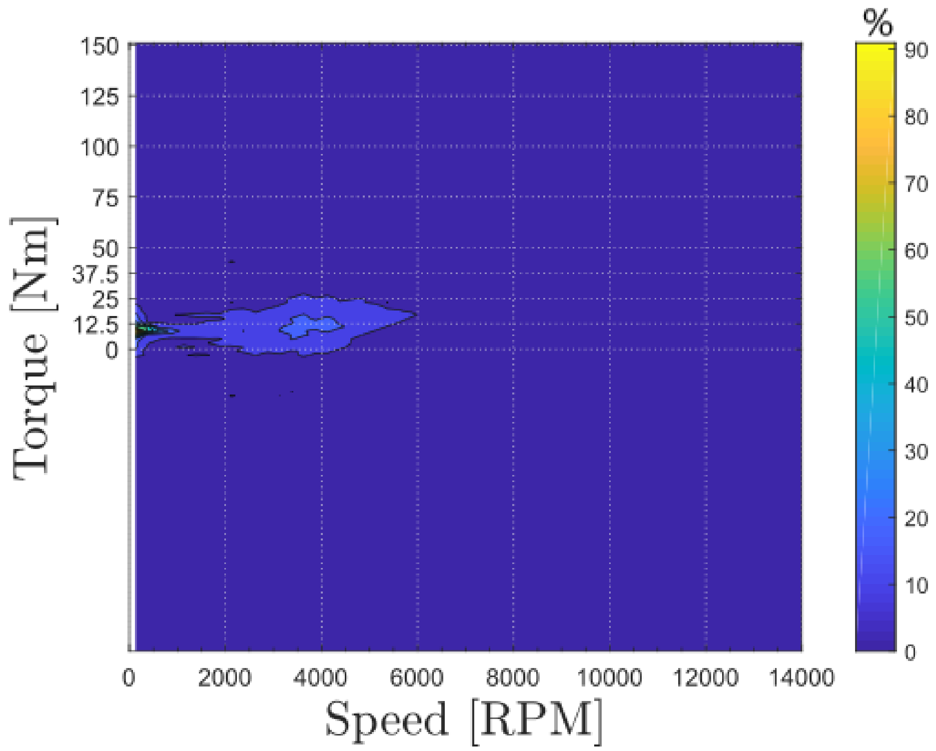

(a) All Urban trips most common operating points.

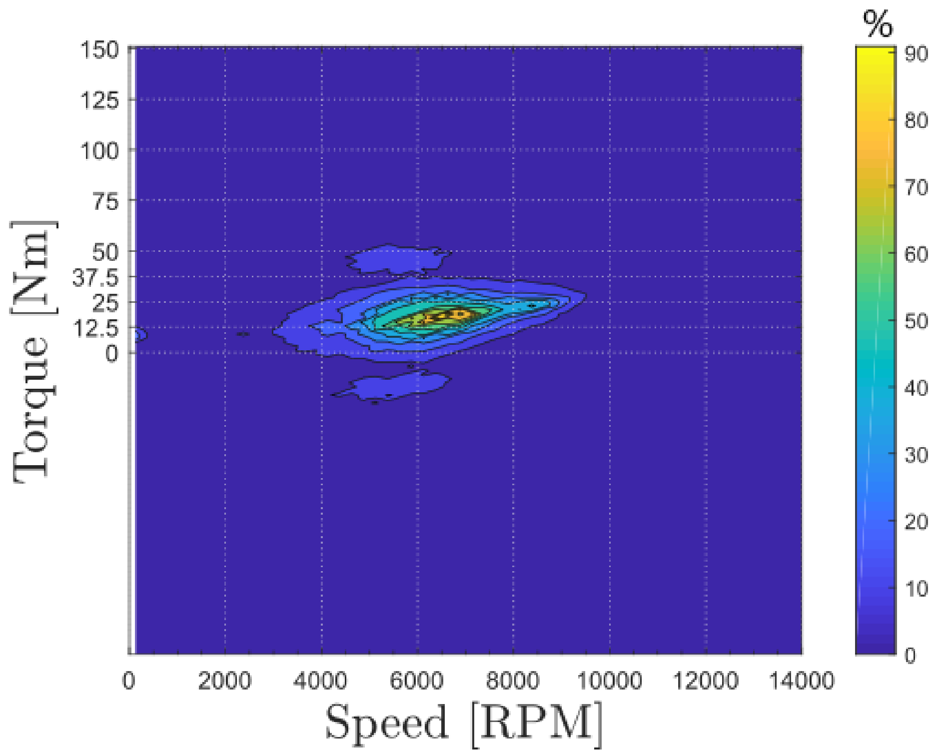

(b) All Rural trips most common operating points.

Figure 3.3: Most common operating points

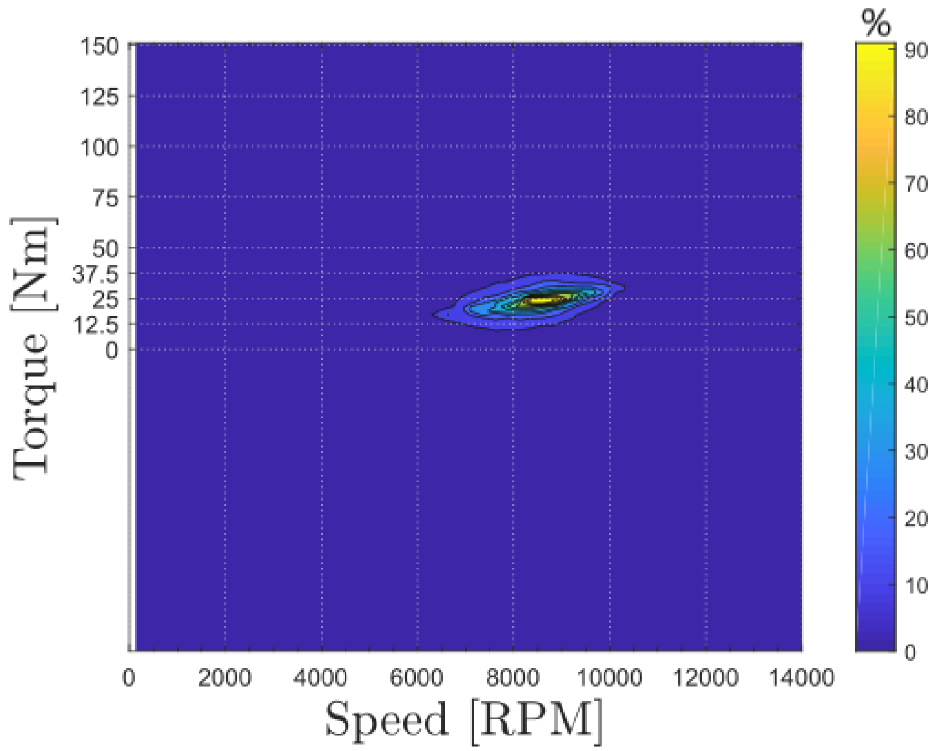

(a) All Highway trips most common operating points.

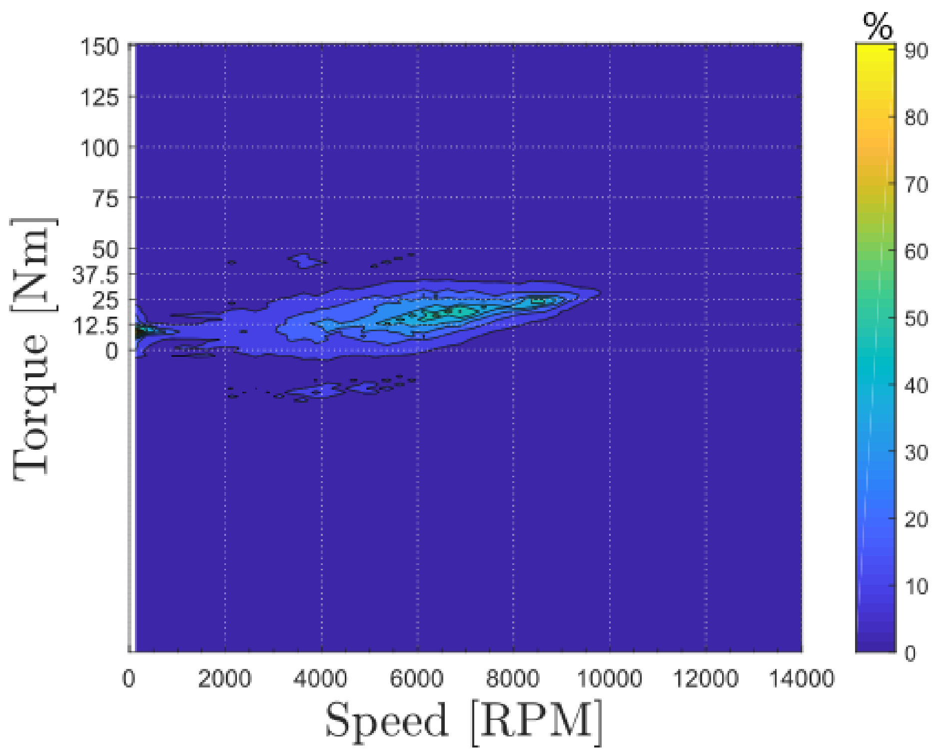

(b) The whole database most common operating points.

Figure 3.4: Most common operating points

Secondly, a trip can be given an RPA value. RPA is and indication of accelerations with high power. The RPA value decreases with lower power accelerations [24]. The RPA is defined as the distance driven with positive acceleration divided by total distance travelled in the trip and given by,

$$RPA = \frac{\int speed(t)\ positive\ acceleration(t)\ dt}{\int speed(t)\ dt = total\ driven\ distance} \tag{3.5}$$

Since analyzing all trips of the database will generate a huge number of data points which cannot be properly presented, a random subset of the database is chosen. For the trips selected, RPA value along with the mean speed of the trip is calculated. This is then repeated for Urban, Rural and Highway categorised trips. The result of this can be seen in figure 3.5. As can be seen, the Urban trips do generally have higher RPA values followed by Rural and last Highway. This indicates that Urban cycles are generally exposed to accelerations with high power. This may be a factor that needs to be taken into consideration when it comes to thermal properties of an electric machine since high power demands result in increased machine temperatures.

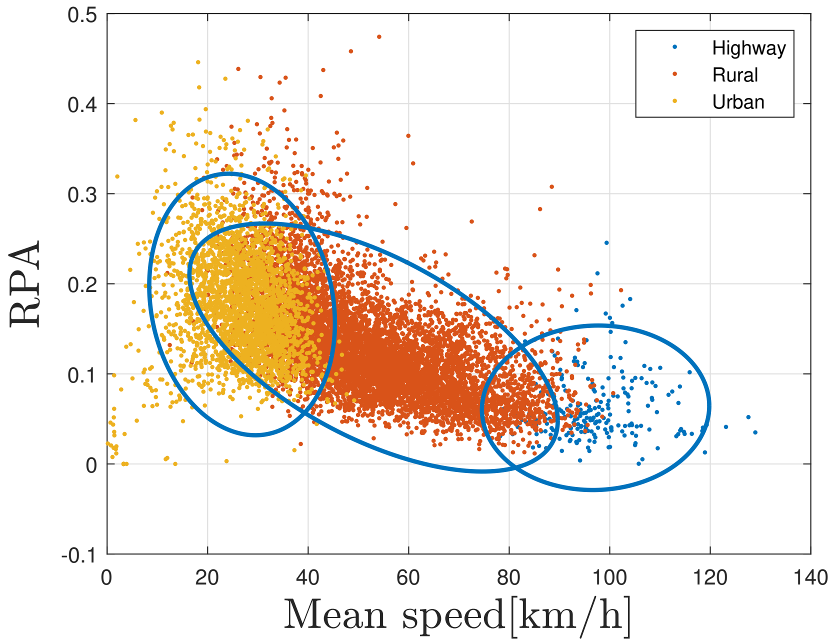

Figure 3.5: RPA values for approximately 6000 trips. Blue circles encloses 95% of each category of data points.

3.5.2 Energy Consummation per driven distance

To further investigate how Urban, Rural and Highway driving differs, their energy consumption per kilometer of driving is calculated. As presented in Fig. 3.6 the energy consumed per km for all three driving categories follow the road load. Here, the road load corresponds to the least amount of force needed to overcome the wind and rolling resistance while driving at a constant speed. Higher energy consumption at the same speed is caused due to the accelerations in the trip. From Fig. 3.5 and Fig. 3.6, we can see that the Urban and Rural cycles diverge more from the road load than the Highway cycles. This indicates that these cycles have more accelerations than the Highway cycles as is also confirmed by the RPA analysis. For this calculation, an efficiency of 70 % is assumed for regenerative braking and an efficiency of 80 % for the energy conversion from the battery to the wheels. It should be noted that the points that lies underneath the road load might represent corrupted data which were not removed during data filtering process.

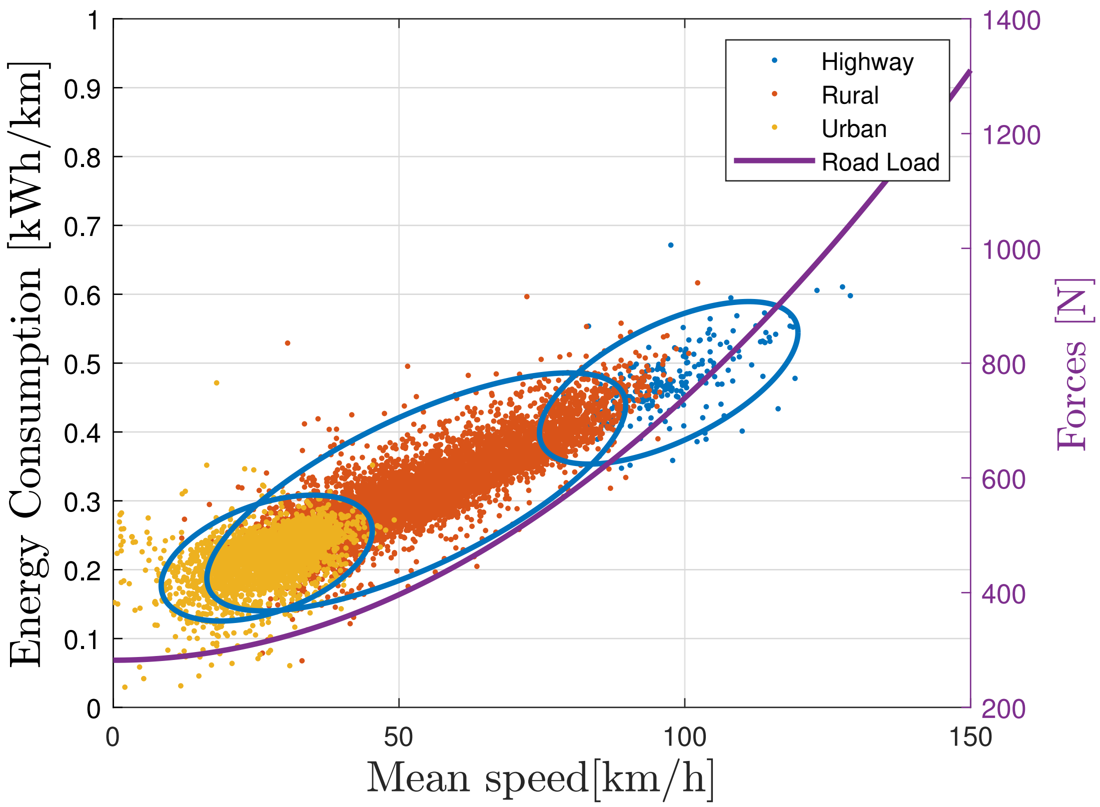

Figure 3.6: Energy consumption of about 6000 trips against the road load.

3.5.3 Device Characterisation

Database is a collection of around 700 cars which are named as devices. These individual cars has been fitted with GPS equipment that logs speed and position while the car is being driven. Each device has a number of trips that has been recorded with the GPS device. The number of trips a device has spanned from just three up to several hundred. To investigate how a car has been driven, all its trips are characterized as either Urban, Rural or Highway according to table 3.1. The outcome can, for example, be that a device has 50% Urban trips and 50 % Highway trips. However, since a trip can be very short, a device that looks like it does Urban trips as often as Highway trips can be miss characterized when it comes to the amount of time spent on the road. By also taking time into consideration for each trip, a different understanding of how a person drives can be developed. Now a device can be characterized in how many "Highway hours" or "Urban Hours" it has. The result can be seen in figure 3.7. As can be seen, do the Urban cycles represent the majority of the trips in the database. However when taking time into consideration Rural and Highway do take up more of the total. This indicates that Urban trips are usually shorter than Rural and Highway trips.

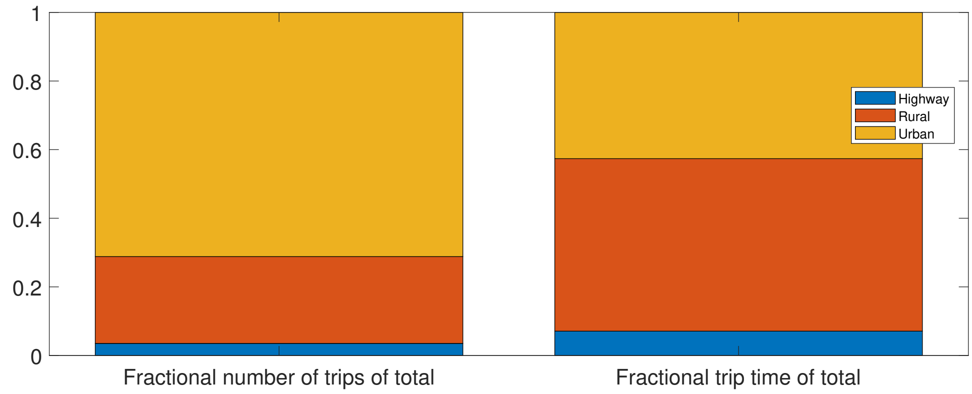

Figure 3.7: Comparison between number of trips and amount of trip time

3.5.4 Are you a city driver or a highway driver?

The initial thought in this thesis was to investigate the possibility that a device can be divided into different categories in terms of Highway, Rural or Urban. Fig. 3.8 presents the fractional time spent by each car in Urban, Rural and Highway cycles and each car is given a number between 1 and 500. From this, we can see that most of the drivers do not drive any particular category of driving but drive in a mixed manner. However, it can be noticed that a less than 50 % of drivers do not do any highway driving.Hence, a new approach should be taken to understand and use the data to meet the driving style of most of the population.

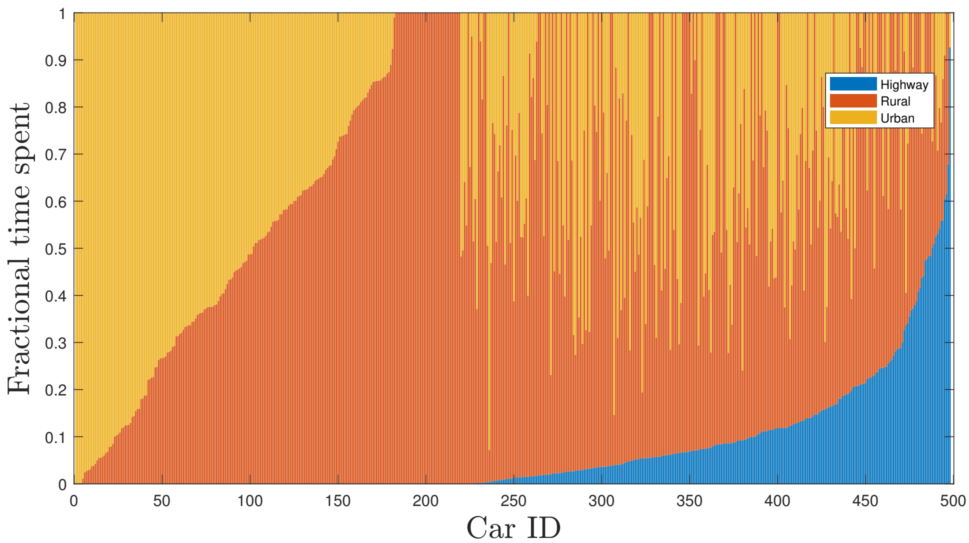

Figure 3.8: Each cars fractional time spend on the different drive categories

3.5.5 Where is most energy consumed?

From the previous sections, it is evident that most common operating points are close to zero. However, these points correspond very low power. This means that a car spends 90 % of its time at this low power regions and 10 % of its time at high power regions. Even though the amount of time spent in high power regions is less, the energy consumed is the highest hence in these regions the electric machine should be efficient. The energy consumption is calculated by taking a trip's operating points, which is torque τ and a speed ω. The power at each point can be determined as $P = \tau\omega$. Energy is then $E = Pt$ where t corresponds to counted points at a certain torque speed point i.e time. This is done iteratively for all Urban, Rural and Highway cycles as well for the population as a whole. The result can be seen in Fig. 3.9 - 3.10. The figures are showing data for the XC90 vehicle.

From Fig. 3.9 - 3.10, it can be observed that for Urban and Rural cycles the most common energy point, or where most energy is burnt is not the same as the most common operating points. If a car only did either only Urban, Rural or Highway cycles, these regions would be good regions to have high electric machine efficiency. It has to be noted that the negative energy points, indicates regenerative braking. It can also be seen that this is more present at Urban cycles than in Highway cycles. The overall energy usage shown in Fig. 3.10b where all the populations highest energy is plotted, would be a good region to have high electric machine efficiency so as to meet the population as a whole. The color bar in the plots is represented in percentage. For example, the deep yellow region indicates that all torque-speed points within this contour are have an energy consumption of at least 80 percent of the highest energy operating point. The negative values in the color bar correspond to negative torques and hence negative energy.

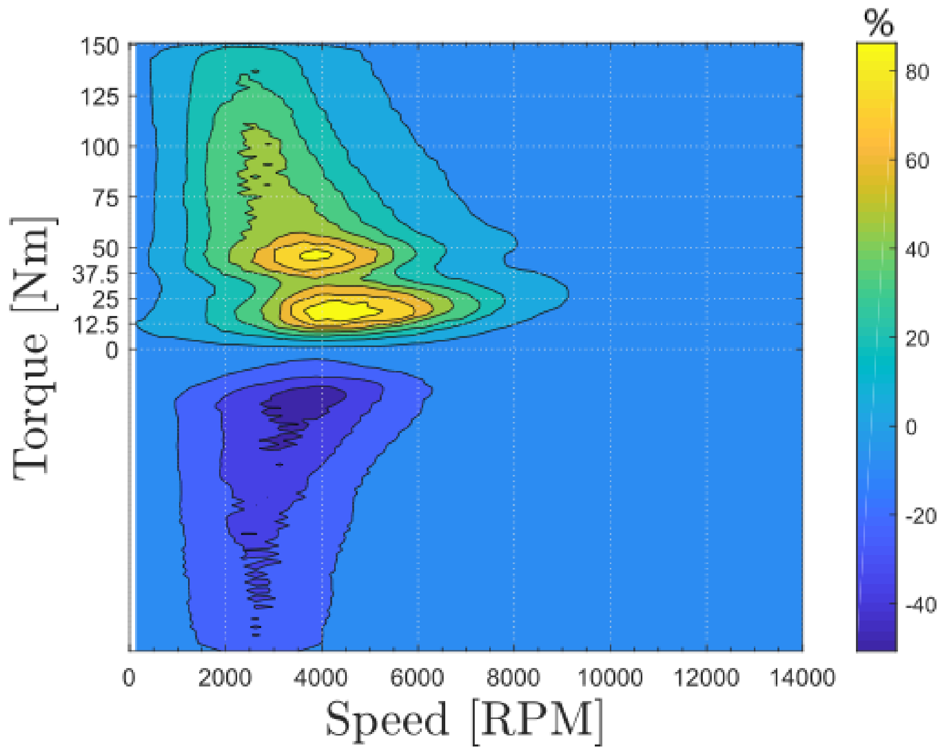

(a) Highest energy demand points for urban trips

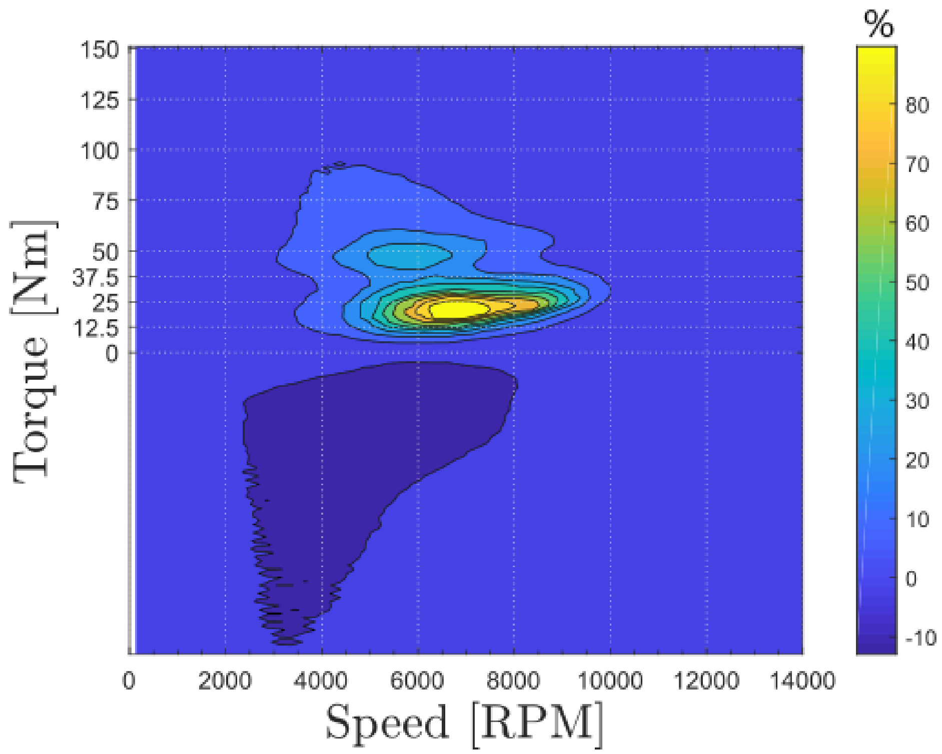

(b) Highest energy demand points for rural trips

Figure 3.9: Highest energy demanding operating points

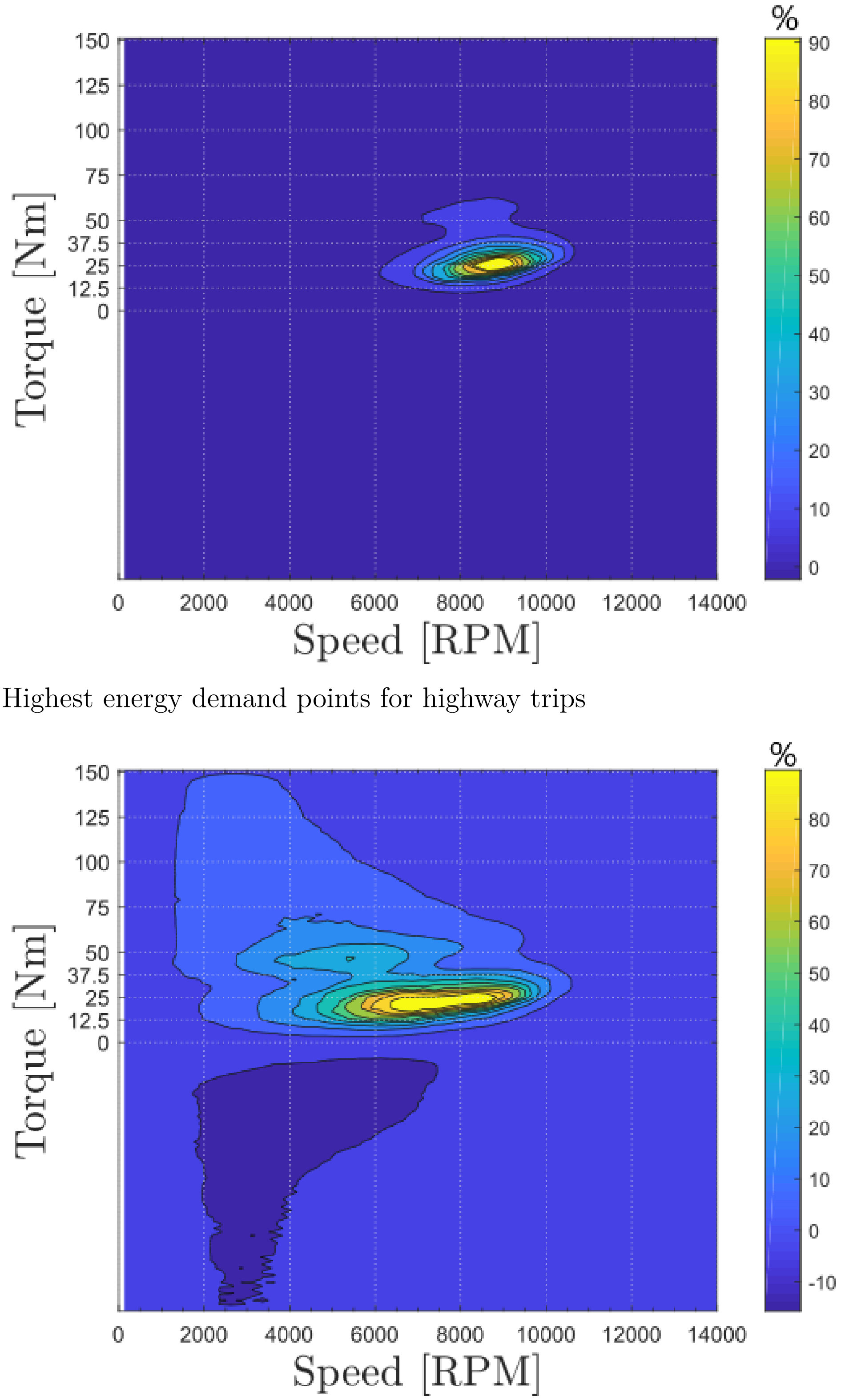

(a) Highest energy demand points for highway trips

(b) Highest energy demand points for all trips

Figure 3.10: Highest energy demanding operating points

To further narrow down the operating points at which most energy is utilized, another method is developed. Since most cars have mixed driving types, it is interesting to observe the operating point at which most of the energy is consumed by each car. The maximum energy point for each car is presented in Fig. 3.11a. This data is then clustered with the help of K-mean clustering algorithm [25] into two groups with corresponding centroids C1 and C2 as seen in Fig. 3.11b. Hence, the objective is to have high efficiency of the electric machines at these centroids, as it would meet the needs of most of the people. It can also be seen that the centroids correspond well to the highest energy points in figure 3.10b were the populations highest energy point as a whole is plotted.

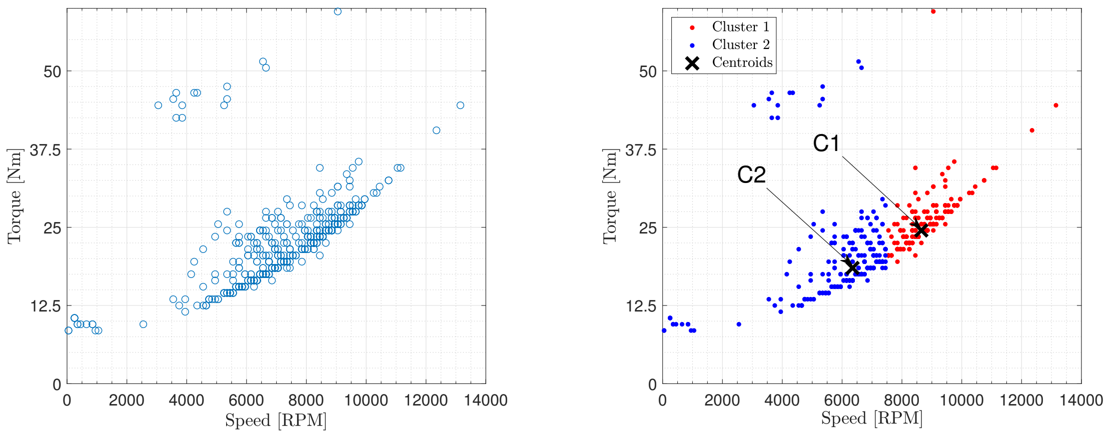

(a) Urban **(b)** Rural

Figure 3.11: Figure 3.11a showing all cars highest demand energy point. Figure 3.11b showing all cars highest demand energy points in two clusters with corresponding centroids.

By using this method for both the XC90 and the S60 vehicles, two sets of operating points are found out. These will be used to compare efficiencies for the machine designs. The points for XC90 and S60 vehicle can be found in Table 3.3.

Table 3.3: Energy centroids

Highest energy centroids		
Parameter	XC90 Machine	S60 Machine
Torque C2	18.5 Nm	13.5 Nm
Speed C2	6360 RPM	6350 RPM
Torque C1	24.5 Nm	18.5 Nm
Speed C1	8350 RPM	8350 RPM

3.5.6 Specifying machine parameters

Electric machine design for automotive propulsion is mainly derived by the parameters of the machine such as maximum torque and speed. In this thesis, drive cycle analysis data is used to decide the requirements for the machines. Considering all the trip requirements in the database leads to an over-dimensioned electric machine which do not satisfy the volume constraints in a typical electric car. If instead,5% of the most demanding trips are discarded, the resulting machine requirements offers poor performance. Hence a new approach to obtain the machine requirements is discussed. First, all trips are analyzed individually. Then each trip's highest torque, highest machine speed and highest machine power points along with corresponding toque and speed points are aggregated. This results in over 330 000 top torque, top speed and top power operating points and can be seen in Fig. 3.12

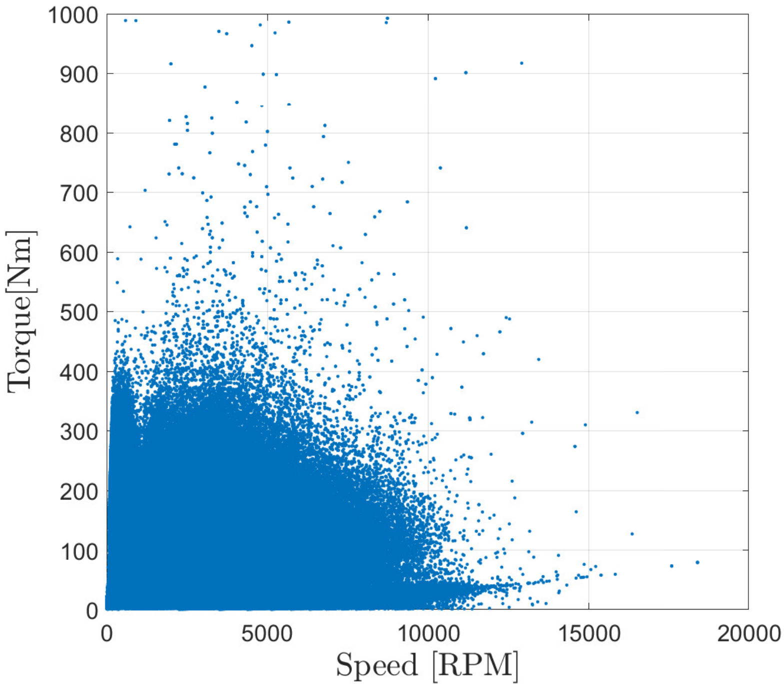

Figure 3.12: Maximum torque, power and speed points from all the trips.

However, as can be seen from figure 3.12 the spread of the points are very large. Some of the points can even be questioned if they are to be trusted or not since they correspond to very high power. To design a machine that will meet all these points will result in a very oversized machine. The goal would be to design an electric machine that will be sufficient enough to meet most of the population. The process for this starts with the required top torque. The maximum torque points are sorted and some percentage of the highest torques are discarded. The first approach that was used was to discard 5 % of the top torques. The result is a top torque of 230 Nm for the XC90. Even though meeting 95 % of maximum torque seems reasonable, the performance from a 230 Nm machine for an XC90 is very poor and also due to the huge amount of data, 5 % of data represents thousands of trips taken by customers. Increase in the torque demand due hill climbing should also be considered. [9] state that at torque demands for 90 km/h at 6 % gradient and 25 % hill gradient at standstill should be met for a city car. By comparing the time taken to perform 0-100 km/h which is a measure of performance and considering the database analysis, the maximum torque of XC90 machine is found to be 400 Nm and 300 Nm of torque. This represents 99.6 % of all the maximum torques in the database. These torque also meeting the torque demands due to gradients. This is presented in Fig. 3.12. With the recent decision by Volvo Cars to limit the speed of its cars to 180 km/h, the maximum speed of the electric machines is taken as 14000 RPM with a gear ratio of 8 . With this in mind, all operating points that correspond to speeds above this are discarded. The remaining points can be seen in Fig. 3.13.

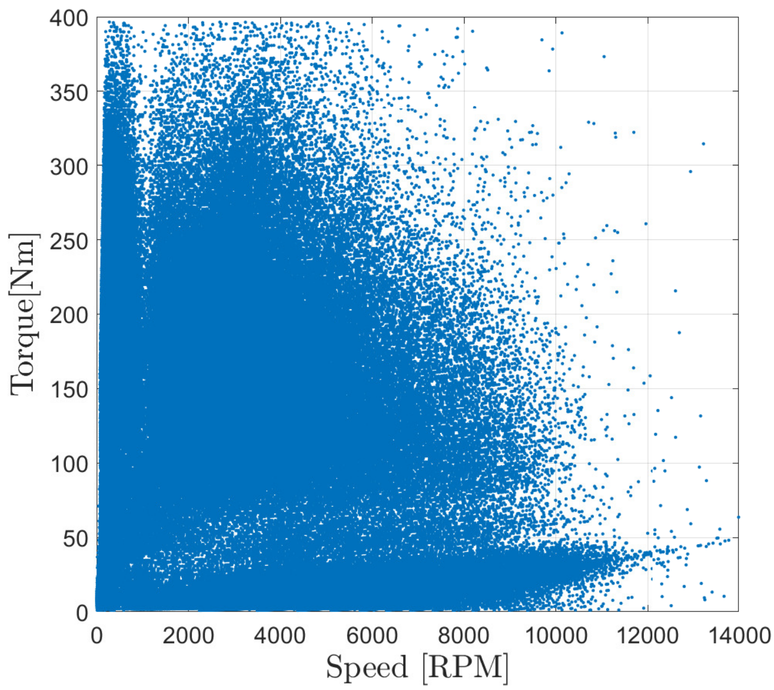

Figure 3.13: 0.4% of the maximum torques removed.

As can be seen from Fig. 3.13, there still exist some points that correspond to very high power. The next step is therefore to discard some of the high power points. This is done by discarding 1 % of the highest powers. The result, can be seen in Fig. 6.1a and this represents the torque-speed envelope that specifies the requirements of the electric machine. The same procedure is repeated for the S60 car. Both the requirements are presented in Fig. 6.1b and is summarized in Table 3.4.

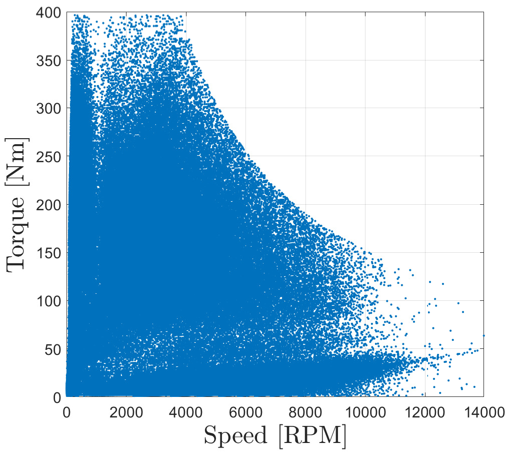

(a) Urban

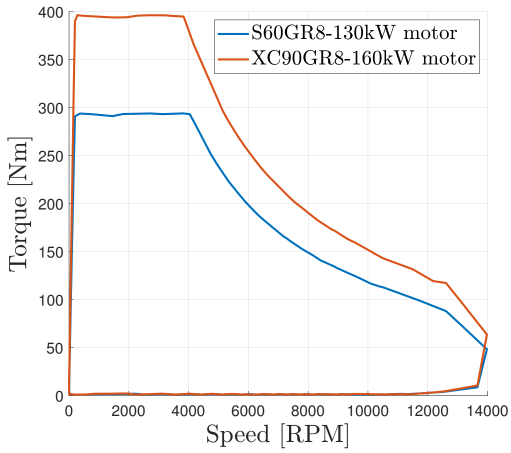

(b) Rural

Figure 3.14: Figure 6.1a showing the modified points for XC90. Figure 6.1b showing the generated torque speed map for both cars.

Table 3.4: Electric machine requirements

Electric machine requirements		
Parameter	XC90 Machine	S60 Machine
Maximum torque	400 Nm	300 Nm
Maximum speed	14000 RPM	14000 RPM
Maximum power	160 kW	130 kW
Base Speed	3800 RPM	4200 RPM

3.6 Summary

In this chapter different methods adopted to analyze the real-world driving cycles and using it to arrive at the requirements for electric machine design was discussed. The requirements in terms of maximum torque and speed of the electric machine and also regions of interest in the torque-speed map were established. The real-world driving cycles were analyzed and was categorized Urban, Rural or Highway driving. It was also shown that each category of driving generates unique areas of interest in terms of electric machine operation.

4

Electric machine design - I

4.1 Machine requirements and dimensions

Based on the drive cycle analysis data, the requirements for the XC90 and S60 electric machines can be seen in table 4.1.

Table 4.1: Electric machine requirements

Electric machine requirements		
Parameter	XC90 Machine	S60 Machine
Maximum Torque	400 Nm	300 Nm
Maximum Speed	14000 RPM	14000 RPM
Maximum Power	160 kW	130 kW
Base speed	3700 RPM	4000 RPM
Torque @ 25% gradient at 0 km/h	241 Nm	180 Nm
Torque @ 6% gradient at 90 km/h	61 Nm	46 Nm

Based on the above requirements and using the analytical design machine process from Chapter 2, and assuming an RMS current density(J_{rms}) of 21.21 A/mm^2 ,the first iteration of the design parameters for XC90 and S60 machines is found in table 4.2

Table 4.2: Electric machine design parameters

Electric machine design parameters		
Parameter	XC90 Machine	S60 Machine
Stator outer Diameter (D_{os})	265 mm	248.3 mm
Rotor outer Diameter (D_{or})	183.08 mm	166.29 mm
Air gap length (δ)	0.9 mm	0.845 mm
Active length (L_{stack})	150 mm	130 mm
Number of poles (P)	8	8
Number of slots (Q_s)	48	48

4.1.1 Winding Layout

Based on the analytical design elaborated in Chapter 2 and the design requirements, an integral slot winding with two parallel paths (a) and two slots per pole per phase

($q = 2$) is chosen. With 48 slots and $q = 2$, the distribution factor is given by,

$$K_{d1} = \frac{1}{4\sin\left(\frac{\pi/6}{2}\right)} = 0.9659 \tag{4.1}$$

and the pitch factor,

$$K_{p1} = \sin\left(\frac{y}{y_Q}\frac{\pi}{2}\right) = 1 \tag{4.2}$$

A representative figure of winding distribution in a 48 slot machine with 8 poles is shown in Fig. 4.1.

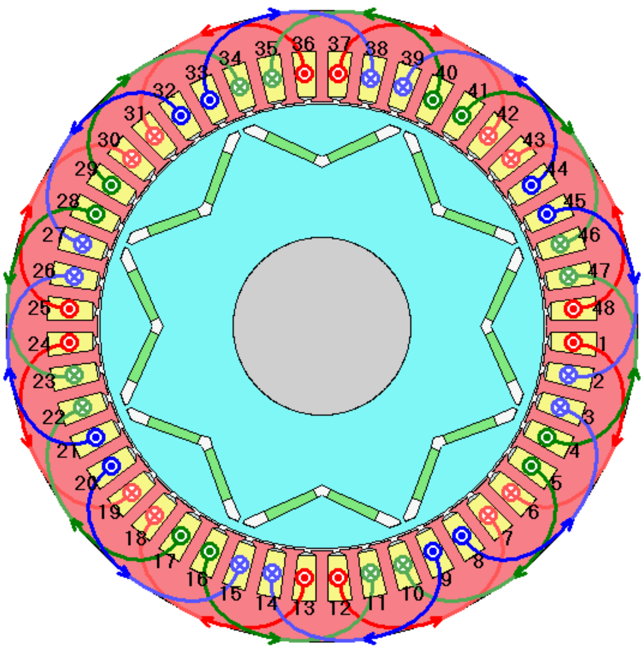

Figure 4.1: Winding pattern

Red color represents Phase A, green is Phase B and blue represents Phase C. The winding details for the XC90 and S60 machines is seen in table 4.3.

Table 4.3: Winding details

Winding details		
Parameter	XC90 Machine	S60 Machine
Number of turns(N_s)	9	10
Number of strands($N_{strands}$)	4	4
Winding factor (K_{w1})	0.9659	0.9659
RMS phase current ($I_{ph,rms}$)	381.98 A	310.36 A
Current density ($J_{rms,act}$)	23.74 A/mm^2	19.29 A/mm^2

Strands of radii of 0.88 mm are considered for the design.
The winding layout showing the start and end of each coil sides and the parallel paths are presented in Appendix 1 [A.1].

4.1.2 Tooth and slot dimensions

Based on the winding parameters and the machine dimensions, a first estimate of the tooth and slot dimensions can be calculated as elaborated in Chapter 2. The slot and tooth details for the XC90 and S60 machine can be seen in table 4.4.

Table 4.4: Tooth and slot dimensions

Tooth and slot dimensions		
Parameter	XC90 Machine	S60 Machine
Slot pitch(τ_s)	12.1 mm	10.9 mm
Tooth width(T_{width})	6.3 mm	5.8 mm
Slot area (A_{slot})	175.16 mm^2	194.62 mm^2
B_{s1}	7.2 mm	6.53 mm
B_{s2}	9 mm	8.16 mm
H_{s2}	21.62 mm	26.47 mm

For the ease of winding, a slot opening (B_{s0}) of 2.5 mm is considered for both the variants.

4.2 Material Properties

Electric machine design is very dependent on the material used for the rotor and stator laminations and as well as the permanent magnet properties.
Stator and rotor lamination's are generally made up of thin lamination's of electrical steel which are made up from an alloy of iron and silicon in varied combinations [26]. Silicon is used so as to reduce the conductivity of the iron and hence reduce losses in the machine. Some of the important magnetic properties of electrical steel that is required to be used for electric machines are small hysteresis area, resulting in low power loss per cycle, low eddy current loss and high permeability. To reduce the eddy current loss further, thin lamination's (≤ 0.5 mm) are generally used.
Electrical steel can be broadly categorized into Non-oriented and Oriented steel. Oriented steel has anisotropic magnetic behavior where in the magnetic properties are aligned in one direction. In Non-oriented steel, the magnetic properties are similar in all directions i.e they exhibit isotropic behaviour. Oriented steel is generally used in applications where the flux direction is in one direction such as transformers and they exhibit low core losses [27]. Non - oriented steel are generally used in electric machines. A commonly used electrical steel $M270-35A$ has been chosen for the first iteration of the design. It has a thickness of $0.35mm$ and a relatively good saturation magnetic flux density. The BH curve of the $M270-35A$ material is presented in fig. 4.2.

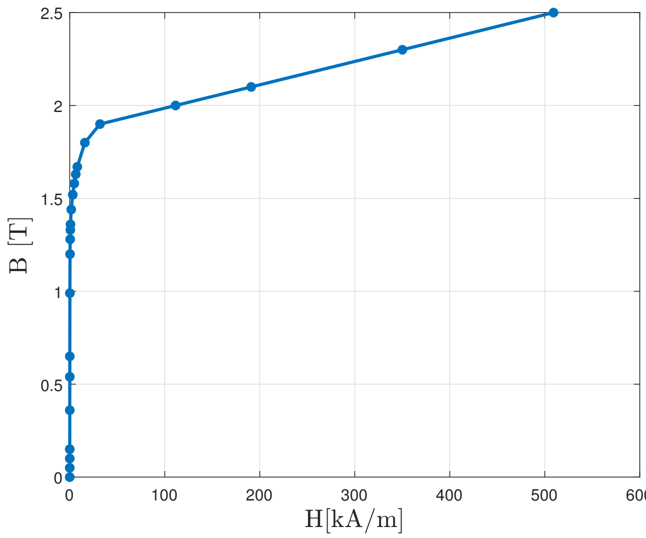

Figure 4.2: BH curve of M270-35A

The loss per kilogram of the $M270-35A$ material for different frequencies of operation is presented in fig. 4.3. As seen from the figure, as the frequency and the magnetic flux density increases, the core loss in the material also increases. The punching effects due to the manufacturing of stator and rotor and the PWM effect due to the interface with an inverter for operation, increases the core losses in the material further. A factor of 1.42 is considered for scaling the losses due to punching effects [28], [29] and a factor of 1.4 is considered for scaling the losses due to PWM effects [30].

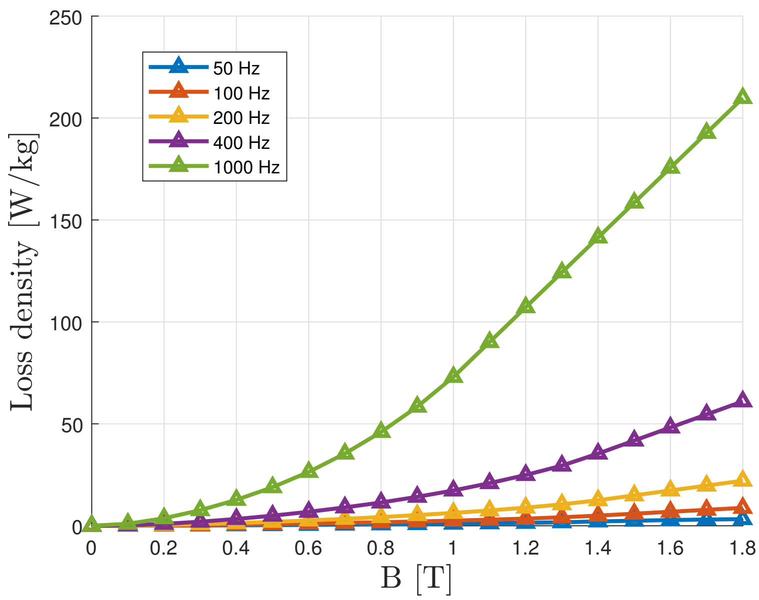

Figure 4.3: Loss/kg of $M270-35A$

Neodymium magnets based electric machines are often used for propulsion applica-

tions due to its high remanence flux density (B_r) and high energy product (BH_{max}) [31]. Neodymium magnets are rare earth material magnets which are made from an alloy of Neodymium, Iron and Boron. Generally, they are also combined with Dysprosium to increase the operating temperature limits. The magnets are manufactured in two different processes namely sintering and bonding.
A typical BH curve of NdFeB magnet is shown in fig. 4.4. As seen in the figure, as the temperature of the magnets increases, the risk of demagnetization increases with increasing current magnitude.

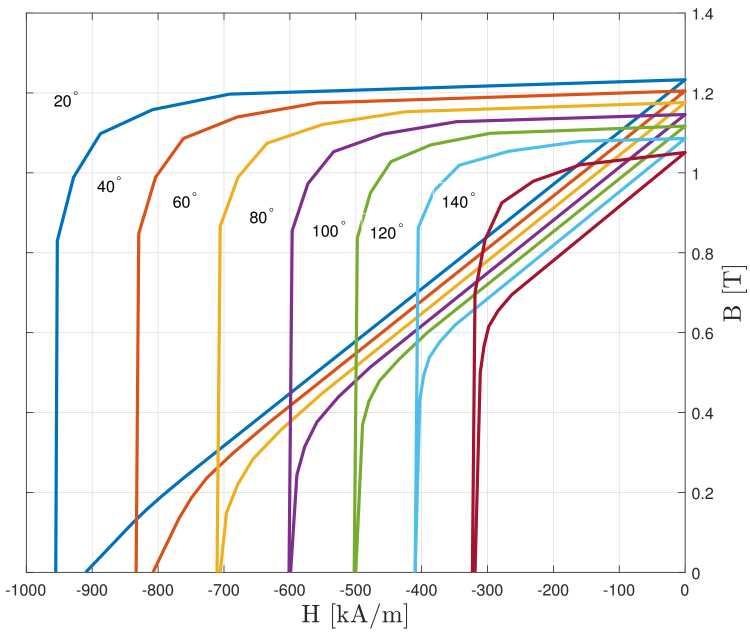

Figure 4.4: BH curve of N35 magnet

In automotive applications, sintered magnets of varied strengths are used depending on the requirements. General nomenclature of sintered magnets starts with letter N which stands for Neodymium magnet followed by two numbers which indicate the strength of the magnets. The values of the two number can range from 28 - 52 , 52 being the strongest magnet having the highest remanence magnetic flux density B_r. In this thesis $N36Z$ Neodymium magnet has been used, which has remanence flux density (B_r) of 1.16 - 1.22 T, coercivity (H_c) of 875 kA/m and maximum energy product (BH_{max}) of 263-294 kJ/m^3 [32].

4.3 Rotor topologies

Automotive manufacturers using PMSM machines for propulsion have opted for different magnet configurations in the rotor [33], but it is evident that most of them use interior permanent magnet machines due to inherent structural strength, availability of reluctance torque component and good field-weakening characteristics as compared to surface mounted PMSM[34].

In this thesis, four different rotor topologies which are used by different automotive manufacturers are investigated and a comparison based on various parameters such as efficiency at the identified operating points, magnet usage, torque ripple, structural integrity and demagnetization analysis is carried out.
The four different rotor topologies are illustrated in fig. 4.5.

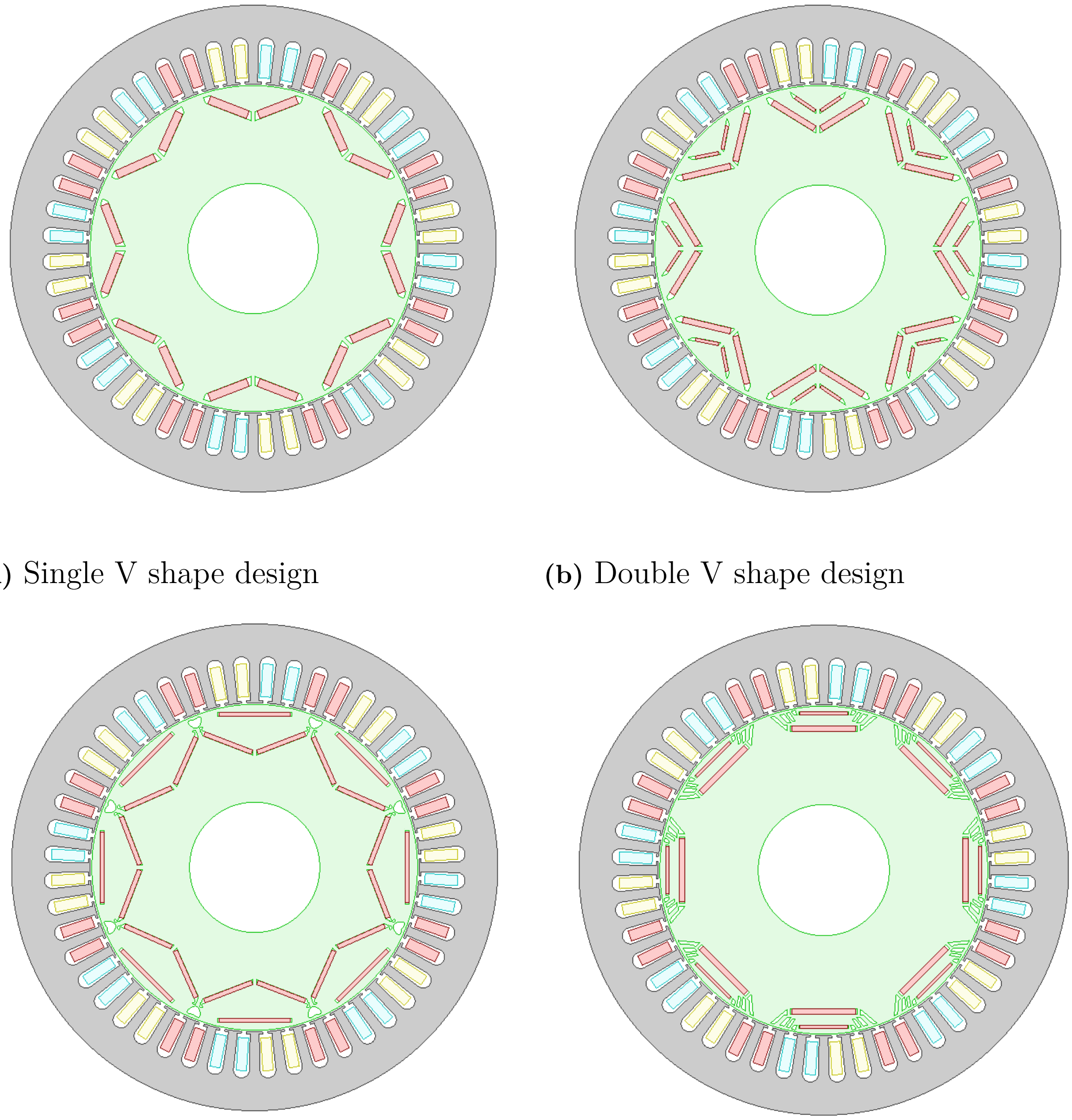

(a) Single V shape design

(b) Double V shape design

(c) Delta shape design

(d) Flat shape design

Figure 4.5: Four different rotor topologies

Fig. 5.16a presents a single layer V shape magnet design which is inspired from Toyota Prius [35] hybrid car. In Fig. 5.16b presents a double layer V shape magnet design which is inspired from General Motors Bolt electric car [36].In Fig. 5.8c presents a delta design which is a mix of single layer V shape and a flat magnet design, this is inspired from Nissan Leaf [35] electric car. In Fig. 5.8d presents a flat shape magnet design where in two layers of flat magnets are embedded within the rotor structure, this kind of design is inspired by the BMW i3 [35] electric car.

4.4 Modeling in Ansys Maxwell

To design, analyze, and compare electric machines a modeling tool is necessary. Ansys Maxwell software package has been used in this thesis to model the electric machines. The software is a mix of a Finite Element Analysis (FEA) and Computer Aided Drawing (CAD) programs with which it is possible to design geometric shapes and perform electromagnetic analysis of these. The software has pre-defined electric-machine components which can be dimensioned according to our needs. Two Independent paths of machine design were taken for the S60 and XC90 vehicles from the initial four rotor topologies. Independent paths were chosen to cover a wider base of possible designs and to better understand the impact of different design parameters. Initial designs were carried out with M270-35A as the electrical steel and N36Z as the magnet material. To better understand the differences of rotor topologies, the stator and the winding configuration was kept constant for each of the S60 and XC90 designs.

4.4.1 Rotor and winding design iterations

Electric machine design is an iterative process to reach the torque-speed requirements. The first iteration of electric machine design was mainly aimed at achieving the required torque and speed and was carried out by numerous iterations on magnet thickness, magnet angles and the number of turns in the windings. The first iteration of designs is not aimed at an optimized design but to meet the requirements. The initial design results for four rotor topologies of XC90 and S60 vehicles are described below. These machines are used as a benchmark for further design improvements.

4.4.2 Machine control in Ansys Maxwell

The analysis of the electric machines in Ansys Maxwell is carried out in three-phase quantities, but control algorithms such as MTPA and Minimum Loss Control as discussed in Chapter 2.7 uses dq reference frame. Hence, the first step in the control of the machines is the transformation of three phase quantities into dq quantities using the familiar Park and Clark transformation. Also all simulations carried out in this thesis are based on current feeding technique wherein a specified magnitude of sinusoidal current at a specified angle is fed to the stator windings. This approach is a simplified method of control where in we assume perfect reproduction of the reference currents calculated in the controller by the inverter. Some of the other methods of feeding are voltage and PWM feeding technique which are more inline with the actual physical process but are not investigated here due to long simulation time in the FEA tool. Once the transformation of quantities are included in the control structure, a series of steps are followed to arrive at important conclusions such as efficiency, core-loss, torque ripple. The steps followed are enumerated below,

1. Calculate the variation of the magnet flux linkage (Ψ_m) with respect to I_q current.
2. Calculation of d and q-axis inductance (L_d - L_q) with respect to different magnitude to current (I_{mag}) and current angle (β) , at one speed.
3. Processing of above data and generation of operating points based on the control strategy to calculate efficiency, core-loss and torque ripple maps.
4. Analyzing the generated operating points in Ansys Maxwell
5. Post processing of results

4.4.3 Post processing

The simulation results are extracted for post-processed with the goal of creating efficiency maps and torque ripple maps. Each of the operating points that is simulated generates corresponding torque, speed, iron loss, mean torque ripple for and is used for post-processing. Total loss ($P_{loss,total}$) at every point is calculated as,

$$P_{loss,total} = P_{cu} + P_{fe,rotor} + P_{fe,stator} \tag{4.3}$$

where $P_{fe,rotor}$,$P_{fe,stator}$ is mean rotor and stator core-loss including punching and PWM effects. P_{cu} corresponds to machine copper loss and is defined as

$$P_{cu} = 3I_{rms}^2 R_s; \tag{4.4}$$

R_s is the effective stator winding resistance including the end windings. Efficiency at every point is calculated as,

$$\frac{P_{out}}{P_{out} + P_{loss,total}} \tag{4.5}$$

P_{out} is the output mechanical power of the machine.

4.5 Initial machine design and observations

The result from the electric machine design, the simulations and the post processing is summarized in efficiency and relative torque ripple maps.The result and initial observations for the four rotor topologies of the XC90 electric machines are described in figures 4.6 - 4.9.

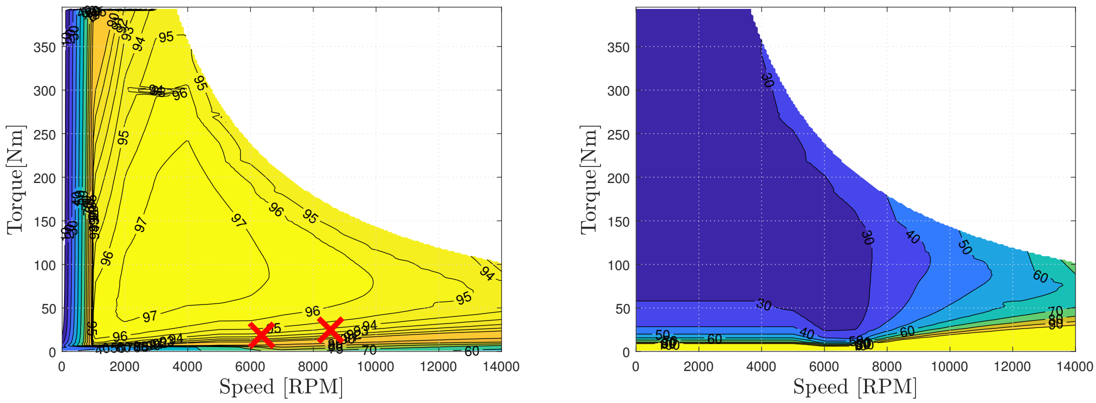

(a) Efficiency map **(b)** Relative torque ripple map

Figure 4.6: Delta design

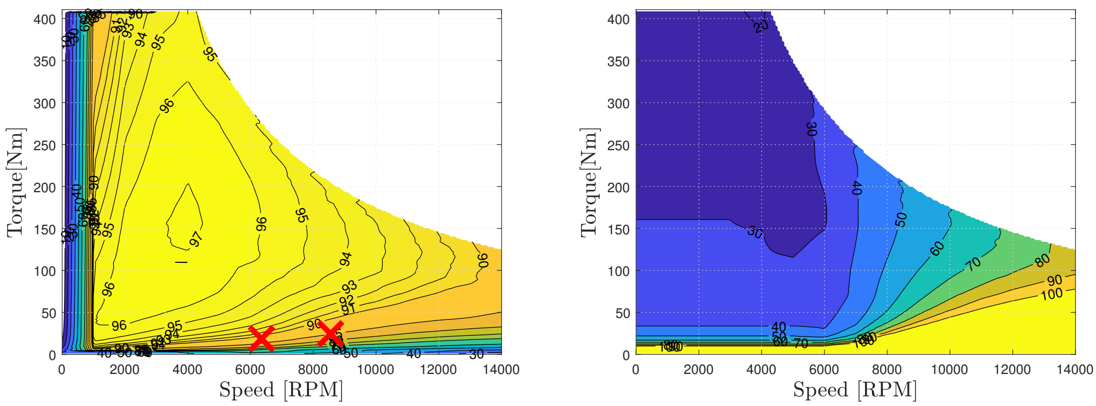

(a) Efficiency map **(b)** Relative torque ripple map

Figure 4.7: Double Flat design

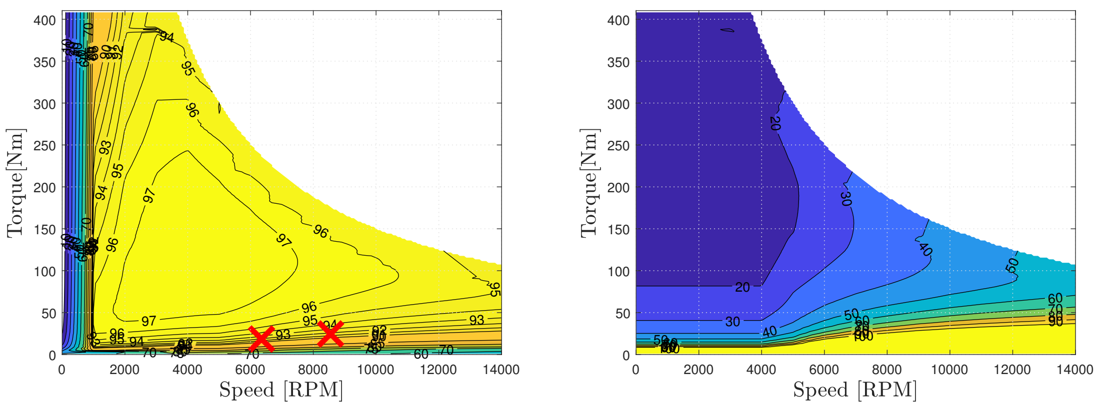

(a) Efficiency map **(b)** Relative torque ripple map

Figure 4.8: Double V design

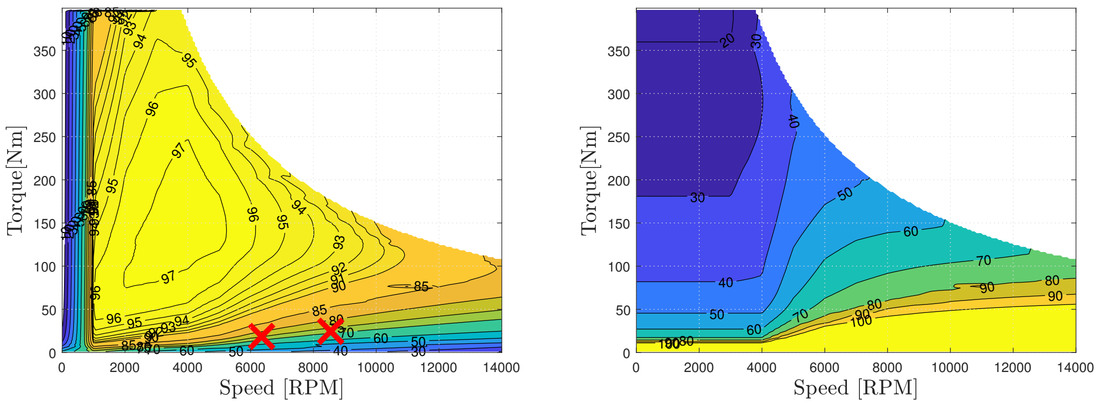

(a) Efficiency map (b) Relative torque ripple map

Figure 4.9: V design

Fig. 4.6 - 4.9 presents the efficiency and relative torque ripple maps of XC90 machines. The two intersections points in red, represent the maximum energy points derived from the database analysis. For the XC90 vehicle, the two points is found in table 4.5,

Table 4.5: Centroid points

Speed [RPM]	Torque [Nm]
6350	18.5
8550	24.5

By analyzing the efficiency at the two operating points described above, efficiencies for the different rotor designs becomes as seen in table 4.6

Table 4.6: Efficiency at the centroid points

Design	6350 RPM, 18.5 Nm	8550 RPM, 24.5 Nm
Delta	93.39	93.64
Double Flat	88.37	85.23
Double V	91.92	91.65
Single V	75.32	72.11

We can see a clear difference in the efficiency for different magnet configurations. From this we can see that the Delta configuration gives the highest efficiency at the operating points compared to any other configuration with a relatively modest torque ripple compared to other designs. By undertaking a similar approach to the S60 vehicle machines, the efficiency and the torque ripple maps are shown in Fig. 4.10 - 5.16 .

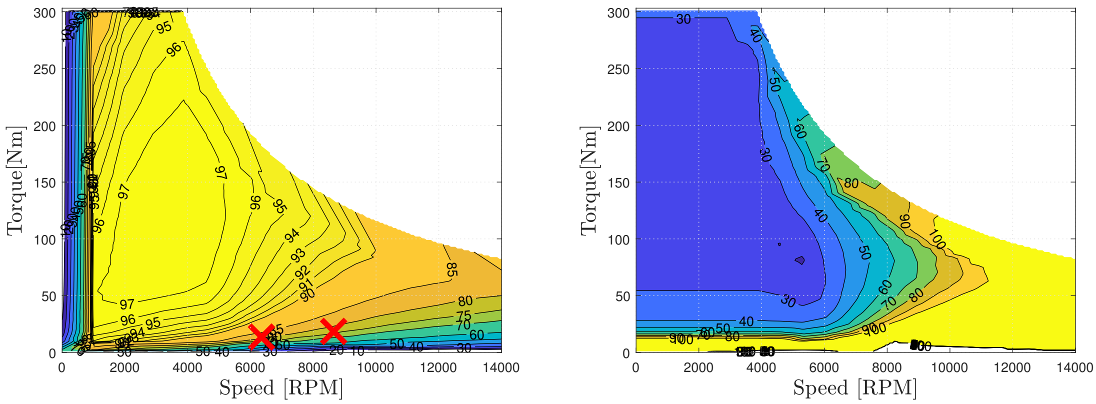

(a) Efficiency map **(b)** Relative torque ripple map

Figure 4.10: Delta design

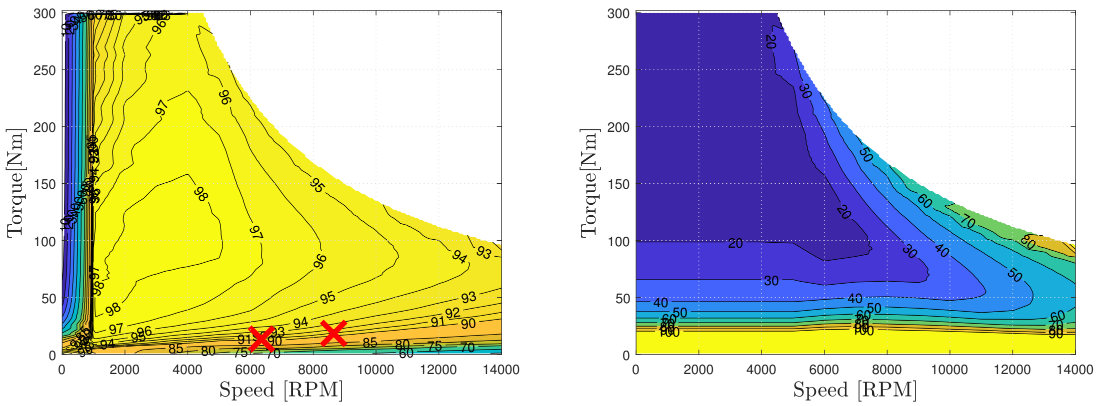

(a) Efficiency map **(b)** Relative torque ripple map

Figure 4.11: Double Flat design

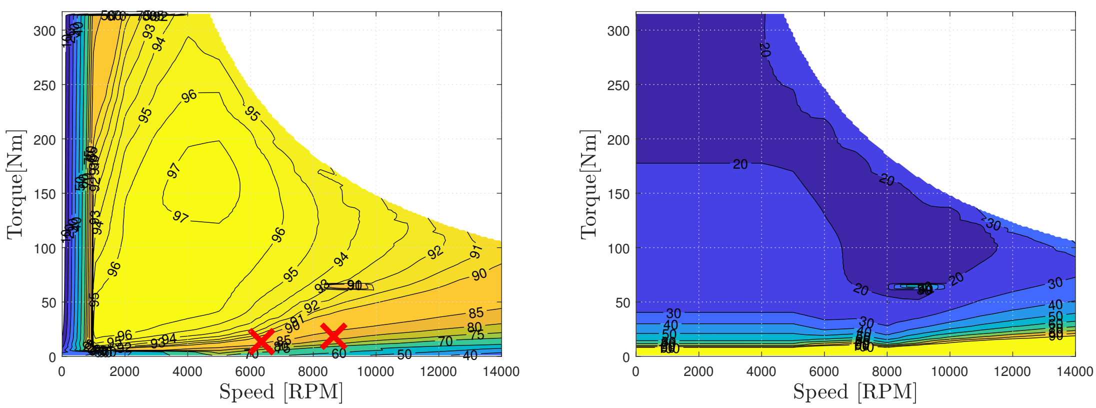

(a) Efficiency map **(b)** Relative torque ripple map

Figure 4.12: Double V design

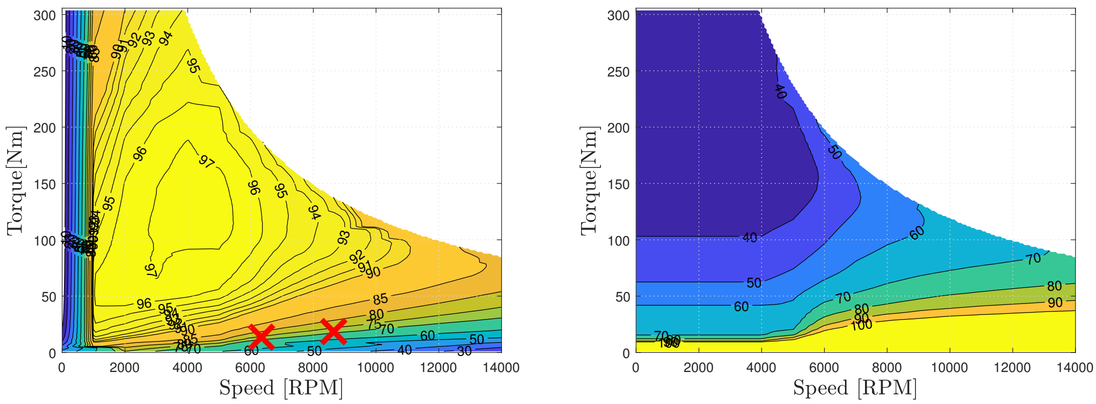

(a) Efficiency map **(b)** Relative torque ripple map

Figure 4.13: V design

The two intersections points in red representing the maximum energy points for the S60 vehicle is seen in table 4.7.

Table 4.7: Centroid points

Speed [RPM]	Torque [Nm]
6350	13.5
8650	18.5

By analyzing the efficiency at the two operating points described above, the efficiencies becomes as seen in table 4.8.

Table 4.8: Efficiency at the centroid points

Design	6350 RPM,13.5 Nm	8550 RPM,18.5 Nm
Delta	76.48	80.92
Double Flat	90.86	90.60
Double V	82.38	86.48
Single V	71.63	74.17

From the data we can see that the double flat design has the highest efficiency at the operating points compared to other designs. Also, it has a better torque ripple profile at low speeds compared to other designs. The two main conclusions from the initial designs are,

1. Efficiency at the operating points are much lower compared to the peak efficiency of the machines
2. Torque ripple at low speeds is ≈ 20 - 30%, which can contribute significantly to the NVH (Noise Vibration and Harshness) characteristics of the electric powertrain [37].

Hence improvement in terms of efficiency and reduced torque ripple will be dealt in the next chapter which yields the final design parameters of the machine.

5
Electric machine design - II

The two main areas of improvement from the initial designs are,

1. Efficiency at the operating points.
2. Reduction in torque ripple at lower speeds.

The improvements stated above can be achieved by varied methods, some of methods investigated in this thesis are,

1. Change in electrical steel material
2. Flux barrier design
3. Skewing

Each of these methods are investigated in detail here and the final design and its analysis is also discussed.

5.1 Change in electrical steel material

As seen from the efficiency plots of the XC90 and S60 vehicle machines, the efficiency at the selected operating points are much lower than the peak value of the efficiency. One of the observation we can make from the operating points is that the operating points lie in the low torque and relatively moderate to high-speed region. Hence to increase the efficiency at these points, a straight forward approach is to reduce the iron losses in the electrical steel of stator and rotor. The material used in the initial designs,$M270 - 35A$, has a lamination thickness of 0.35 mm and relatively moderate loss/kg as shown in Fig. 4.3. We know that iron losses are mainly divided into hysteresis and eddy current losses and eddy current losses form a major part of the iron losses [26]. One of the straight forward approach to reduce eddy current losses is to reduce the lamination thickness of the electrical steel. Arnon 7 electrical steel manufactured by Arnold magnetics [38] is found to have lower loss/kg and is also available in lamination thickness of 0.178 mm. Hence, this material is used to investigate the change in efficiency due to material change. The BH curve of the Arnon 7 electrical steel compared to the $M270 - 35A$ material is presented in Fig. 5.1.

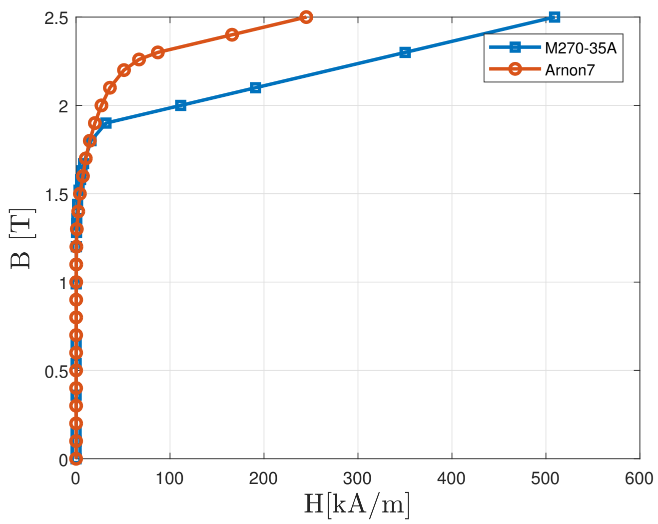

Figure 5.1: BH curve of Arnon 7

As seen from figure 5.1, the knee of the magnetizing curve is higher for Arnon 7 compared to the latter. This is also beneficial as this allows us to further reduce the size of machine due to higher saturating flux density in the steel. The loss per kilogram of the Arnon 7 material for different frequencies of operation is presented in fig. 5.2. Also, the Loss density of $M270 - 35A$ material at 1000 Hz is presented for comparison. As seen from the figure, as the frequency and the magnetic flux density increases, the core loss in the material also increases. A scaling factor of 1.42 for punching effects and a factor of 1.4 for the losses due to PWM effects is considered as before.

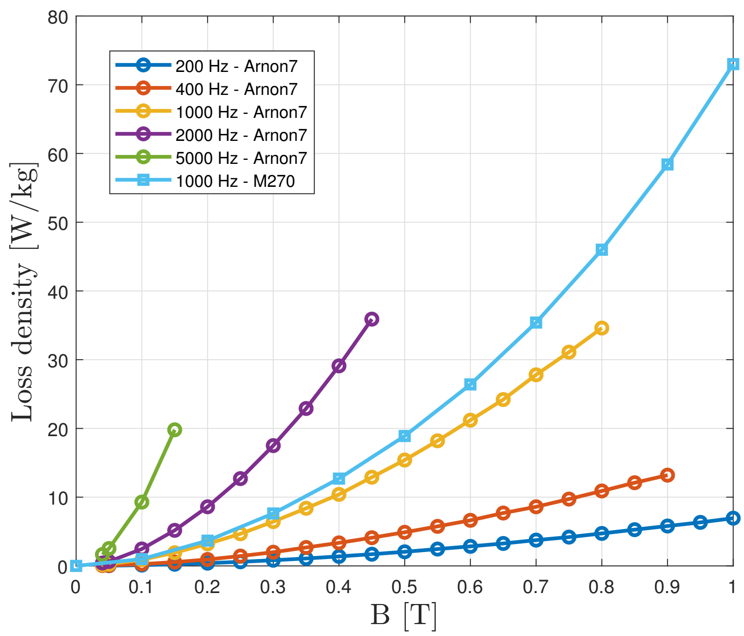

Figure 5.2: Loss/kg of Arnon 7

To study the effect of the material change, a Double V shape magnet machine for the XC90 vehicle with M270-35A material was changed to Arnon 7 material instead and the results are presented in Fig. 5.3.

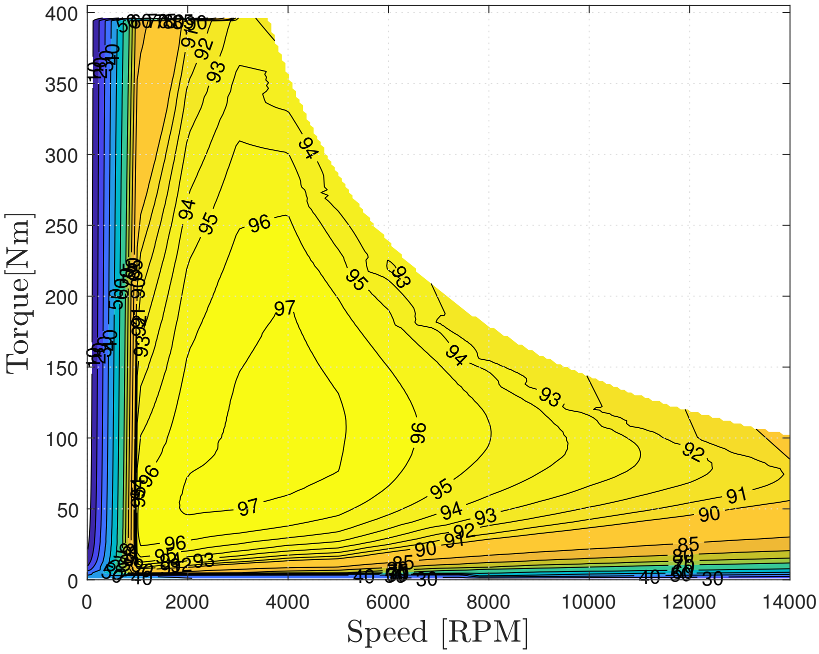

(a) M270 - 35A

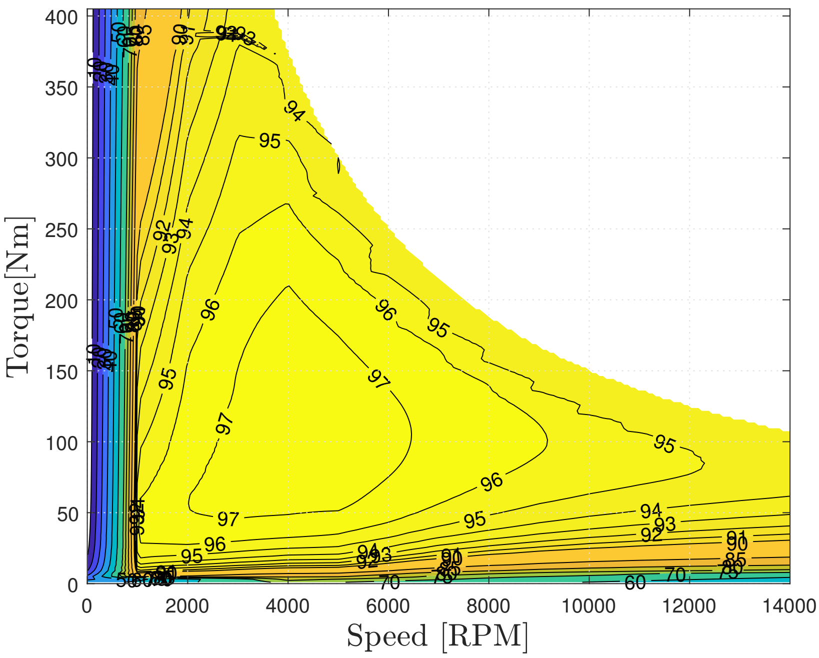

(b) Arnon 7

Figure 5.3: Comparison of M270 vs Arnon 7 material

As seen from Fig. 5.3, the change in material has caused a notable expansion of the most efficient regions of the machine. In terms of efficiency at the selected operating points we can see 2 - 3 % increase in efficiency due to the change of material.

5.2 Flux barrier design

Flux barrier design is one of the important aspects in interior permanent magnet machine design, due to the placement of magnet in the interior of the rotor. Flux barriers mainly refers to air pockets in the structure of the rotor which are around the magnets, whose purpose is to reduce the leakage magnet flux by concentrating them towards the air-gap. A typical flux barrier of the single V shape machine design is presented in Fig. 5.4 encircled by the black circle .

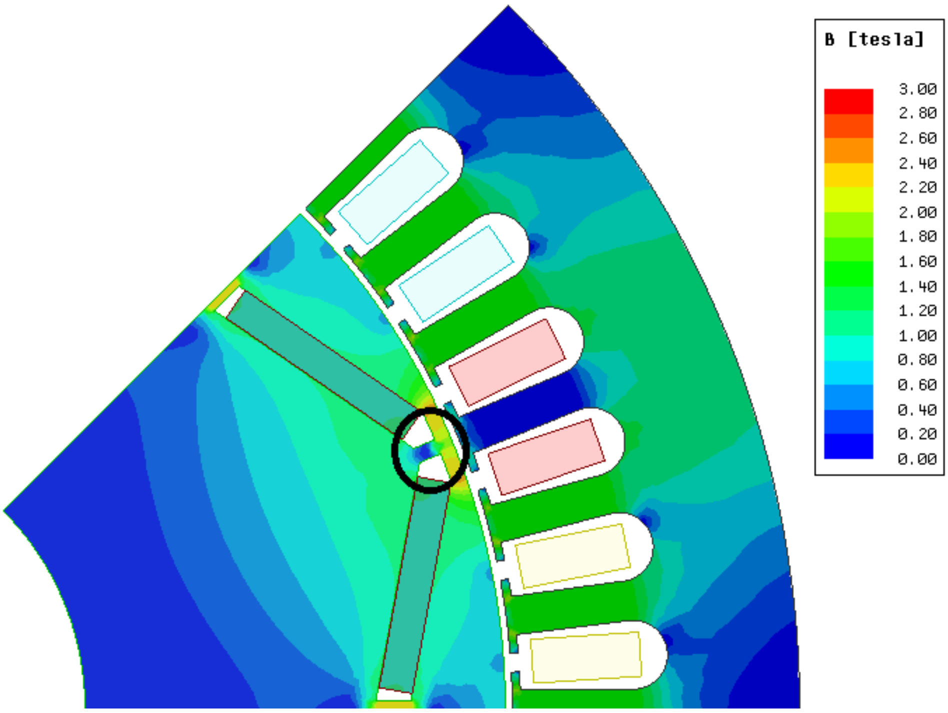

Figure 5.4: Flux barriers in a V shape rotor design

As the flux barriers primary purpose is to reduce the leakage flux, magnetically, it is favorable to extend the flux barrier till the air gap. But this make the rotor structurally fragile and hence a small area of iron (bridge) is required to hold structural integrity and hence the flux barriers are generally 2 - 2.5 *mm* away from the air gap. Due to the small cross-sectional area of the bridge, the flux density at the bridge saturates the iron and hence magnetically it is similar to have no bridges. This can also be seen as red regions near the flux barriers in Fig. 5.4. Flux barrier design also has a strong impact on core-losses and torque ripple [39] . Since the current profile of the machines is sinusoidal in nature, reduction in torque ripple can be achieved by concentrating the magnet flux [40],[41]. Different flux barrier designs for the four different rotor topologies were investigated and studied as part of the thesis.

However, the design of flux barriers is a complex topic and the outcome of the final rotor flux barrier designs are not thoroughly investigated. For the S60 machines, the Double Flat and the Delta topology is considered to have the most complex design and the barriers are inspired by the Nissan Leaf and the BMW i3 designs. However, there have been no improvement strategies for the flux barriers and the resulting designs have not gone through any optimization. For the XC90 rotor designs, the approach was to make the flux barriers as simple as possible. Due to the decrease in leakage flux after the flux barrier design, thinner magnets were used to achieve the required machine characteristics.

5.3 Skewing

Skewing in an effective method of torque ripple reduction [40], [42]. A view of an unskewed rotor with inset magnets in the rotor is presented in Fig. 5.5a.

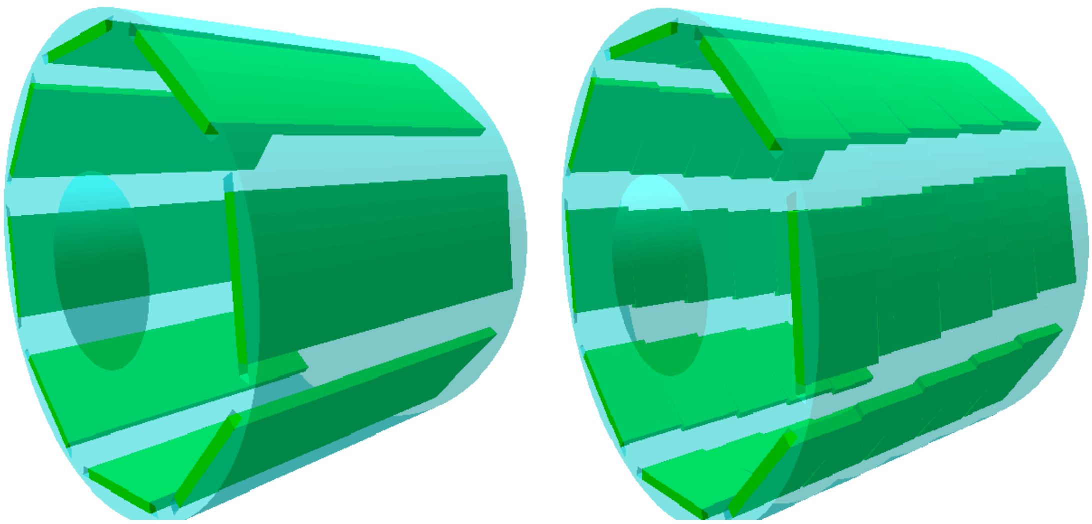

(a) Unskewed rotor **(b)** Skewed rotor

Figure 5.5: Comparison of the Unskewed and Skewed rotor

As seen from the Fig 5.5a and 5.5b, the magnet extends to the entire length of the rotor. Fig. 5.5b presents skewed rotor as a modification of Fig. 5.5a. The skewed rotor consists of 5 slices of equal steps where in each rotor slice is skewed by an angle of 1.5° with the middle slice acting as the zero slice. Hence with respect to the middle slice the relative angles of the slices are - 3°, - 1.5°, 0°, + 1.5° and + 3°. Skewing achieves reduction in torque ripple by (1) reducing the variation of reluctance as seen by the rotor magnets and (2) reducing the higher order back-EMF harmonics in the machine [43]. This also has a positive effect on reduce the cogging torque of the machine. Even though skewing is an effective approach to reduce the torque ripple , it reduces the peak torque by 2-3 % and increases the leakage and stray losses [44]. It also adds complexity during the construction of the machine. Torque ripple map in percentage for the skewed and unskewed Double V shape magnet design is presented in Fig. 5.6.

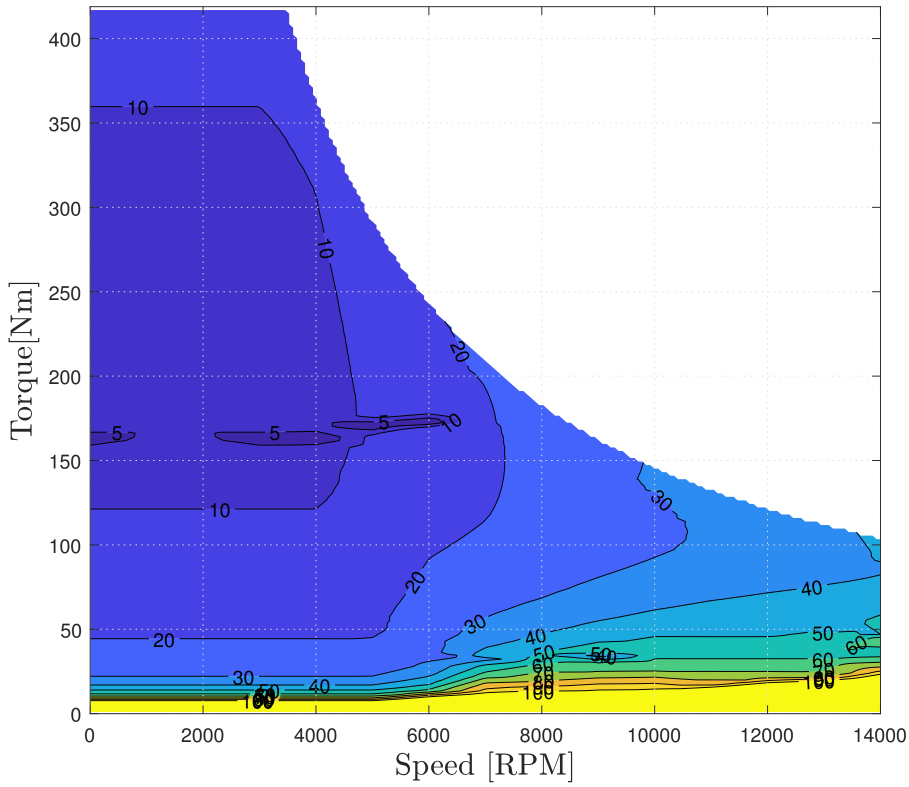

(a) Relative torque ripple of unskewed rotor

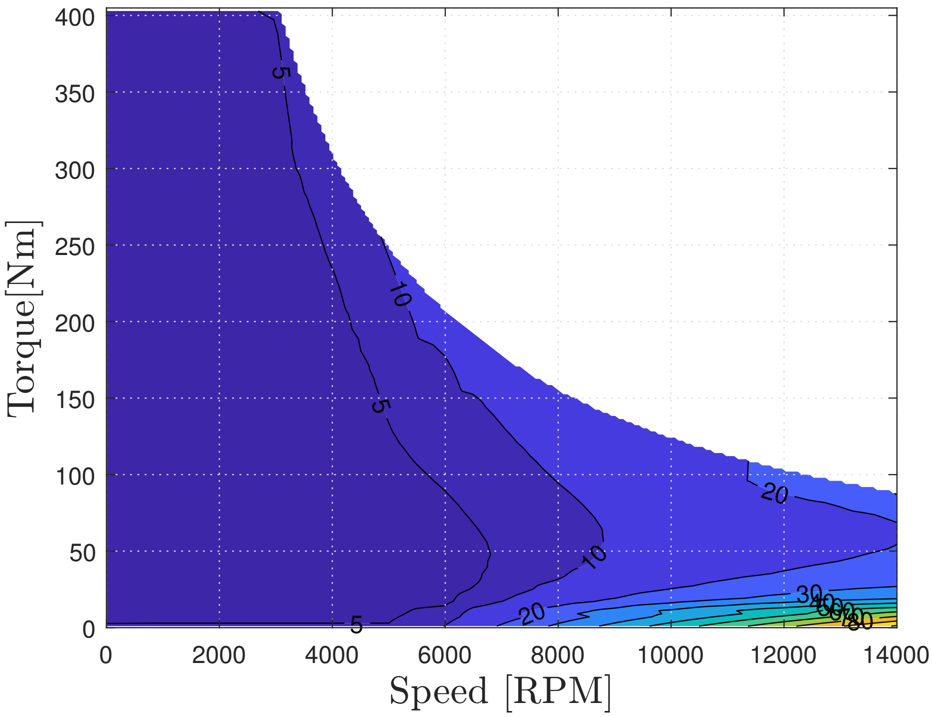

(b) Relative torque ripple of skewed rotor

Figure 5.6: Relative torque ripple in Double V design

The skewed rotor was sliced into 5 separate slices with a total skew angle of 7.5°, which corresponds to one slot angle. Two main observations from Fig. 5.6 are,

1. Significant reduction in torque ripple at low speeds.
2. 2-3 % reduction in the peak torque as anticipated.

5.4 Final design iteration

Based on the above discussed methods of improving the efficiency and torque-ripple, the final design of the S60 and XC90 based machines are presented in Fig. 5.7 and 5.8 respectively.

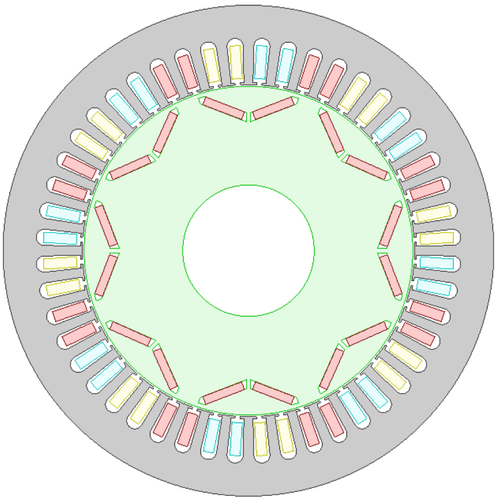

(a) Single V shape design

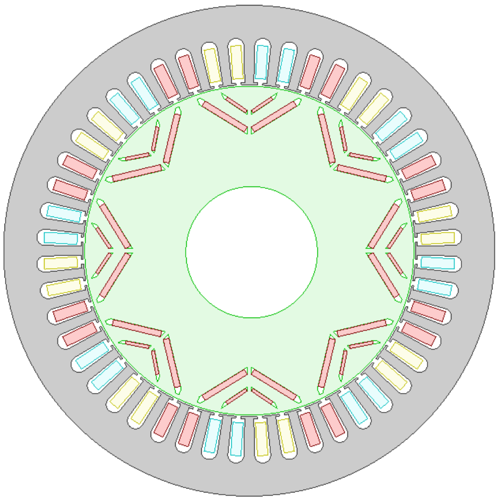

(b) Double V shape design

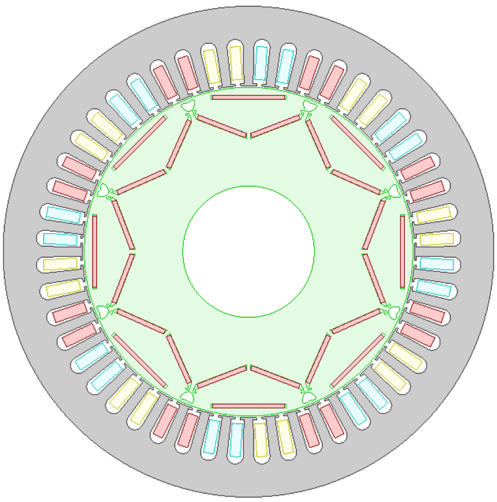

(c) Delta shape design

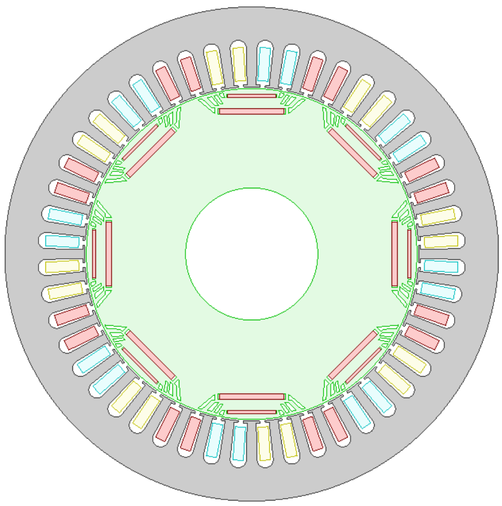

(d) Double Flat shape design

Figure 5.7: S60 machines

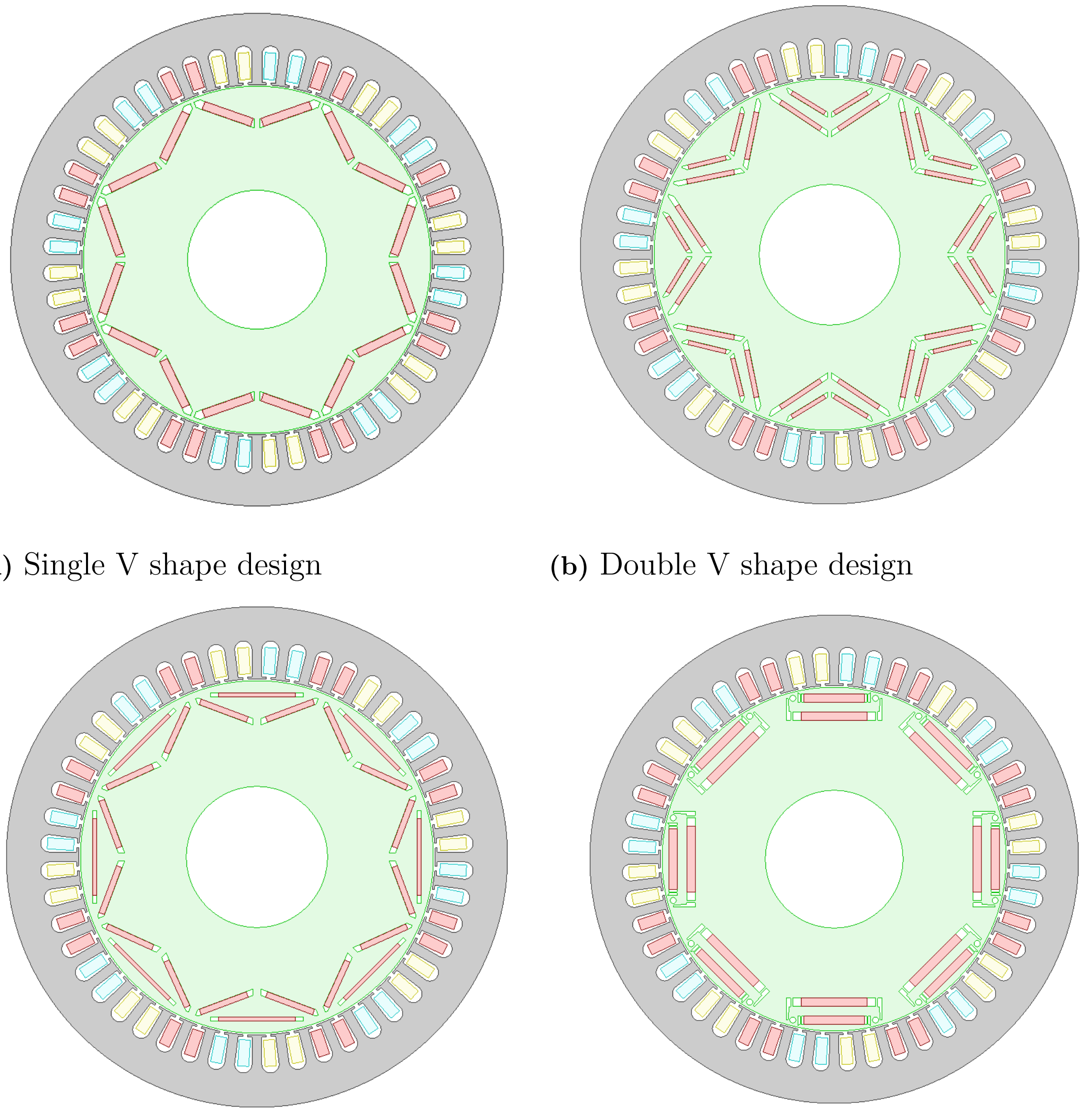

(a) Single V shape design

(b) Double V shape design

(c) Delta shape design

(d) Double Flat shape design

Figure 5.8: XC90 machines

5.5 Results and Observations

The efficiency (in percentage) and core loss (in kW) maps of the S60 machines are shown below,

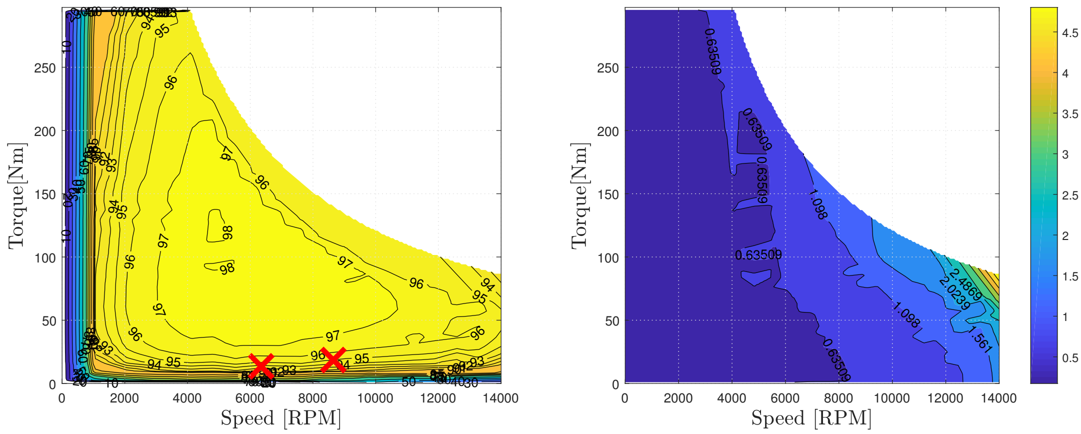

(a) Efficiency map

(b) Core loss map

Figure 5.9: Delta design

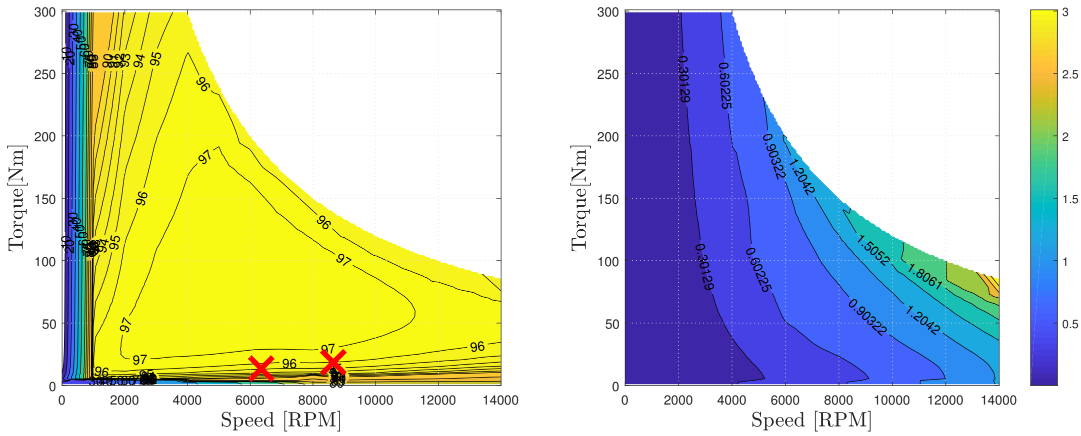

(a) Efficiency map

(b) Core loss map

Figure 5.10: Double flat design

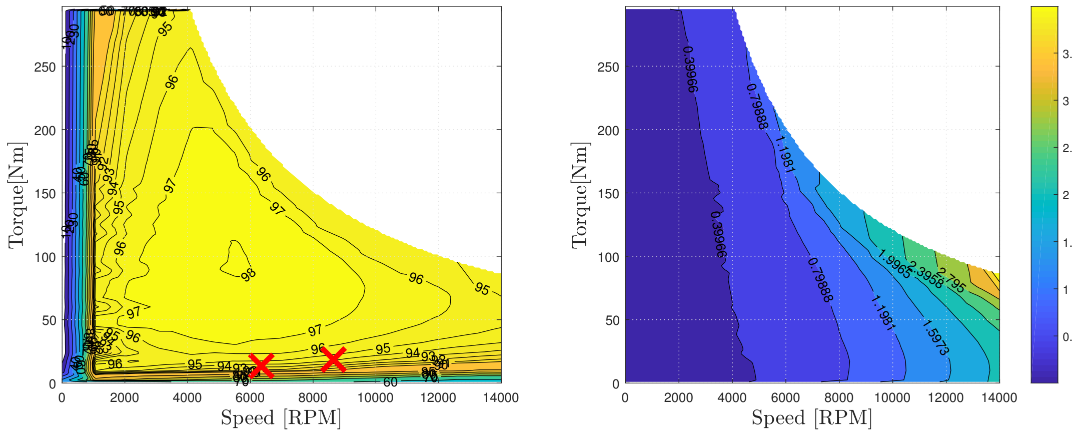

(a) Efficiency map **(b)** Core loss map

Figure 5.11: Double V design

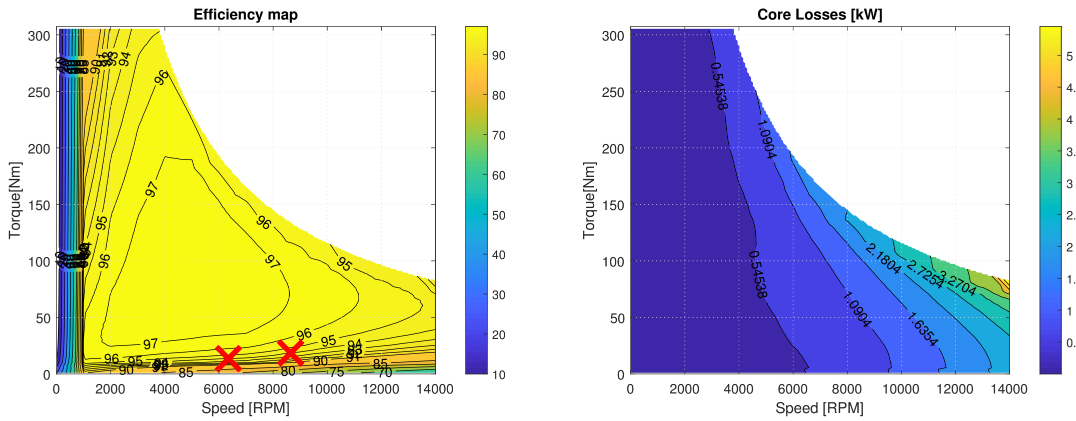

(a) Efficiency map **(b)** Core loss map

Figure 5.12: Single V design

The efficiencies at the identified centroid's for the S60 design are ,

Table 5.1: Efficiency at the centroid points

Design	6350 RPM,13.5 Nm	8550 RPM,18.5 Nm
Delta	93.73	94.98
Double Flat	95.96	95.14
Double V	93.36	94.15
Single V	93.95	93.97

As seen from the above table data, there is a considerable increase in the efficiency at the operating points mainly due to improvements in the design of flux barriers, magnet dimensions and also the change of material from $M270-35A$ to Arnon 7.

The efficiency (in percentage) and core loss (in kW) maps of the XC90 machines are as follows,

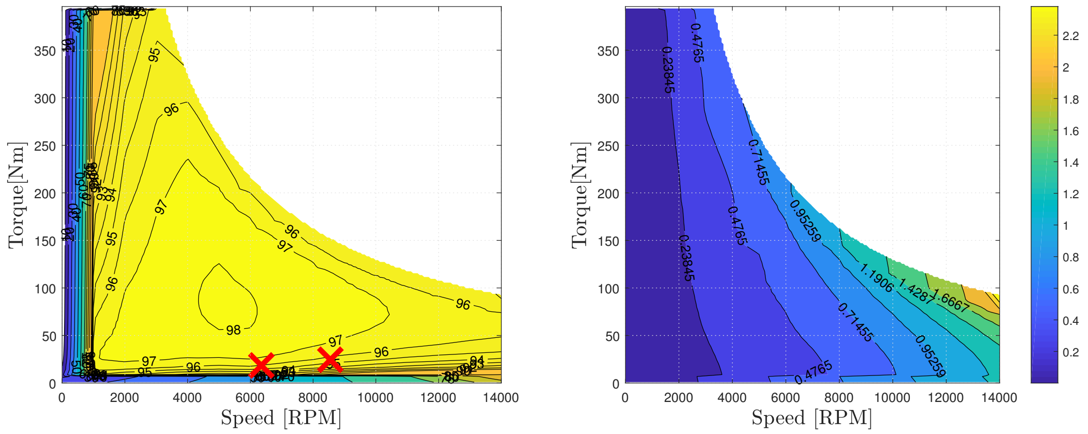

(a) Efficiency map **(b)** Core loss map

Figure 5.13: Delta design

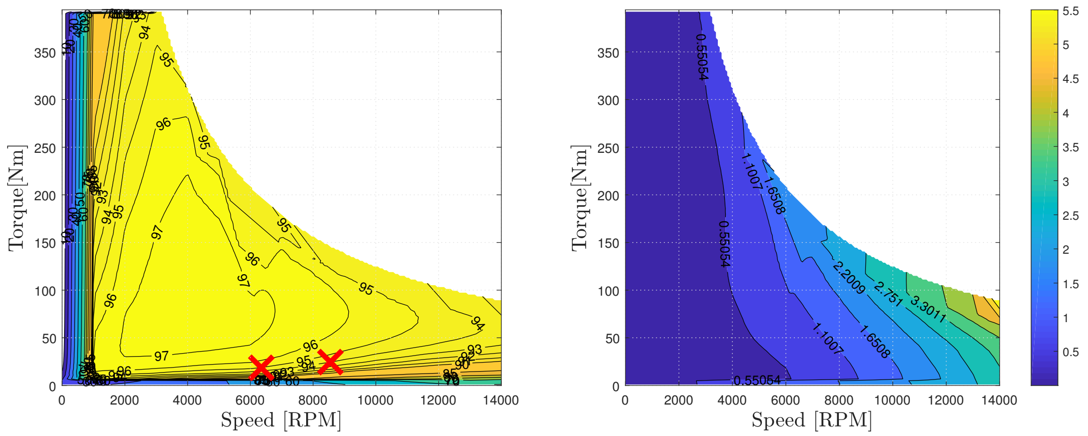

(a) Efficiency map **(b)** Core loss map

Figure 5.14: Double flat design

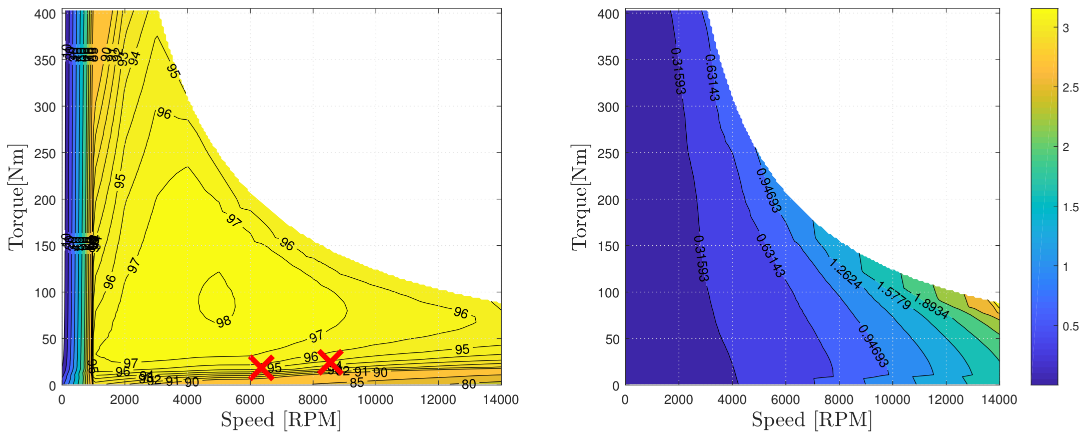

(a) Efficiency map **(b)** Core loss map

Figure 5.15: Double V design

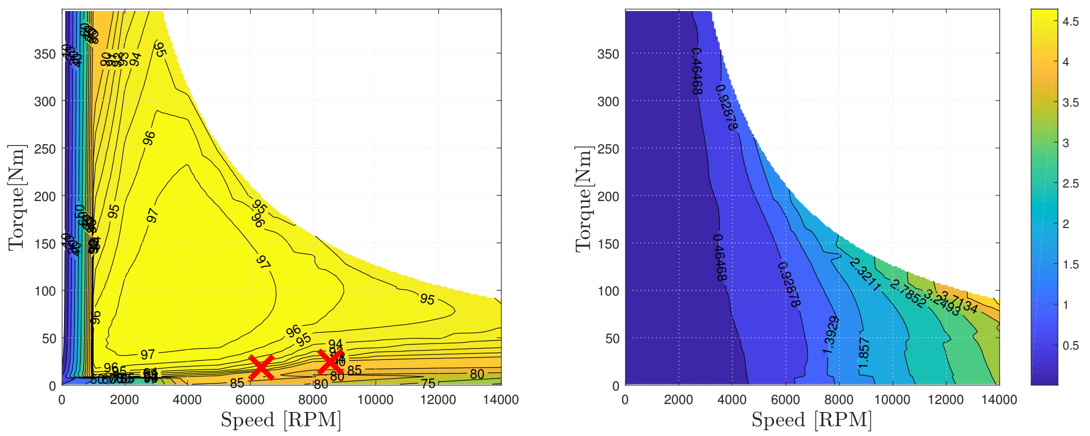

(a) Efficiency map **(b)** Core loss map

Figure 5.16: Single V design

The efficiencies at the identified centroid's for the XC90 design are,

Table 5.2: Efficiency at the centroid points

Design	6350 RPM,18.5 Nm	8550 RPM,24.5 Nm
Delta	95.7	95.96
Double Flat	94.02	94.95
Double V	94.71	95.14
Single V	89.62	92.09

Similar to the S60 design, here also we can see improvements in the efficiency at the operating points with the changes aforementioned.

Some of the observations we can make from the results of XC90 and S60 machines are,

1. Improvements in the efficiency at the operating points compared to the initial design results.

2. The core loss in all the designs are the higher at high speeds and reaches its maximum value at the maximum torque level achievable at the highest speed. This is due to the field weakening of the machine which causes highly distorted zigzag air-gap flux density [45].

3. The core losses of the single layer V - shape design for both XC90 and S60 machines are generally higher compared to any other designs. This is due to the increased stator core-loss in single layer magnet design for a 48 slot machine with 8 poles[46].

4. The double V shape design for the XC90 and S60 machines shows a similar core-loss map due to similar rotor design.

5. The core loss map of the Double Flat design of XC90 and S60 vehicles shows contrasting results. It is observed that the XC90 machine has a higher core loss compared to the S60 machine. By studying the design of both the machines, we can observe that the XC90 machines use thicker magnets and the channel width between the two layers of magnets is smaller compared to S60 machine. Due to the smaller channel width and thicker magnets, the rotor eddy current losses might be higher [47] ,[46] which we be can seen as the difference in core loss map.

6. We can see a similar discrepancy, in the losses in the delta design of the XC90 and S60 machines. The S60 machine has higher core losses compared to the XC90 machine. By studying the design of both the machines, we can see that the magnets of the S60 machine goes deeper into the rotor core compared to the XC90 which has a very shallow rotor structure. Due to this the eddy current losses in the rotor of S60 machine can be higher as compared to XC90 as the magnets are closer to the air gap and shield the rotor core from the air gap field harmonics[46].

The difference in core losses for different machines can also be studied in terms of the harmonics content in the current and voltages of the machine. Since, all the simulations are based on current feeding method, the harmonic content of the induced voltage at no load is studied next. The harmonic content of the induced voltage gives a fair representation of the space harmonics present in the air gap. Fig. 5.17a and 5.17b present the fundamental and the harmonic content of the induced voltage for XC90 and S60 machines.

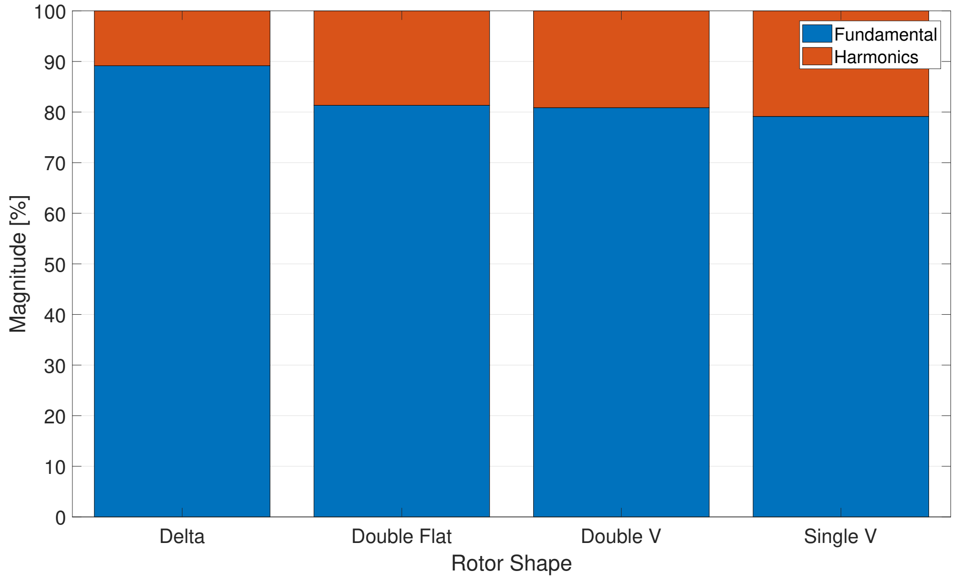

(a) Harmonic analysis of XC90 machines

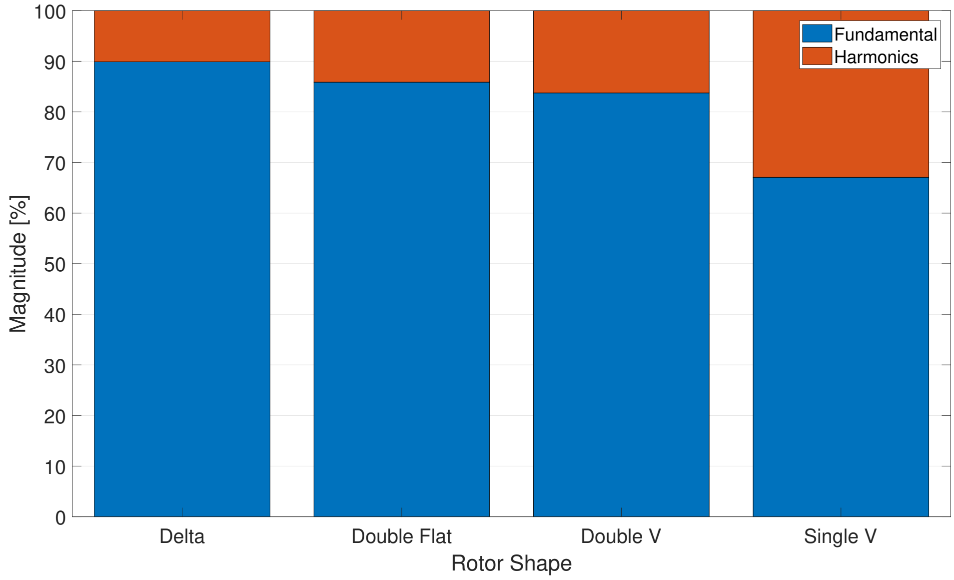

(b) Harmonic analysis of S60 machines

Figure 5.17: Back EMF harmonic analysis

The harmonic analysis of back EMF for different machines presents a similar picture as that of the core loss discussion before. The Single layer V shape design has the highest harmonic content for both XC90 and S60 machines and they have the highest core losses as well. The Double Flat design of XC90 machine has higher harmonic content compared to the S60 machine and also in terms of core losses, the XC90 machine had higher core losses compared to S60 machines. Even though, the Delta design of XC90 had lower core losses compared to S60 machine, there is very little difference in the induced voltage harmonics of these machines.

5.6 Further Analysis

As the electric machines designed are to be used for automotive propulsion, some of the other important aspects which has to investigated are related to safety issues in handling the machine and also on further improvement of the efficiency by using different control strategies. Some of the safety issues such as demagnetization analysis of the magnets and mechanical rigidity of the rotor is studied here along with results of Minimum loss control on the designed machines.

5.6.1 Short circuit and demagnetization analysis

As discussed in chapter 4.1, permanent magnets are very sensitive to high temperatures. And hence, care must be taken to make sure that the permanent magnet do not demagnetize during the normal and adverse operating conditions of the machine. As discussed in Chapter 2.5.1, the MTPA control of the PMSM varies the current angle (β) and the current magnitude (I_{mag}) for producing the requested torque. It is also known that I_{sq} is mainly responsible for torque production whereas I_{sd} for flux control in the machine. During field weakening operation of the machine, the I_{sd} current is increased so as to achieve the required speed and the remaining current ($\sqrt{I_{max}^2 - I_{sd}^2}$) is used for torque generation. Hence, the first investigation to be carried out for demagnetization is to apply maximum current (I_{max}) along the negative d - axis i.e. I_{sd} = -I_{max} and check for demagnetization. $N36Z$ magnets used in this thesis, have a maximum operating temperature of 100° and is assumed to begin the process of demagnetization if the flux density of the magnets is lower than 0.3T. The flux density in the double flat design magnets of S60 design at I_{sd} = I_{max} condition is shown in Fig. 5.18.

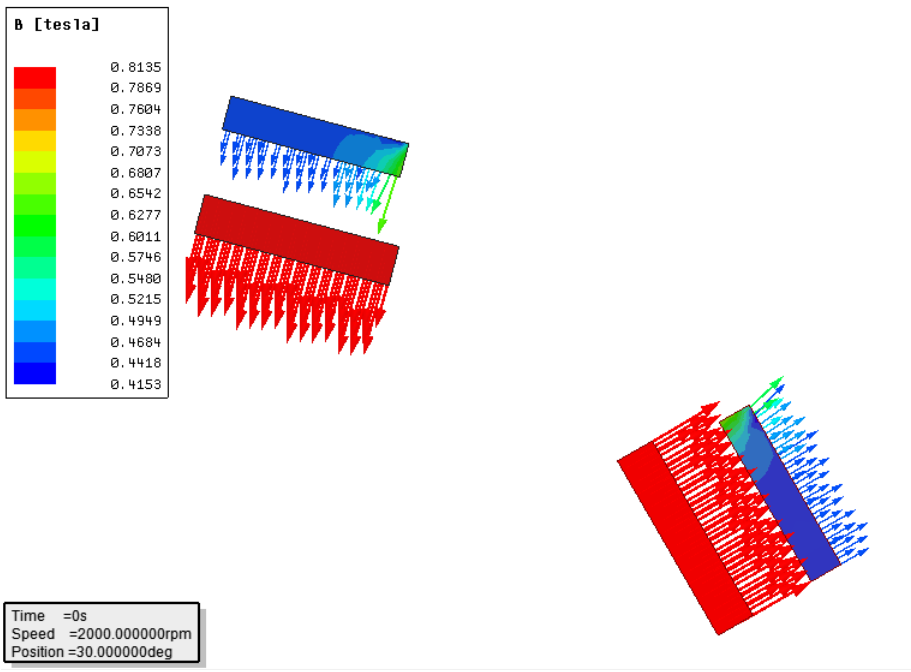

Figure 5.18: Magnet Analysis , I_{sd} =- I_{max}

As seen in the Fig. 5.18, the flux density in the magnets is higher than 0.3 T and hence the design survives the first investigation. All the designs of the XC90 and S60 machines survive $I_{sd} = -I_{max}$ condition. Short circuit of the machines is one of the severe cases of machine operation and the survivability of the PMSM are more relevant at short circuits compared to other machines, due to the use of permanent magnets. Here, the dynamics of a PMSM under short circuit condition is first discussed and then effect of short circuit on the permanent magnets is studied next.

Short circuit - Steady state analysis

The voltage equations of the PMSM machine in dq reference frame is given by,

$$U_{sd} = R_s i_{sd} + L_{sd}\frac{di_{sd}}{dt} - \omega_r L_{sq} i_{sq} \tag{5.1}$$

$$U_{sq} = R_s i_{sq} + L_{sq}\frac{di_{sq}}{dt} + \omega_r L_{sd} i_{sd} + \omega_r \Psi_m \tag{5.2}$$

neglecting $L_{sd}\frac{di_{sd}}{dt}$ and $L_{sq}\frac{di_{sq}}{dt}$ terms from the above voltage equations and assuming steady state operation,

$$U_{sd,ss} = R_s i_{sd} - \omega_r L_{sq} i_{sq} \tag{5.3}$$

$$U_{sq,ss} = R_s i_{sq} + \omega_r L_{sd} i_{sd} + \omega_r \Psi_m \tag{5.4}$$

In a three phase short circuit of the machine, the value of $U_{sd,ss}$ and $U_{sq,ss}$ is zero and hence,

$$0 = R_s i_{sd} - \omega_r L_{sq} i_{sq} \tag{5.5}$$

$$0 = R_s i_{sq} + \omega_r L_{sd} i_{sd} + \omega_r \Psi_m \tag{5.6}$$

From (5.5) and (5.6), I_{sd} and I_{sq} can be written as,

$$I_{sd} = \frac{-\omega_r^2 L_{sq} \Psi_m}{R_s^2 + \omega_r^2 L_{sd} L_{sq}} \tag{5.7}$$

$$I_{sq} = \frac{-\omega_r R_s \Psi_m}{R_s^2 + \omega_r^2 L_{sd} L_{sq}} \tag{5.8}$$

The variation of I_{sd} and I_{sq} with respect to speed for the XC90 delta design machine with $R_s = 3e - 3\ \Omega$, $L_{sd} = 2e - 4\ H$, $L_{sq} = 3.5e - 4\ H$ and $\Psi_m = 0.0656\ Wb$ is presented in Fig. 5.19.

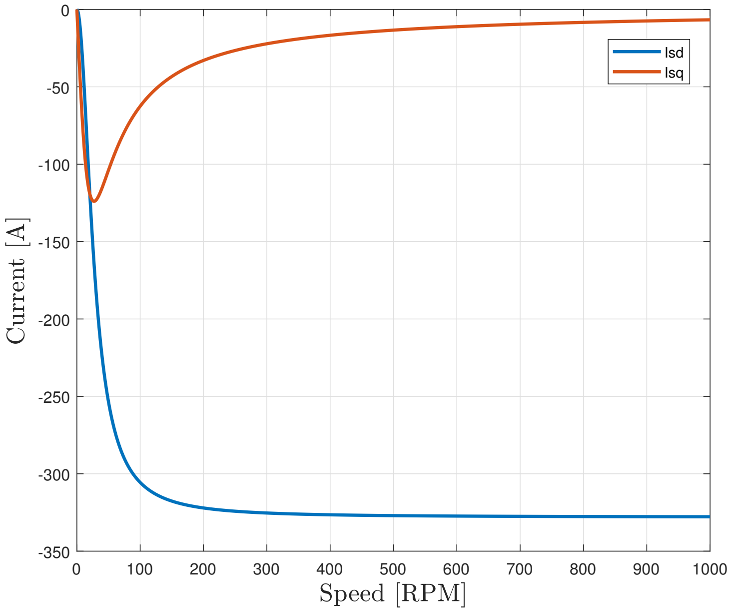

Figure 5.19: Short circuit currents in steady state

As can be seen from Fig. 5.19, the I_{sq} current is negative and decays to zero as speed increases and I_{sd} increases from zero and reaches a steady state value of $-\frac{\Psi_m}{L_{sd}}$, which is referred to as the characteristic current (I_{ch}) of the machine [48]. Analysing the torque behaviour in Fig. 5.20 ,

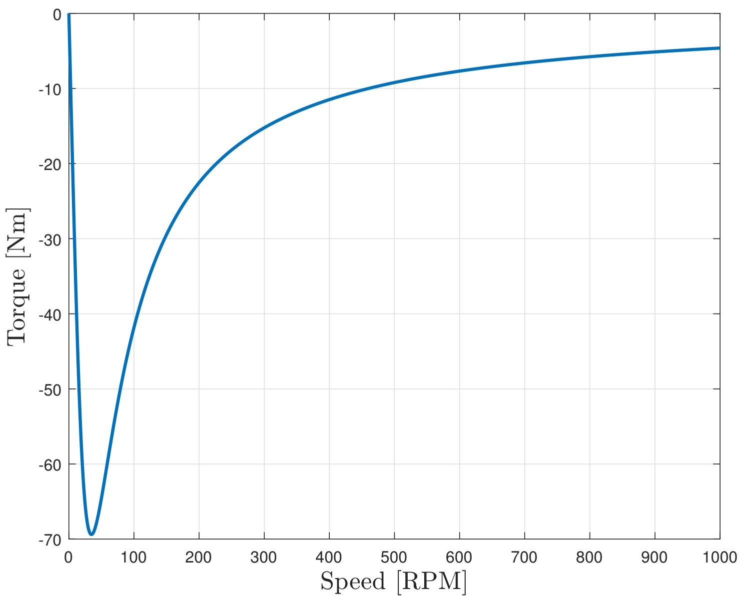

Figure 5.20: Short circuit torque in steady state

we can see that, the generated electromagnetic torque is negative during short circuit and then decays to zero as the speed increases and is consistent with the behaviour of I_{sq}.

Short circuit - Transient analysis

As discussed before, the voltage equations of the PMSM machine in dq reference frame is given by,

$$U_{sd} = R_s i_{sd} + L_{sd}\frac{di_{sd}}{dt} - \omega_r L_{sq} i_{sq} \tag{5.9}$$

$$U_{sq} = R_s i_{sq} + L_{sq}\frac{di_{sq}}{dt} + \omega_r L_{sd} i_{sd} + \omega_r \Psi_m \tag{5.10}$$

Applying Laplace transform to the above equations, equating U_{sd} and U_{sq} to zero and assuming zero initial currents ($I_{sd}(0)$,$I_{sq}(0) = 0$),

$$0 = R_s I_{sd}(s) + sL_{sd} I_{sd}(s) - \omega_r L_{sq} I_{sq}(s) \tag{5.11}$$

$$0 = R_s I_{sq}(s) + sL_{sq} I_{sq}(s) + \omega_r L_{sd} I_{sd}(s) + \frac{\omega_r \Psi_m}{s} \tag{5.12}$$

Writing them in matrix form,

$$\begin{bmatrix} R_s + sL_{sd} & -\omega_r L_{sq} \\ \omega_r L_{sd} & R_s + sL_{sq} \end{bmatrix} \begin{bmatrix} I_{sd}(s) \\ I_{sq}(s) \end{bmatrix} = \begin{bmatrix} 0 \\ -\frac{\omega_r \Psi_m}{s} \end{bmatrix}$$

and $I_{sd}(s)$ and $I_{sq}(s)$ can be written as,

$$\begin{bmatrix} I_{sd}(s) \\ I_{sq}(s) \end{bmatrix} = \begin{bmatrix} R_s + sL_{sd} & -\omega_r L_{sq} \\ \omega_r L_{sd} & R_s + sL_{sq} \end{bmatrix}^{-1} \begin{bmatrix} 0 \\ -\frac{\omega_r \Psi_m}{s} \end{bmatrix}$$

which leads to,

$$I_{sd}(s) = \frac{-\omega_r^2 L_{sq} \Psi_m}{s(s^2 L_{sd} L_{sq} + sR_s[L_{sd} + L_{sq}] + R_s^2 + \omega_r^2 L_{sq} L_{sd})} \tag{5.13}$$

$$I_{sq}(s) = \frac{-R_s \omega_r \Psi_m - sL_{sd}\omega_r \Psi_m}{s(s^2 L_{sd} L_{sq} + sR_s[L_{sd} + L_{sq}] + R_s^2 + \omega_r^2 L_{sq} L_{sd})} \tag{5.14}$$

Applying the inverse Laplace transform to (5.13) and (5.14), the transient solution of $I_{sd}(t)$ and $I_{sq}(t)$ is presented in Fig. 5.21.

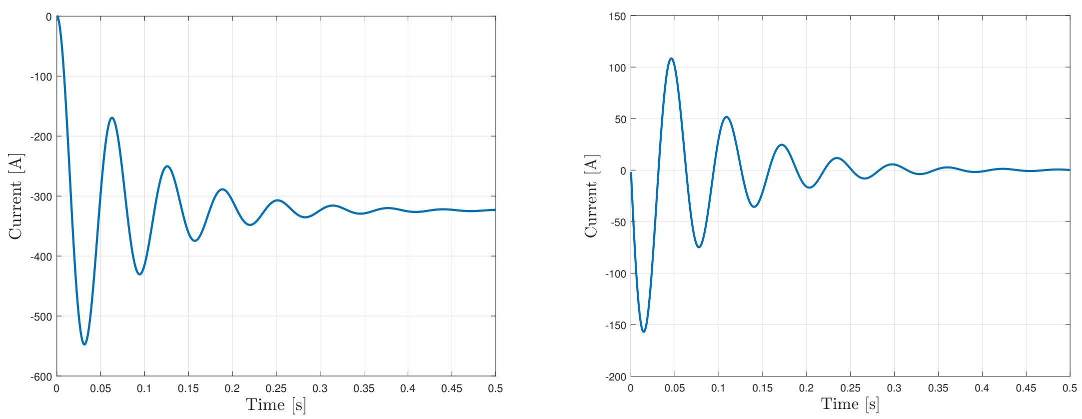

(a) I_{sd} **(b)** I_{sq}

Figure 5.21: Transient short circuit currents

As seen from Fig. 5.21, the transient solutions of I_{sd} and I_{sq} follows the steady state response as presented in Fig. 5.19. The I_{sd} vs I_{sq} trajectory and the electromagnetic torque generated are presented in Fig. 5.22.

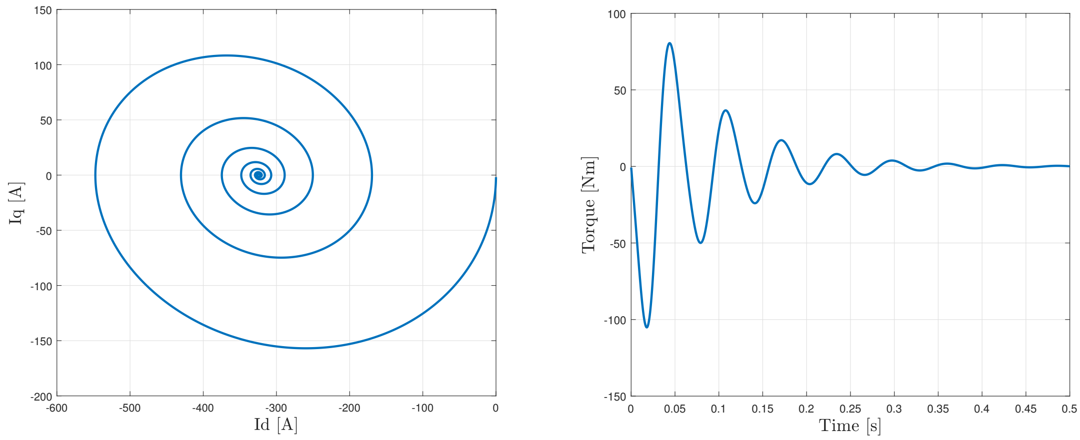

(a) I_{sd} vs I_{sq} **(b)** Electromagnetic torque

Figure 5.22: Transient trajectory and electromagnetic torque

Short circuit - Permanent magnet analysis

As seen from Fig. 5.19 and 5.21, the maximum value of the d - axis transient short circuit current ($I_{max,sd}$) is close to 1.7 times the steady state short circuit current (I_{ch}). Also from literature we see that, $I_{max,sd} \approx 1.7 I_{ch}$ [49], hence an investigation where $I_{sd} = 1.7 I_{ch}$ is carried out next to analyze the survivability of the magnets during the short circuit. The flux density of the double flat design magnets when $I_{sd} = 1.7 I_{ch}$ is shown in Fig. 5.23.

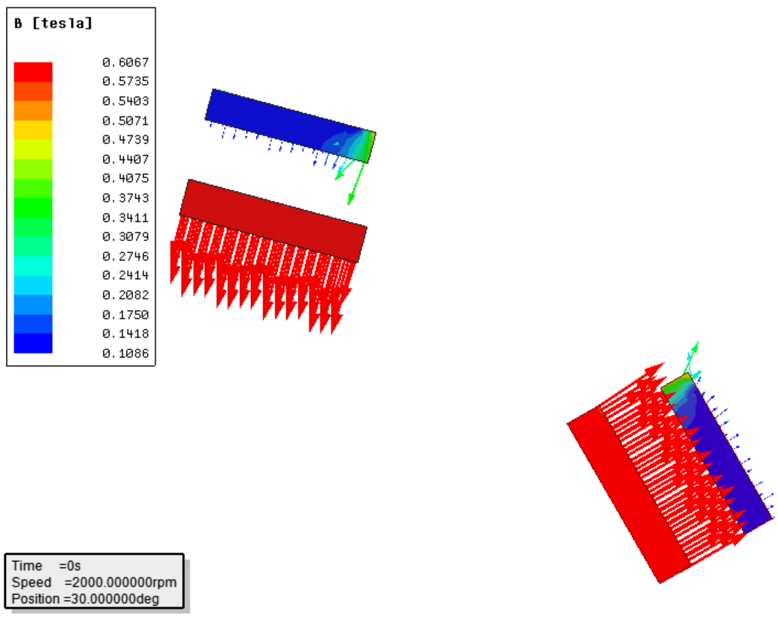

Figure 5.23: Magnet Analysis , $I_{sd} = 1.7 I_{ch}$

As seen from Fig. 5.23, the flux density in some parts of the magnets are lower than the threshold of 0.3 T and hence there is a risk of demagnetization. This is also observed in all other designs of the XC90 and S60 machines. Hence, different magnets with better demagnetization properties has to be considered.

5.6.2 Mechanical stress test

Mechanical rigidity of electric machines is one of the important parameters in the overall design and development processes. Due to the complex shape of the flux barriers and the placement of magnets, it is even more important to check the mechanical strength of the PMSM's. In this thesis, mechanical rigidity of the rotor to the centripetal forces acting on it due to the rotation of the rotor up to 14000 RPM is studied. The maximum tensile stress and the maximum expansion of the rotor structure is analyzed. For Arnon 7 the maximum allowable tensile strength is 450 GPa and maximum expansion limit is set to 0.05 mm. Fig. 5.24 presents the simulation result of the tensile strength distribution around the rotor structure.

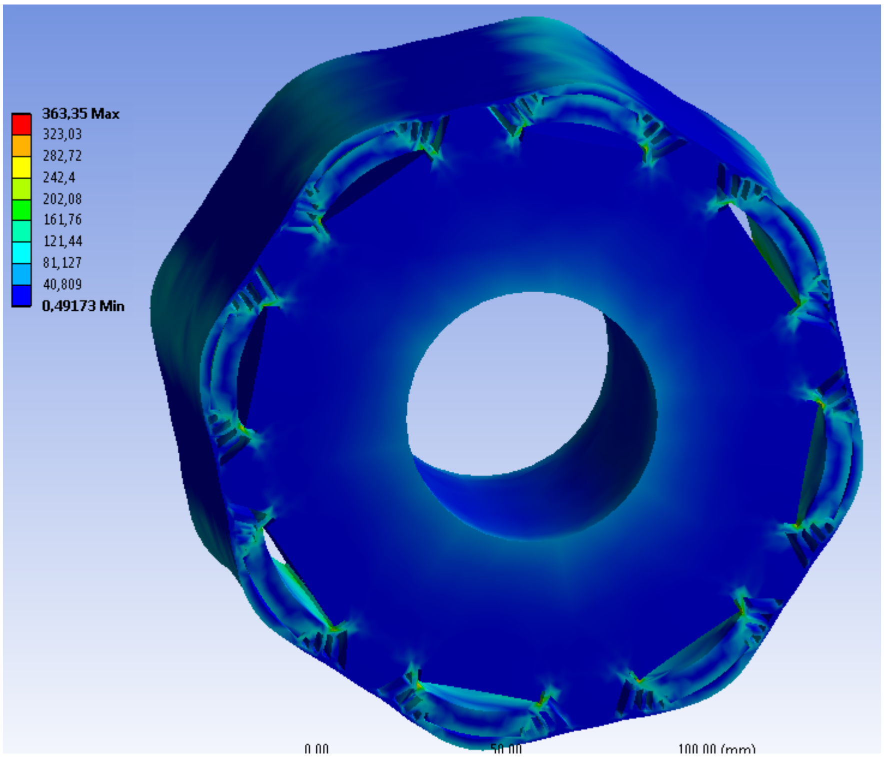

Figure 5.24: Tensile strength analysis

Fig. 5.25 presents the expansion of the rotor structure due to centripetal forces.

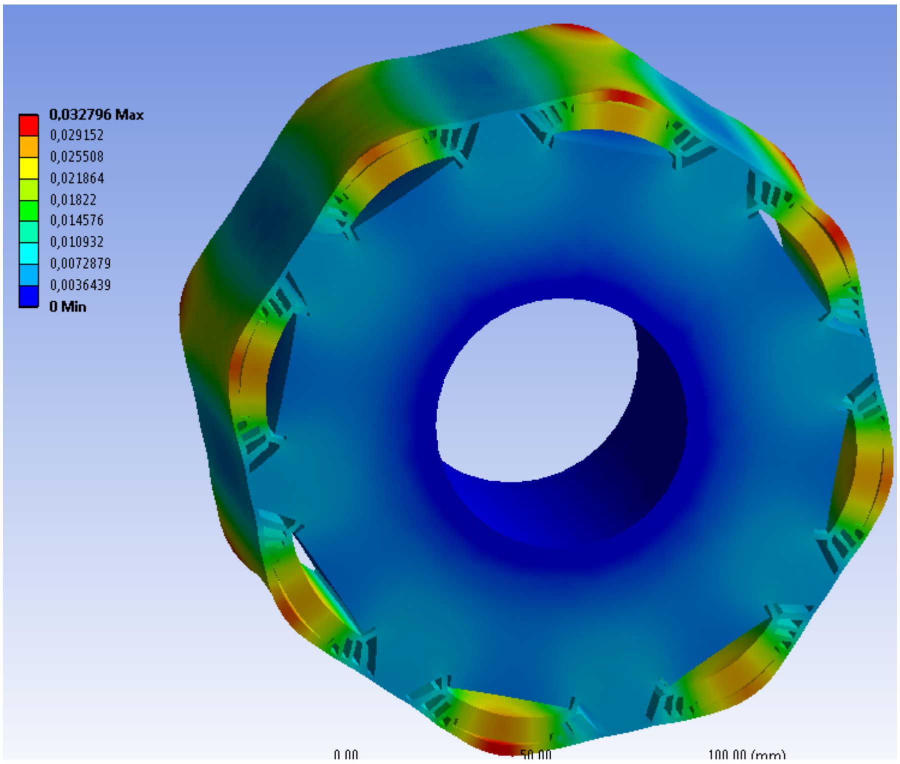

Figure 5.25: Rotor structure expansion

All eight rotor designs pass the simulation. Due to its complex duct design and magnet configuration, the double flat design come out as the weakest while the single V appears to be the strongest. The V shape and double V-shape also comes out to be the strongest since it it structurally supported in three places compared to the two places in double flat design.

5.6.3 Minimum Loss control

Apart from the MTPA control algorithm , minimum loss control technique was tried on some of the final designs of the machines. Even though a reduction in the core losses was observed for the same operating point as compared to MTPA , an excess current is needed to satisfy the torque demand was noted. No significant improvement in efficiency was observed. Due to the excess current, the converter losses also increases and can decrease the overall system efficiency. Hence, we do not see any drastic changes in terms of efficiency to advocate minimum loss control over MTPA control.

6

Design comparison and cost analysis

This result chapter will present the comparison between the designs as well as some additional cost analysis.

6.1 Cost Analysis for Arnon 7

Electric machines designed for automotive propulsion applications are inherently designed for mass production and hence a high emphasis on initial and running cost are placed on machine design. In this thesis, it is a trade-off between materials which can increase efficiency and the cost. Hence a cost analysis on the usage of new material and its impact is studied here. A simplified model is used where only gain in the machine efficiency is taken into account and improvements in the inverter losses is neglected. Hence, modest results are expected and in practical, improvements in cost benefit will be even more than predicted. Due to an extended field weakening region of operation, the main losses in the electric machine are the iron losses in the rotor and stator iron. Hence, materials with low $loss/kg$ is beneficial and hence thinner laminations are preferred. In this thesis, Arnon 7 [38] having 0.178 mm lamination thickness as compared to 0.35 mm of $M270-35A$ is used. However, the cost of this material is almost 8 times as that of $M270-35A$, where the $M270-35A$ costs 2.354 € per kg while the Arnon 7 costs 15.75 € per kg. A cost analysis is therefore performed to see if the increase in cost can be motivated in terms of money saved from energy savings. Cost per driven km depends on (with only electrical energy taken in to consideration) the electric energy consumption and the price of electricity.

$$P_{operatingpoints}T_{km}C_{energy} = 0.05€/km \tag{6.1}$$

Where P is the power (kW) at the defined operating points , T is the time it takes to drive one km (h/km) and C is the cost per kwh(€/kWh) . The cost C is the cost for charging and is taken as 0.29€ as this is the mean cost of charging between house and charging stations. A mean increase of 3 % efficiency at the centroids is observed between machines made from Arnon-7 and $M270-35A$ material as seen in Fig. 5.3. The cost savings due to increase in machine efficiency from a battery perspective and a 100 kWh battery with a battery cost of 134 €/ kWh is

$$100kWh * 0.03 * 134€/kWh = 403€ \tag{6.2}$$

The cost savings from decreased battery size is removed from the increased cost of the more expensive Arnon material. The amount of iron material used in each of the machines is calculated by taking the machine as a cylinder. Assuming a steel density ρ_{steel} of 7740 kg/m^3, the total weight of the material (W_m) for each machine is,

$$W_m = (\frac{D_s}{2})^2 \pi L_{st} \rho_{steel} \tag{6.3}$$

where D_s is the outer diameter of the stator and L_{st} is the stack length. Fig. 6.1 presents the distance vehicles have to be driven before the extra cost incurred due to the use of Arnon 7 evens out with savings in energy due to higher efficiency.

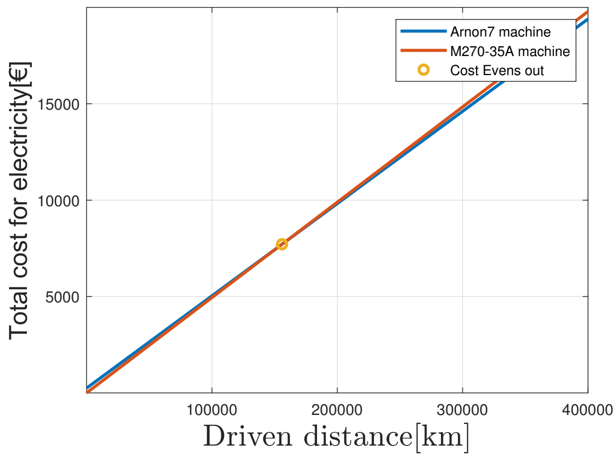

(a) S60

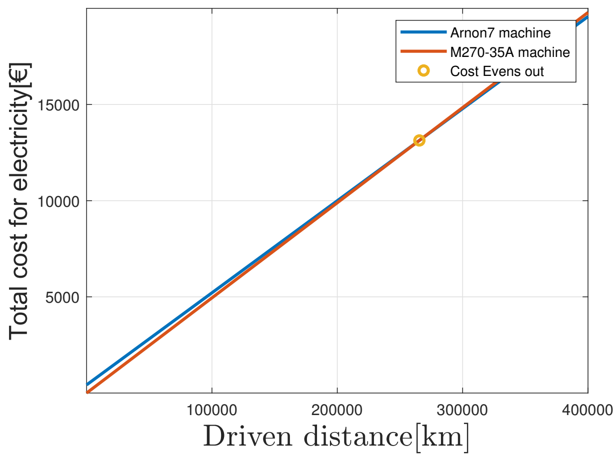

(b) XC90

Figure 6.1: Driven distance where energy cost savings vs. material cost difference evens out.

The total material cost for the S60 machine is 114€ for the $M270-35A$ material and 766€ for the Arnon 7 material. For the heavier XC90 machine the total material cost is 145€ for the $M270-35A$ material and 972€ for the Arnon 7 material. Since the Arnon 7 material is more expensive, the starting point in Fig. 6.1 of $M270-35A$

and Arnon 7 is different. It can be seen that after around 150500 *km* for the S60 and 260000 *km* for the XC90, the cost difference evens out since the Arnon 7 material saves money in terms of lower energy consumption. Since the costs evens out within the lifespan of a car it is recommended to pick the more expensive material due to its higher efficiency. It is also likely that a large order of Arnon 7 material will lower the costs of the material.

6.2 Design comparison

In addition to the comparison of efficiency at the centroids, two additional means have been adopted to make a more informed decision. The first method is comparing the efficiency of the machines with Urban, Rural and Highway cycles of the entire database when it is in motoring mode and generating mode and the second method is comparison with WLTP class 3 legislative drive cycle which is being rolled out for electric vehicle certification [50]. Representative Urban, Rural and Highway drive-cycles are presented in Fig. 6.2b and their corresponding operating points for the XC90 vehicle is shown in Fig. 6.2a. The WLTP legislative drive-cycle is also presented in Fig. 6.3.

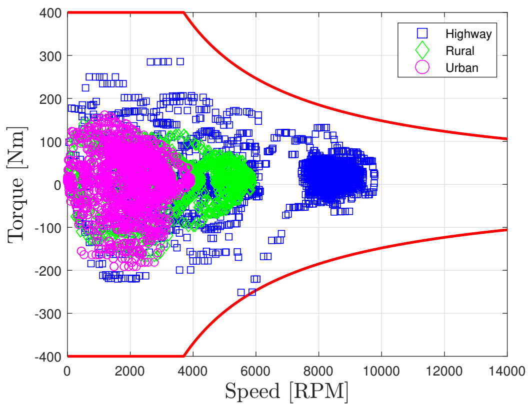

(a) Operating points

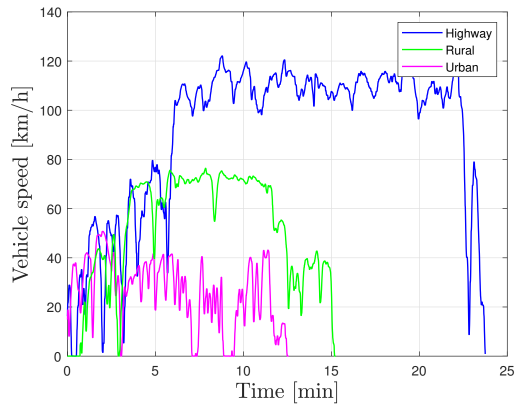

(b) Drive-cycles

Figure 6.2: Drive cycles and its corresponding operating points

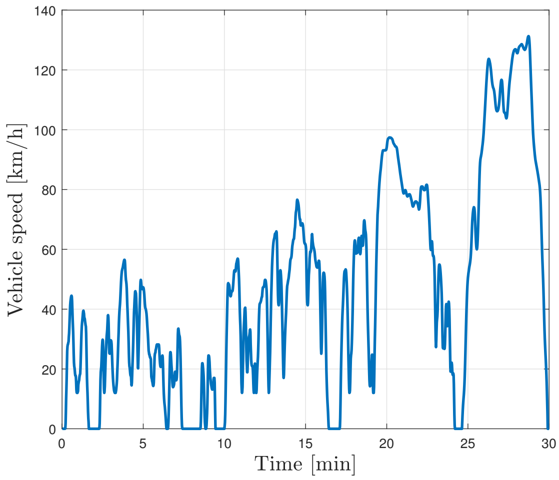

Figure 6.3: WLTP drive cycle

As seen in Fig. 6.3, the WLTP drive cycle is a combination of various driving scenarios and can be equated to be a combination of Urban, Rural and Highway driving. A weighted efficiency calculation approach is considered to compare the different electric machine designs. For this approach, the results obtained from analysis of the entire database is used. The procedure to calculated the weighted efficiency is described below,

1. Energy data binned in terms of torque and speed for all of the Urban, Rural and Highway driving-cycle category is collected. All the trips in the entire database is used for this process.
2. The operating points of the Urban, Rural and Highway drive-cycles for all the trips in the database is collected.
3. The weighted efficiency (η_w) for each category of driving is calculated as per (6.4) for motoring mode and (6.5) for generating mode.
4. This is repeated for each of the category and also for the entire database as a whole.

The calculation of weighted efficiency in motoring mode is given by,

$$\eta_{w,motor} = \frac{O_1 + O_2 + ... + O_n}{\frac{O_1}{\eta_1} + \frac{O_2}{\eta_2} + ... + \frac{O_n}{\eta_n}} \tag{6.4}$$

and in generating mode is given by,

$$\eta_{w,generator} = \frac{\eta_1 G_1 + \eta_2 G_2 + ... + \eta_n G_n}{G_1 + G_2 ... G_n} \tag{6.5}$$

where η_n is the efficiency at each of the operating points, O_n is the output mechanical energy in motoring mode and G_n is the input mechanical energy in generating mode. The result for the S60 machines in motoring and generating mode are presented in Table 6.1 and 6.2. Green marks the "winner" for each cycle.

Table 6.1: Weighted efficiency of S60 machines for drive cycles from the database

S60 - Motoring mode				
	Double Flat	Single V	Double V	Delta
Weighted Urban	93.04	93.65	92.75	88.01
Weighted Rural	95.50	95.03	94.56	93.38
Weighted Highway	95.99	94.55	94.50	94.82
Weighted Total	94.89	94.59	94.06	92.04

Table 6.2: Weighted efficiency of S60 machines for drive cycles from the database

S60 - Generating mode				
	Double Flat	Single V	Double V	Delta
Weighted Urban	95.25	95.55	94.89	94.10
Weighted Rural	95.81	95.76	95.20	94.87
Weighted Highway	95.73	95.10	94.58	94.57
Weighted Total	95.55	95.63	95.02	94.50

Similarly, the results for the XC90 machines in motoring and regenerating mode are presented in Table 6.3 and 6.4.

Table 6.3: Weighted efficiency of X90 machines for drive cycles from the database

XC90 - Motoring mode				
	Double Flat	Single V	Double V	Delta
Weighted Urban	92.49	93.51	94.45	91.77
Weighted Rural	94.30	93.42	95.68	94.55
Weighted Highway	94.12	91.46	95.16	95.42
Weighted Total	93.80	93.17	95.29	93.92

Table 6.4: Weighted efficiency of XC90 machines for drive cycles from the database

XC90 - Generating mode				
	Double Flat	Single V	Double V	Delta
Weighted Urban	94.94	95.27	95.89	94.97
Weighted Rural	95.10	95.03	96.22	95.36
Weighted Highway	94.22	93.50	95.63	94.84
Weighted Total	94.99	95.07	96.04	95.16

By taking a similar approach to calculate efficiency for the WLTP drive-cycle, the efficiency of the S60 machines is presented in Table 6.5.

Table 6.5: Weighted efficiency of S60 machines in WLTP cycle

S60 - WLTP				
	Double Flat	Single V	Double V	Delta
Motoring	95.42	95.18	94.82	85.28
Generating	95.64	95.83	95.28	94.64

and for the XC90 machines in Table 6.6,

Table 6.6: Weighted efficiency of XC90 machines in WLTP cycle

XC90 - WLTP				
	Double Flat	Single V	Double V	Delta
Motoring	93.51	93.24	95.24	93.54
Generating	94.22	93.50	95.63	94.84

6.2.1 Observations

Some of the observations that can be made from the above results are,

1. The Double V design seems to be an optimal solution for the XC90 vehicle as it has the highest efficiency for the different drive cycles as compared to other designs except for Highway cycles.
2. The Delta design of the XC90 vehicle had the highest efficiency in terms of the centroids. As the centroids are close to the Highway operating regions, in the weighted efficiency calculation too, we can see that the delta design has the highest highway efficiency.
3. The Double Flat design of the S60 vehicle seems to perform well at high speed - low torque operations which is similar to Rural and Highway driving cases.
4. For low speed - high torque operations of S60 vehicle, the single V shape design seems to be the optimal solution.
5. For the WLTP cycle, Double V shape design seems to be the optimal design for the XC90 and the Double Flat design for the S60 vehicles.

6.3 Discussion

Drive-cycle analysis

With the high volume of real world driving data used in this thesis, we believe that the results obtained gives a fair representation of the the actual driving conditions. The results on energy consumption in different driving scenarios is one of the interesting findings of this thesis. While analyzing the database, extreme torque, speed and power values have been observed, which seem to indicate data corruption while recording the data and these trips have been neglected for further analysis. Filtering of the data was performed to smoothen out unrealistic values from the database. Even though most of data after filtering seems reasonable, we cannot fully ascertain the validity of the entire data used for analysis. During the analysis of the data in terms of speed, a step size of 3.2 km/h was used. This does not fully capture the dynamics during stop and go traffic where the speed is generally less than 5 km/h. It would be interesting to fully understand this driving scenario as electric vehicles consume much less energy during stop and go traffic as compared to combustion vehicles.

Machine design

The results from the efficiency analysis and the design process of the machines are discussed here. The designs comes very close to each other in the terms of efficiency and hence it is difficult choose one rotor topology as compared to others.Also, due to the design of 8 different machines, the degree of optimization reached for each machine differs and hence we cannot state with certainty that one rotor topology is better than others.From this thesis we can state with high level of confidence that two vehicles with vastly different masses will need two different machines if both performance and efficiency are to be as high as possible. However, it is hard to say if the size difference of the machines will play a key role when finding efficient rotor designs for the requested operating points. It is therefore believed that a more accurate result could have been achieved if only one car model was used and maximum three rotor topologies were analyzed.

7
Conclusion

7.1 Conclusion

In this thesis, electric machine design based on analysis of real-world driving cycles was investigated. The database from the Swedish car movement data project was used as input data to collect and analyze the driving cycles of more than 500 privately owned cars around the Gothenburg region, Sweden. In Chapter 1, some of the previous work carried out in this field was studied and it was found that most of the investigations use legislative cycles for electric machine design as compared to real-world driving cycles.

In Chapter 2, the underlying principles for analysis of drive-cycles and electric machine design was introduced. In Chapter 2.2, the basics of vehicle dynamics which are used to construct a vehicle model are discussed. The vehicle model is then used for analysing the drive cycle and mapping the drive cycle data into electric machine torque-speed data. In Chapter 2.5, analytical design equations for the design of a PMSM was introduced. This formed the basis of the initial design of electric machines.

In Chapter 3, analysis of the drive-cycles was carried out. The drive cycles are categorized into Urban, Rural and Highway driving and are mapped into electric machine operating points. Also, energy consumption in different driving scenarios are calculated. It is followed by specifying the electric machine requirements for two different vehicle models Volvo XC90 and S60. In Chapter 4, based on the electric machine requirements, the initial analytical machine design was carried out and the four rotor topologies under investigation are presented. The results based on efficiency at the centroids and the torque ripple maps for all the eight designs are also presented.

In Chapter 5, improvements in the design from Chapter 4 are discussed. Improvements in terms of change of electric steel material, flux barrier design and skewing are discussed in detail. From these improvements, the final design of the machines is presented along with the results. Also, further analysis in terms of demagnetization and mechanical stress tests are also presented. In Chapter 6, efficiency analysis on all the eight designs based on legislative and different driving styles are presented and commented on.

The findings regarding the driving styles of customers and the regions of high energy usage are invaluable for the design of electric machines for automotive propulsion applications. The findings helped in arriving at the electric machine requirements for the two vehicles, XC90 and S60, and also showed that different vehicles require different electric machines. From the requirements of electric machines, electric machine design in a FEA simulation tool was carried out and significant improvements in efficiency (3 % gain at the centroids) and torque ripple (< 5 %) were found through the change of material from $M270-35A$ to Arnon 7 and skewing of the rotors. From the analysis of different drive-cycles on the electric machines, it was found that the Double V is an optimal solution for the XC90 vehicle for most of the operations. For the S60 vehicle the Double Flat design was found to be better for highway and rural driving and single the V shape for urban driving scenarios.

7.2 Sustainability aspects

The three main pillars of sustainable product development are its ecological, economic and social impacts. Transportation has been one of the important factors for advancements in human civilization. It has been a major player in improving the economic and social status of a large set of population. With increasing emissions from the transportation sector, global warming has caused a massive deterioration of the environment and this also affects the society both economically and socially. This thesis aims at creating viable electric machines for electric propulsion applications so as to negate the effects on global warming from the transportation sector.

7.2.1 Ecological aspects

Investigating the ecological impacts of electric vehicles and especially electric machines, we can see that they do not contribute to local emissions during their usage as compared to combustion vehicles. This is since most of the electricity production till now has been done in power plants far away from city centers. Electric vehicles, in comparison to fuel-burning vehicles, do not produce any tailpipe emissions and can contribute significantly to improving the air quality in the city centers. But if electricity production is purely based on fossil fuels such as coal or natural gas, might the advantages of electric vehicles to negate deterioration in air quality and climate change can be compromised. But with the increased interest in renewable sources of energy such as solar, hydropower and wind energy, electric vehicles will become more sustainable in the future.

The main energy source in an electric vehicle is the battery. With a need for an increased range and performance of electric vehicles, the battery becomes a complex and heavy component in an electric vehicle. Also to achieve the performance and range requirements, rare earth materials are often used in the batteries which are a cause of concern. The use of rare earth materials is not only unsustainable but also the extraction of them from the earth can lead to significant ecological deterioration, as most extraction methods also have a risk of radiation exposure. But with more than 100 years of experience in the extraction of fossil fuels from the earth, these risks are mitigated in the fossil fuel industry. The two most widely used electric machines for propulsion applications are Induction machines (IM) and PMSM's. Even though PMSM offers better efficiency and lower size as compared to IM, PMSM can become unsustainable due to the use of permanent magnets in their design. These permanent magnets are generally made up of elements such as Neodymium which are classified as rare earth materials and are very scarce to find and extract. Hence from a sustainability point of view, IMs are preferred over PMSMs. With active research in the field of using less or no rare earth material in PMSM design, the sustainability of PMSM can be improved in the future. Also, both IM and PMSM use copper for winding the machine, the extraction of copper is significantly difficult and dangerous to the environment as compared to aluminum. Also, a IM uses more copper compared to a PMSM due to the requirement of a copper rotor for better performance and hence in this regards PMSM are more favorable. Regardless of the electric machines used, the efficiency of the electric machines are many folds greater than that of the combustion engines and they also have the opportunity to recuperate the energy during braking, which also not only saves energy but also reduces wear and tear on the brake disks. All these factors favor electric vehicles with either IM or PMSM compared to a combustion engine vehicle.

7.2.2 Economical aspects

Due to the high price of batteries, electric vehicles are currently expensive compared to combustion engine vehicles. But there has been a drastic decrease in the price of batteries year after year and it is very likely that EVs can be priced similar to combustion engine vehicles in a few years. Also, with the decrease in oil reserves around the world and continued legislative actions to decrease the amount of emissions produced by combustion engine vehicles, we can see an increase in the operating cost of the combustion cars as compared to electric cars which are more and more powered by renewable sources of energy. This will also give an additional boost to reduce the cost of electric vehicles. The efficiency of the PMSM machines are higher compared to IM, this helps in saving energy during the lifetime of the machine and reduces the operating cost. This reduction in energy consumption will also have a direct effect on the sizing of the battery. As the battery is the most expensive part of an electric vehicle, this directly translates to a reduction to prices. But in terms of economic sustainability the IM might be a more sustainable option than the PMSM. Due to the high demand for rare earth materials used in PMSM there has been a rapid increase in the prices. In a span of 2009 - 2012, the cost of rare earth metal dysprosium (Dy) grew from \$150/kg to \$2500/kg. The price even spiked at \$3500/kg for a short period during 2011 [51]. Even though by 2017, the prices stabilized, it is predicted that with increased demand, the prices are set to rise again. These trends indicate an uncertain market price for essential constituents of the PMSM. Furthermore, if we are to reduce the CO_2 concentration in the atmosphere to 450 ppm as agreed by the Paris Climate Summit, there has to be a huge push toward electrification of automobiles.[52] predicts a 2400 % increase in the price of Dysprosium and 600 % Neodymium by the year of 2035 due to the increased demand for electric vehicles. Also it has to be noted that China controls 96-97 % of all rare earth material extraction and production [53], making other countries heavily dependent on the trade with a single country for the continued use of PMSMs.

7.2.3 Social aspects

Electric vehicle powertrain has few moving parts compared to combustion engine vehicles and there is also no combustion of any fuel. Hence, electric vehicles are quieter compared to combustion vehicles thereby reducing noise pollution. This also allows for free movement of heavy electric vehicles in the Urban environment during nights which are restricted for combustion vehicles. Also with fewer moving parts in the electric vehicle powertrain, the chances of breakage of components is lower and the maintenance required is also lower. While comparing electric machines, PMSM have a higher power density compared to the IM and this leads to a reduced volume of a PMSM machine for the same power level [11]. This is an important advantage of the PMSM for automotive propulsion applications as the available space in the vehicle chassis is limited. This also allows more luggage space in the electric vehicle as compared to combustion vehicles. Negative effects of the use of permanent magnets, will be the working conditions at the mines where the rare earth elements for the PMSM are extracted [53] as these are deplorable. These mining areas can have a risk of radiation exposure and are also heavily polluted with chemicals, creating a poor environment for the workers [54]. Also, in case of a sudden shut down of the machine, due to the presence of permanent magnets in the PMSM, the rotor will continue to induce voltage in the stator windings whereas the IM rotor is de-excited. This can be a safety issue as it can damage the other components of the powertrain.

With all the above inputs, in terms of sustainable development electric vehicles show a clear advantage as compared to combustion vehicles. Also with respect to electric machines, rare earth material permanent magnets do not provide a strong case of sustainability. Also due to mining hazards and potential bottlenecks in supply and cost of rare earth materials, PMSM are at a disadvantage. However, increased efficiency and lower volume combined with lower battery size are the beneficial factor of PMSM. Hence, a comprehensive strategy by a combined leadership from automotive, mining and legislator sectors are needed to analyze the situation more thoroughly. Also, sustainable development in terms of life cycle analysis is also required.

7.3 Future work

Some of the aspects which can be studied in future are,

1. In this thesis, altitude variations of the cars recorded in the database are neglected. Effort can be made to add altitude data into analysis.

2. The Swedish car movement data project has a separate database where information regarding only pure electric vehicles is aggregated. A similar analysis as carried out in this thesis can be made on the electric vehicle data and any

differences can be identified.

3. Most of the database analysis in thesis is primarily based on speed. Analysis based on distance travelled and acceleration profiles can be made.

4. Validating the database results with own driving recording of different driving scenarios.

5. Thermal modelling of a electric machine can be carried out and can be coupled with acceleration data to have more broad understanding of drive-cycles and electric machine design.

6. An integral slot distributed winding configuration was used in all of the machine designs, investigation on fractional slot winding and concentrated winding can be carried out.

7. Loss in performance due to partial demagnetization of the magnets can be included in the analysis.

8. Geometrical variations of slot and teeth dimensions of the electric machines can be investigated.

9. Investigation on the use of aluminium windings and ferrite magnets instead of copper windings and rare earth material magnets.

Bibliography

[1] G. Choi and T. M. Jahns, "Design of electric machines for electric vehicles based on driving schedules," *Proceedings of the 2013 IEEE International Electric Machines and Drives Conference, IEMDC 2013*, vol. 06, pp. 54–61, 2013.

[2] L. Chen, J. Wang, P. Lazari, and X. Chen, "Optimizations of a permanent magnet machine targeting different driving cycles for electric vehicles," *Proceedings of the 2013 IEEE International Electric Machines and Drives Conference, IEMDC 2013*, pp. 855–862, 2013.

[3] S. Gunther, S. Ulbrich, and W. Hofmann, "Driving cycle-based design optimization of interior permanent magnet synchronous motor drives for electric vehicle application," *2014 International Symposium on Power Electronics, Electrical Drives, Automation and Motion, SPEEDAM 2014*, pp. 25–30, 2014.

[4] E. Carraro, M. Morandin, and N. Bianchi, "Traction PMASR motor optimization according to a given driving cycle," *IEEE Transactions on Industry Applications*, vol. 52, no. 1, pp. 209–216, 2016.

[5] Q. Li, T. Fan, X. Wen, Y. Li, Z. Wang, and J. Guo, "Design optimization of interior permanent magnet sychronous machines for traction application over a given driving cycle," *Proceedings IECON 2017 - 43rd Annual Conference of the IEEE Industrial Electronics Society*, vol. 2017-Janua, pp. 1900–1904, 2017.

[6] S. Karlsson, "The Swedish car movement data project Final report," 2013.

[7] "Volvo cars s60 specifications." `https://www.media.volvocars.com/se/sv-se/models/new-s60/2020/specifications/`, 2019.

[8] "Volvo cars xc90 specifications." `https://www.media.volvocars.com/se/sv-se/models/xc90/2020/specifications/`, 2019.

[9] E. A. Grunditz, *Design and Assessment of Battery Electric Vehicle Powertrain , with Respect to Performance , Energy Consumption and Electric Motor Thermal Capability.* PhD thesis, Chalmers University of Technology, 2016.

[10] W. Xu, J. Zhu, Y. Guo, S. Wang, Y. Wang, and Z. Shi, "Survey on electrical machines in electrical vehicles," *2009 International Conference on Applied Superconductivity and Electromagnetic Devices, ASEMD 2009*, no. c, pp. 167–170, 2009.

[11] G. Pellegrino, A. Vagati, B. Boazzo, and P. Guglielmi, "Comparison of induction and PM synchronous motor drives for EV application including design

examples," in *IEEE Transactions on Industry Applications*, vol. 48, pp. 2322–2332, 2012.

[12] V. M. Bida, D. V. Samokhvalov, and F. S. Al-mahturi, "PMSM Vector Control Techniques – a Survey," *2018 IEEE Conference of Russian Young Researchers in Electrical and Electronic Engineering (EIConRus)*, no. VVC, pp. 577–581, 2018.

[13] C. T. Pan and S. M. Sue, "A Linear Maximum Torque Per Ampere Control for IPMSM Drives Over Full-Speed Range," *IEEE Transactions on Energy Conversion*, vol. 20, no. 2, pp. 359–366, 2005.

[14] C. Mademlis and N. Margaris, "Loss minimization in vector-controlled interior permanent-magnet synchronous motor drives," *IEEE Transactions on Industrial Electronics*, vol. 49, no. 6, pp. 1344–1347, 2002.

[15] J. Lee, K. Nam, S. Choi, and S. Kwon, "Loss-Minimizing Control of PMSM With the Use of Polynomial Approximations," *IEEE Transactions on Power Electronics*, vol. 24, no. 4, pp. 1071–1082, 2009.

[16] Z. Huang, *Thermal Design of Electrical Machines Performances.* PhD thesis, Lund University, 2013.

[17] J.Pyrhonen T.Jokinen V.Hrabovcova, *Design of Rotating Electric Machines.* 2014.

[18] T. Lipo, *Introduction to AC machine design.* 2017.

[19] Z. Q. Zhu, S. Member, S. Ruangsinchaiwanich, N. Schofield, and D. Howe, "Reduction of Cogging Torque in Interior-Magnet Brushless Machines," *IEEE Transactions on Magnetics*, vol. 395, no. 5, 2003.

[20] K.-h. Shin, J.-s. Yu, J.-y. Choi, and H.-w. Cho, "Design and Analysis of Interior Permanent Magnet Synchronous Motor Considering Saturated Rotor Bridge using Equivalent Magnetic Circuit," *The Korean Magnetics Society*, vol. 19, no. 4, pp. 404–410, 2014.

[21] M. Farshadnia, *Advanced Theory of Fractional-Slot Concentrated- Wound Permanent Magnet Synchronous Machines.* PhD thesis, The University of New South Wales.

[22] L. Chong, *Design of an Interior Permanent Magnet Machine with Concentrated Windings for Field Weakening Applications.* PhD thesis, The University of New South Wales, 2011.

[23] TeslaMotors, "2012 TESLA MODEL S SPECIFICATIONS AND FEATURES," pp. 1–5, 2012.

[24] E. Ericsson, *Driving pattern in urban areas – descriptive analysis and initial prediction model.* PhD thesis, Lund Institute of Technology, 2000.

[25] T. Kanungo, S. Member, D. M. Mount, N. S. Netanyahu, C. D. Piatko, R. Silverman, A. Y. Wu, and S. Member, "An Efficient k -Means Clustering Algo-

rithm : Analysis and Implementation," *IEEE Transactions on Pattern Analysis and Machine Intelligence*, vol. 24, no. 7, pp. 881–892, 2002.

[26] J.Gyselinck J.Melkebeek P.Dular F.Henrotte W.Legros, "Calculation of Eddy Currents and Associated Losses in Electrical Steel Laminations '," *IEEE Transactions on Magnetics*, vol. 35, no. 3, pp. 1191–1194, 1999.

[27] M. Tietz, F. Herget, G. V. Pfingsten, S. Steentjes, K. Telger, K. H. Senior, M. Ieee, T. Steel, E. Ag, and S. Steentjes, "Effects and advantages of high-strength non grain oriented (NGO) electrical steel for traction drives," *2013 3rd International Electric Drives Production Conference (EDPC)*, pp. 1–6, 2013.

[28] A. Krings, *Iron Losses in Electrical Machines — Influence of Material Properties , Manufacturing Processes , and Inverter Operation.* PhD thesis, Royal Institute of Technology Stockholm, 2014.

[29] K. Bourchas, "Manufacturing Effects on Iron Losses in Electrical Machines," 2015.

[30] M.Lazzari, A.Boglietti, and P.Ferraris, "Iron losses in magnetic materials with six-step and pwm inverter supply," *IEEE Transactions on Magnetics*, vol. 27, no. 6, pp. 5334–5336, 1991.

[31] M. Rahman and G. Slemon, "Promising applications of neodymium boron Iron magnets in electrical machines," *IEEE Transactions on Magnetics*, vol. 21, no. 5, pp. 1712–1716, 1985.

[32] Magnetic Materials Producers Association, "Standard Specifications for Permanent Magnet Materials," Tech. Rep. 0100.

[33] P.Sekerak V.Hrabovcova J.Pyrhonen L.Kalamen, "Comparison of Synchronous Motors With Different Permanent Magnet and Winding Types," *IEEE Transactions on Industry Applications*, vol. 49, no. 3, pp. 1256–1263, 2013.

[34] W. L. Soong, S. Han, and T. M. Jahns, "Design of Interior PM Machines for Field-Weakening Applications," in *International Conference on Electrical Machines and Systems*, pp. 654–664, 2007.

[35] G. James and S. David, "Open Source Electric Motor Models for Commercial EV & Hybrid Traction Motors," *Motor Design Limited*, 2017.

[36] F. Momen, K. M. Rahman, Y. Son, and P. Savagian, "Electric Motor Design of General Motors ' Chevrolet Bolt Electric Vehicle," *SAE Int. J. Alt. Power*, vol. 5, no. 2, pp. 286–293, 2019.

[37] M. Rahman and P. J. Savagian, "Design , Optimization and Development of Electric Machine for Traction Application in GM Battery Electric Vehicle," in *2015 IEEE International Electric Machines & Drives Conference (IEMDC)*, pp. 1814–1819, 2015.

[38] "Arnon 7 Silicon Steel." `https://www.arnoldmagnetics.com/materials/thin-and-ultra-thin-silicon-steels/`, 2019.

[39] S.-h. Han, T. M. Jahns, and Z. Q. Zhu, “Design Tradeoffs Between Stator Core Loss and Torque Ripple in IPM Machines,” *IEEE Transactions on Industry Applications*, vol. 46, no. 1, pp. 187–195, 2010.

[40] T. M. Jahns and W. L. Soong, “Pulsating Torque Minimization Techniques for Permanent Magnet AC Motor Drives-A Review,” *IEEE Transactions on Industrial Electronics*, vol. 43, no. 2, 1996.

[41] S. Rick, M. Felden, M. Hombitzer, and K. Hameyer, “Permanent Magnet Synchronous Reluctance Machine - bridge design for two-layer applications,” *2013 International Electric Machines & Drives Conference*, pp. 1376–1383, 2013.

[42] T. Lipo and W. Zhao, “Torque Pulsation Minimization in Spoke-type Interior Permanent Permanent Magnet Configurations,” *IEEE Transactions on Magnetics*, vol. 51, no. 11, pp. 1–4, 2015.

[43] W. Q. Chu and Z. Q. Zhu, “Investigation of Torque Ripples in Permanent Magnet Synchronous Machines With Skewing,” *IEEE Transactions on Magnetics*, vol. 49, no. 2, pp. 1211–1220, 2013.

[44] A. Wang, W. Lu, H. Zhao, and A. D. Procedure, “Influence of Skewed and Segmented Magnet Rotor on IPM Machine Performance and Ripple Torque for Electric Traction,” *2009 IEEE International Electric Machines and Drives Conference*, pp. 305–310.

[45] T. Lipo and R. Schiferl, “Core Loss in Buried Magnet Permanent Magnet Synchronous Motors,” *IEEE Transactions on Energy Conversion*, vol. 4, no. 2, pp. 279–284, 1989.

[46] S.-h. Han, T. M. Jahns, Z. Q. Zhu, A. S. Magnetic, and F. Case, “Analysis of Rotor Core Eddy-Current Losses in Interior Permanent-Magnet Synchronous Machines,” *IEEE Transactions on Industry Applications*, vol. 46, no. 1, pp. 196–205, 2010.

[47] A. H. Zarei, K. Abbaszadeh, and K. Safari, “The Analytical Analysis of the Rotor Losses in the PMSM Motors,” in *World Congress on Engineering and Computer Science*, vol. II, 2012.

[48] G. Choi and T. Jahns, “Interior Permanent Magnet Synchronous Machine Rotor Demagnetization Characteristics under Fault Conditions,” *2013 IEEE Energy Conversion Congress and Exposition*, pp. 2500–2507, 2013.

[49] B. A. Welchko, T. M. Jahns, W. L. Soong, and J. M. Nagashima, “IPM Synchronous Machine Drive Response to Symmetrical and Asymmetrical Short Circuit Faults,” *IEEE Transactions on Energy Conversion*, vol. 18, no. 2, pp. 291–298, 2003.

[50] “WLTP Class 3 driving cycle.” `https://wiki.unece.org/pages/viewpage.action?pageId=2523179`, 2019.

[51] M. J. Kramer, R. W. McCallum, I. A. Anderson, and S. Constantinides,

"Prospects for non-rare earth permanent magnets for traction motors and generators," *Jom*, vol. 64, no. 7, pp. 752–763, 2012.

[52] E. Alonso, A. M. Sherman, T. J. Wallington, M. P. Everson, F. R. Field, R. Roth, and R. E. Kirchain, "Evaluating Rare Earth Element Availability: A Case with Revolutionary Demand from Clean Technologies," *Environ. Sci. Technol.2012*, vol. 46, no. 8, 2012.

[53] B. C. Hurst, "China ' s Rare Earth Elements Industry : What Can the West Learn ?," *Institute for the Analysis of Global Security (IAGS)*, no. March, 2010.

[54] G. Bailey, N. Mancheri, and K. Van Acker, "Sustainability of Permanent Rare Earth Magnet Motors in (H)EV Industry," *Journal of Sustainable Metallurgy*, vol. 3, no. 3, pp. 611–626, 2017.

A

Appendix 1

Winding layout of the electric machines is shown below.

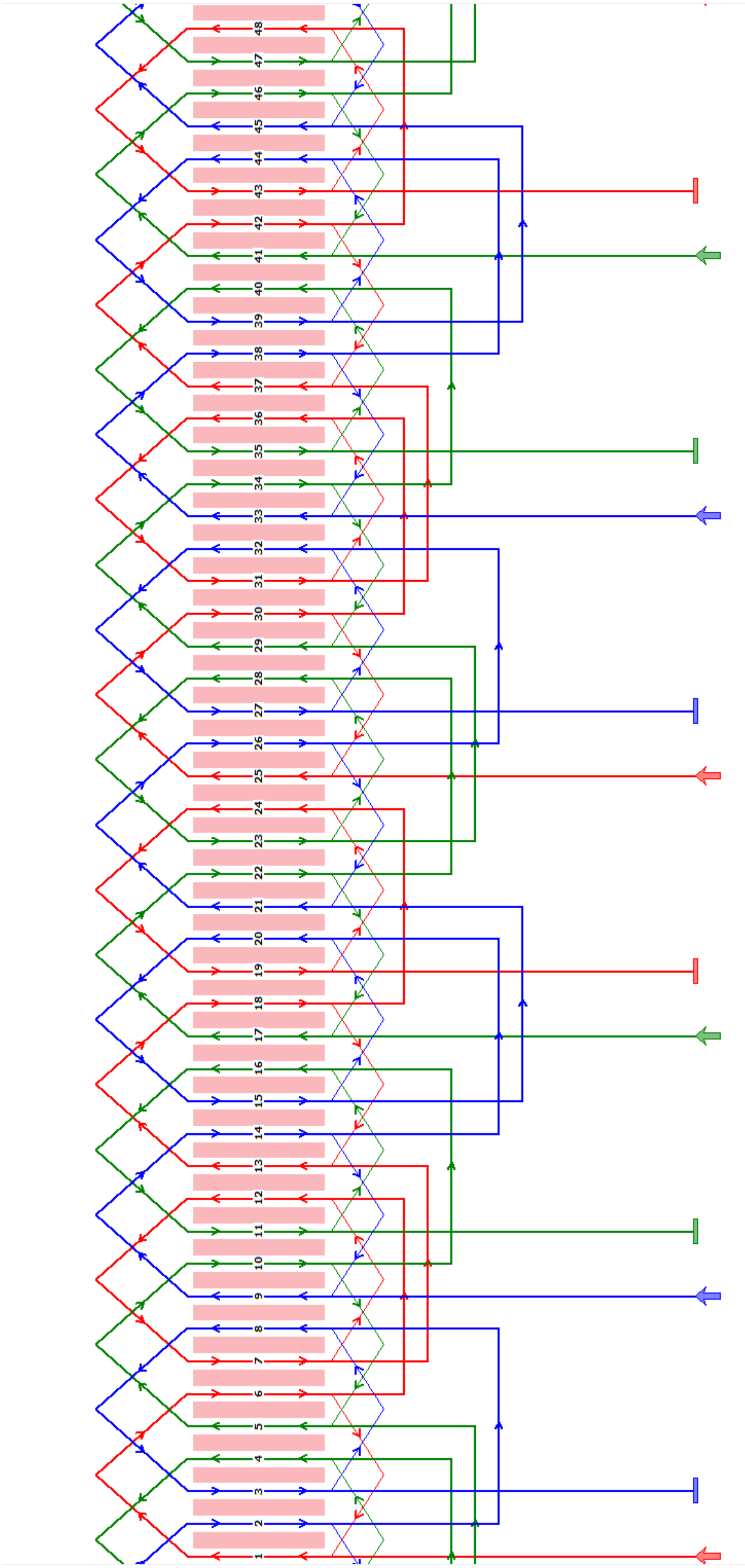

Figure A.1: Winding pattern